

Functional thin films for high-efficiency solar cells

Citation for published version (APA):

Hoex, B. (2008). *Functional thin films for high-efficiency solar cells*. [Phd Thesis 1 (Research TU/e / Graduation TU/e), Applied Physics and Science Education]. Technische Universiteit Eindhoven.
<https://doi.org/10.6100/IR634627>

DOI:

[10.6100/IR634627](https://doi.org/10.6100/IR634627)

Document status and date:

Published: 01/01/2008

Document Version:

Publisher's PDF, also known as Version of Record (includes final page, issue and volume numbers)

Please check the document version of this publication:

- A submitted manuscript is the version of the article upon submission and before peer-review. There can be important differences between the submitted version and the official published version of record. People interested in the research are advised to contact the author for the final version of the publication, or visit the DOI to the publisher's website.
- The final author version and the galley proof are versions of the publication after peer review.
- The final published version features the final layout of the paper including the volume, issue and page numbers.

[Link to publication](#)

General rights

Copyright and moral rights for the publications made accessible in the public portal are retained by the authors and/or other copyright owners and it is a condition of accessing publications that users recognise and abide by the legal requirements associated with these rights.

- Users may download and print one copy of any publication from the public portal for the purpose of private study or research.
- You may not further distribute the material or use it for any profit-making activity or commercial gain
- You may freely distribute the URL identifying the publication in the public portal.

If the publication is distributed under the terms of Article 25fa of the Dutch Copyright Act, indicated by the "Taverne" license above, please follow below link for the End User Agreement:

www.tue.nl/taverne

Take down policy

If you believe that this document breaches copyright please contact us at:

openaccess@tue.nl

providing details and we will investigate your claim.

Functional Thin Films for High-Efficiency Solar Cells

PROEFSCHRIFT

ter verkrijging van de graad van doctor aan de
Technische Universiteit Eindhoven, op gezag van de
Rector Magnificus, prof.dr.ir. C.J. van Duijn, voor een
commissie aangewezen door het College voor
Promoties in het openbaar te verdedigen
op donderdag 8 mei 2008 om 16.00 uur

door

Bram Hoex

geboren te Horst

Dit proefschrift is goedgekeurd door de promotor:

prof.dr.ir. M.C.M. van de Sanden

Copromotor:

dr.ir. W.M.M. Kessels

The work described in this thesis was partly conducted in the “HR-CEL” project within the Economy, Ecology and Technology program funded by the Netherlands Ministry of Economic Affairs, the Ministry of Education, Culture and Science and the Ministry of Housing, Spatial Planning and the Environment.

Printed and bound by Universiteitsdrukkerij Technische Universiteit Eindhoven.
Cover design by Jorrit van der Rijt, Oranje Vormgevers.

CIP-DATA LIBRARY TECHNISCHE UNIVERSITEIT EINDHOVEN

Hoex, Bram

Functional thin films for high-efficiency solar cells / door Bram Hoex. – Eindhoven : Technische Universiteit Eindhoven, 2008. – Proefschrift.

ISBN 978-90-386-1255-3

NUR 926

Trefwoorden: zonnecellen / silicium / oppervlaktepassivatie / levensduurmetingen / atomaire-laagdepositie / plasmadepositie

Subject headings: solar cells / silicon / surface passivation / carrier lifetime / atomic layer deposition / plasma deposition

Contents

Chapter 1	Introduction	1
Chapter 2	Industrial High-rate ($\sim 5\text{nm/s}$) Deposited Silicon Nitride Yielding High Quality Bulk and Surface Passivation under Optimum Antireflection Coating Behavior <i>B. Hoex, A.J.M. van Erven, R.C.M. Bosch, W.T.M. Stals, M.D. Bijker, P.J. van den Oever, W.M.M. Kessels, and M.C.M. van de Sanden, Progr. Photovoltaics 13, 705 (2005).</i>	47
Chapter 3	High-Rate Plasma Deposited SiO_2 Films for Surface Passivation of Crystalline Silicon <i>B. Hoex, F.J.J. Peeters, M. Creatore, M.A. Blauw, W.M.M. Kessels, and M.C.M. van de Sanden, J. Vac. Sci. Technol. A 24, 1823 (2006).</i>	59
Chapter 4	Ultralow Surface Recombination of c-Si Substrates Passivated by Plasma-Assisted Atomic Layer Deposited Al_2O_3 <i>B. Hoex, S.B.S. Heil, E. Langereis, M.C.M. van de Sanden, W.M.M. Kessels, Appl. Phys. Lett. 89, 0412112 (2006).</i>	79
Chapter 5	Silicon Surface Passivation by Atomic Layer Deposited Al_2O_3 <i>Submitted for publication: B. Hoex, J. Schmidt, P. Pohl, M.C.M. van de Sanden, and W.M.M. Kessels.</i>	87
Chapter 6	Excellent Passivation of Highly Doped <i>p</i> -type Si Surfaces by the Negative-Charge-Dielectric Al_2O_3 <i>B. Hoex, J. Schmidt, R. Bock, P. P. Altermatt, M. C. M. van de Sanden, and W. M. M. Kessels, Appl. Phys. Lett. 91, 112107 (2007).</i>	115
Chapter 7	On the c-Si Surface Passivation mechanism by the Negative-Charge-Dielectric Al_2O_3 <i>In preparation for publication: B. Hoex, J.J.H. Gielis, M.C.M. van de Sanden, and W.M.M. Kessels.</i>	125
Chapter 8	Surface Passivation of High-Efficiency Solar Cells by Atomic-Layer-Deposited Al_2O_3 <i>Accepted for publication: J. Schmidt, A. Merkle, R. Brendel, B. Hoex, M.C.M. van de Sanden, and W.M.M. Kessels, Progr. Photovoltaics (2008).</i>	143
Summary		155
Publications related to this research		157
Acknowledgments		161
Curriculum Vitae		163

Chapter 1

Introduction

I. General introduction and framework of this research

A. Electricity from sunlight: a promising renewable energy option

In recent years, public opinion on climate change has changed dramatically. Since 1990 the International Panel on Climate Change (IPCC) has been publishing reports periodically on the collective scientific understanding of climate change and its correlation to human activity.¹ According to the UN Secretary General “the IPCC has now unequivocally confirmed the warming of our climate system and linked it directly to human activity”.² Former U.S. Vice President Al Gore’s “An Inconvenient Truth” movie in 2006 had a considerable impact on the general public by showing the link between human-induced CO₂ levels and rising global temperature and its, albeit dramatized and slightly exaggerated, impact on the earth and on mankind.³ The IPCC and Al Gore were awarded the Nobel Peace Prize in 2007 “for their efforts to build up and disseminate greater knowledge about man-made climate change, and to lay the foundations for the measures that are needed to counteract such change”.⁴ Moreover, the Stern report, which was published in 2006, clearly illustrated the dramatic *economical* consequences of global warming in various scenarios. It demonstrated that “business as usual” would be an economical unwise option and is actually one of the worst case scenarios.⁴ Together with the limited availability of fossil fuels it is now clear that mankind has to change its way of life, especially in terms of energy production and usage.

When looking into more detail at the projected future energy mix, as shown in Fig. 1, it can be seen that several so-called renewable energy options are expected to

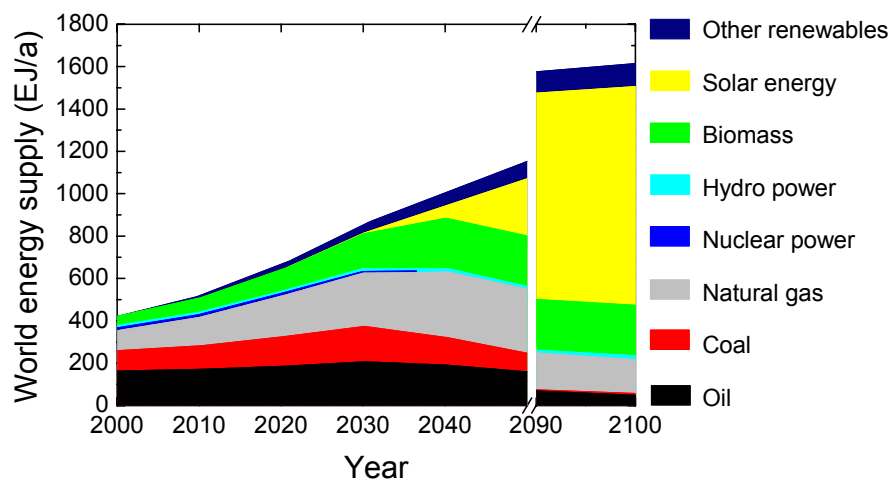


Figure 1: The future energy mix as projected by German Advisory Council on Global Change.⁵

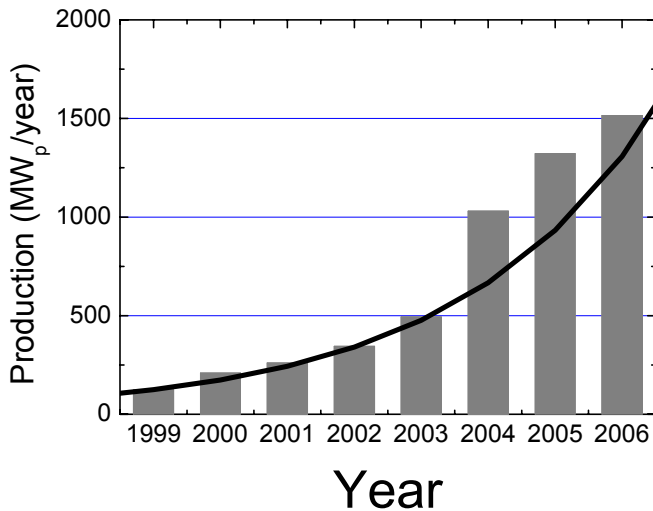


Figure 2: Worldwide annual production of solar cell modules expressed in rated peak power (W_p) output.⁶ The solid line represents a 40 % annual growth from the year 1999.

become more important in the future.⁵ Traditional fossil fuels such as coal, oil and natural gas are not expected to be depleted by 2100. Their relative share in the future energy supply will, however, significantly decrease. Renewable energy options such as wind, biomass, water and solar are expected to be dominating in the energy supply in the twenty-second century. Solar energy is even expected to account for more than 60 % of the energy mix. Solar energy can be harvested in the form of heat and electricity. In the remainder of this thesis the focus will be on the direct conversion of solar irradiation to electricity.

The photovoltaic effect was discovered by Becquerel in 1839 demonstrating that electrons could interact with electromagnetic radiation.⁷ This interaction is the physical principle of photovoltaic (PV) devices that convert solar light into electricity. The first PV device based on crystalline silicon (c-Si) with a reasonable conversion efficiency was demonstrated in 1954 by Chapin *et al.* at AT&T Bell labs.⁸ This c-Si solar cell demonstrated an energy conversion efficiency of ~6 %,⁸ and in recent years the record efficiency has been increased up to 24.7 %.⁹ Although c-Si solar cells were perceived as far too expensive for terrestrial application in the past, they currently still dominate the PV market with a market share of over 90 %. The remainder of the PV market is taken by solar cells based on thin film technologies such as a-Si:H, CdTe and CuIn(Ga)Se₂ (CI(G)S). As illustrated in Fig. 2 the PV market has been growing at 40 % (or more) per annum and is currently a multi-billion euro market. In a recent article, Swanson discussed

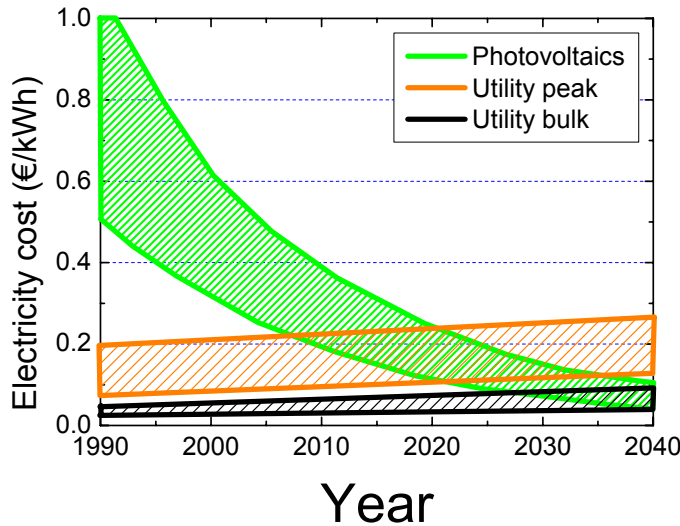


Figure 3: Projected cost of electricity produced by photovoltaics for high solar irradiation (Southern Europe, solar irradiation 1800 kWh/a m⁻²) and low solar irradiation (Northern Europe, solar irradiation 900 kWh/a m⁻²). For comparison the projected typical (utility bulk) and peak (peak utility) cost of electricity stemming from conventional coal or gas driven electricity plants. Data courtesy of EPIA.¹⁰

the economic strength of the c-Si PV versus alternative technologies such as thin film solar cells (so-called “second generation solar cells”) and concentrator solar cells (part of the so-called “third generation solar cells”).^{11,12} This paper argued that the c-Si is most likely to stay the dominant technology for at least another decade. C-Si PV is a proven technology with long-term stability (current warranty of 25 years) which will be a challenging moving target to match for alternative technologies. Moreover, the high energy conversion efficiency of c-Si solar cells results in a more modest share of solar cells in the total installment costs of, e.g., a rooftop system, if compared to lower efficiency alternatives.^a

As shown in Fig. 3 the cost of PV electricity is currently significantly higher than the prices of bulk electricity stemming from conventional coal or gas driven electricity plants. The cost of PV electricity is, however, matching the peak utility prices in summer on the electricity spot-market in most of Europe.¹³ The enormous growth which the PV market has experienced in recent years is primarily policy-driven. For example by programs such as the feed-in tariff that is currently applied in various European countries including Germany. In Germany a producer of solar energy is receiving a fixed price per

^a Swanson argued that a thin-film technology with a conversion efficiency of 8 % would need unrealistically low production costs of 0.02 \$/W_p to be costs-competitive to 18 % efficient c-Si solar cells assuming similar area lamination and balance of system costs for both technologies.¹²

kWh for a period of 20 years. This feed-in tariff is paid by all electricity consumers such that this program is independent of the Government budget and that continuity is assured. In 2007 the feed-in tariff was 0.38-0.54 €/kWh depending on the configuration of the PV-system.¹³ From Fig. 3 it can be seen that the German feed-in tariff is higher than the projected cost of solar electricity, making PV a lucrative investment. As a consequence the significant up-front investment costs associated with a PV installation are easily financed by a commercial bank loan.

B. Cost-driven trends for c-Si PV

The German feed-in tariff also includes a strong incentive to reduce the costs for PV electricity. The feed-in tariff is reduced by 5 % each year for newly installed PV systems. Consequently, solar cell producers are forced to reduce their costs accordingly. Part of the cost-reduction of PV electricity can still be obtained by economy-of-scale, but other cost-reduction trends are pursued in c-Si PV as well. These trends can mostly be related to the relatively large share of the c-Si base material in PV electricity costs. A first obvious trend is the reduction of the c-Si wafer thickness that is used for the production of solar cells. In 2002 solar cells were produced from > 300 µm thick c-Si wafers, whereas in 2007 wafers with a thickness < 200 µm were industrially used.¹² Moreover, alternative technologies have been developed that significantly reduce the amount of silicon required for c-Si solar cells. The most notable examples in this respect are the ribbon technology as used by Evergreen Solar¹⁴ and the Sliver technology developed at the Australian National University and currently commercialized by Origin Energy.¹⁵ In the ribbon technology c-Si wafers are directly produced from the Si melt thereby avoiding sawing losses. In the Sliver technology 60 µm thick solar cells are produced from ~2 mm thick c-Si wafers, decreasing Si usage by a factor of 12.^{14,15}

The second major trend is related to the production of c-Si base material for c-Si solar cells. In 2006 the amount of c-Si consumed by the PV industry was matching that of the semiconductor industry, and the PV share will continue to increase.¹² This rapid growth was not anticipated by the producers of c-Si feedstock and the growth of the c-Si PV in 2007 was even severely limited by the c-Si feedstock supply.¹² As a result alternative feedstock production processes are intensively investigated, and future material standards can be set by the PV industry instead of the semiconductor industry. At the moment most c-Si solar cells are produced from *p*-type base material as this material proved to be more stable for space applications in the past.¹⁶ Recently it was, however, found that most metallic impurities are less detrimental for the c-Si solar cell performance in *n*-type c-Si as compared to *p*-type c-Si. This could obviously be beneficial from a production-cost point of view.¹⁷ These advantages could result in a dedicated production of *n*-type c-Si for PV, thereby requiring new solar cell

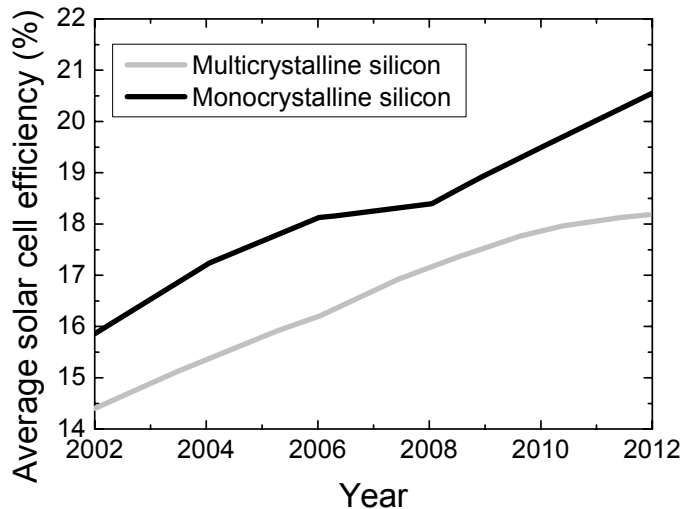


Figure 4: Projected average solar cell efficiency for mono- and multicrystalline silicon solar cell in industrial production.¹⁸

designs. The advantage of *n*-type c-Si over *p*-type c-Si is currently already exploited in commercial solar cells with the highest energy conversion efficiencies produced by Sanyo and SunPower.^{19,20} Also alternative low-cost production schemes for *p*-type c-Si are investigated such as upgrading of metallurgical grade Si to solar grade Si.²¹

The last, and most important, trend that can be observed in c-Si PV is the increase in energy conversion efficiency of commercial c-Si solar cells. In this way more electricity can be extracted from the same amount of c-Si base material. The energy conversion efficiency of industrial c-Si solar cells has been steadily increasing in recent years, and was typically 15-16 % on cell level for solar cells based on multi-crystalline (mc) Si in 2007 as shown in Fig. 4.¹² By continuous technological advances and new solar cell designs, energy conversion efficiency is expected to increase up to 18-20 % in the upcoming years.¹² For an industrial 25 MW production line an 1 % absolute increase in solar cell efficiency nowadays accounts for ~3.3 M€ additional yearly revenue.^b Currently c-Si solar cells with a conversion efficiency of over 22 % are already commercially produced by SunPower.²² Numerous other companies, such as Q-cells,²³ have announced production of high-efficiency concepts in the near future.^c

^b Assuming an energy conversion efficiency of 15 % and a selling price of 2 €/W_p for a solar cell manufacturer.

^c The average module efficiency is always lower than the cell efficiency. For example the first commercial solar cell module with a 20 % efficiency was presented by SunPower at the 22nd EU-PVSEC meeting in Milan, consisting of solar cells with an average efficiency of 22.4 %.²⁴

C. Technological requirements to support the cost driven trends

The three main cost-driven trends lead to various technological requirements as summarized in Table I. All these technological requirements are in essence based on a cost-effective optimization of the c-Si solar cell efficiency, and are currently intensively investigated in industry and academia.

Reduction of the solar cell thickness will significantly increase the surface-to-volume ratio, and therefore electronic losses at the front and the rear surface of the c-Si solar cell will become more detrimental for its performance. A reduction of surface recombination by adequate surface passivation will, consequently, become more important. Moreover, due to the relatively low light absorption in c-Si a significant portion of solar irradiation will reach the rear side of the solar cell if the solar cell thickness is further reduced. Adequate light-trapping schemes should be applied for thinner c-Si solar cells to achieve a similar optical performance when compared to thicker c-Si solar cells. The industry standard aluminum back-surface field (Al-BSF) that is applied at the rear side of c-Si solar cells cannot fulfill the desired optical

Table I: Technological requirements derived from the three main cost-driven trends in c-Si PV. This list is not exhaustive but summarizes the main topics currently investigated in academia and in industry.

Trend I: Reduction of the solar cell thickness
<ul style="list-style-type: none">• Production and handling of thinner c-Si wafers• Improvement of light trapping properties• Good surface passivation of front and rear side• Avoidance of wafer bow• Development of metal pastes for thin c-Si wafers
Trend II: Alternative c-Si feedstock
<ul style="list-style-type: none">• Production of high electronic quality c-Si• New feedstock technologies• Alternative solar cell designs when using <i>n</i>-type c-Si
Trend III: Higher conversion efficiencies
<ul style="list-style-type: none">• Improvement of light trapping properties• Reduction of losses in emitter region• Improvement of c-Si bulk lifetime• Improved surface passivation of front and rear side• Alternative solar cell designs (e.g. back contact or heterojunction concept)• Reduction losses due to the front and rear side electrical contacts (e.g. shading and electrical losses)• Photon up- and down-conversion

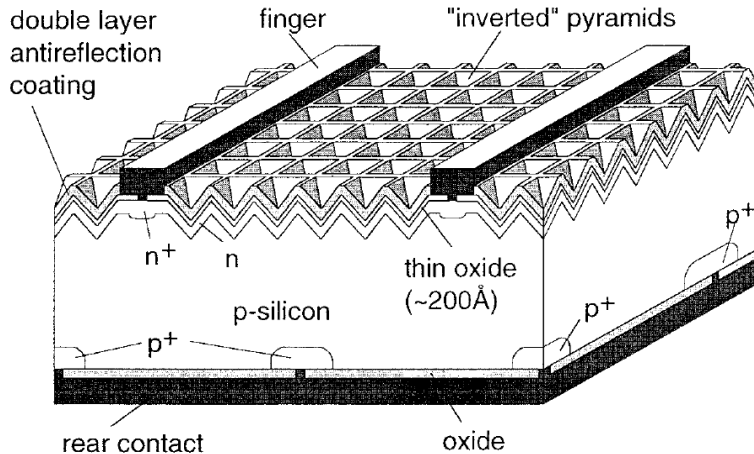


Figure 5: Schematic illustration of the world record Passivated Emitter Rear Locally diffused (PERL) c-Si solar cell structure developed at the University of New South Wales.⁹

and electrical requirements when the solar cell thickness is further reduced. Moreover, the significant difference in the thermal expansion coefficient of Al and Si even results in an unacceptable wafer bow. Therefore it is expected that the reduction of the c-Si solar cell thickness could lead to an (inevitable) replacement of the Al-BSF for an alternative technology in the near future.

A dedicated low-cost feedstock production for c-Si PV will most probably lead to c-Si with a higher impurity (e.g. metallic) content, which leads to higher electronic recombination losses in the bulk of c-Si. It is therefore desired that the bulk recombination activity is further reduced in the solar cell manufacturing process. Fortunately, several impurities can effectively be gettered from c-Si in the P-diffusion process during emitter formation in c-Si solar cell production.²⁵ Moreover, some bulk c-Si defects can also be neutralized by atomic H supplied during the c-Si solar cell production process. As mentioned, a dedicated c-Si production could also result in a shift to *n*-type c-Si base material instead of the current industry standard *p*-type c-Si. Both formation and passivation of a *p*⁺-type emitter are currently still technologically challenging. For this reason alternative solar cell designs based on *n*-type c-Si are heavily investigated as well. A notable example in this respect is the HIT (heterojunction with intrinsic thin film) solar cell design of Sanyo, which is elaborated further in Section III (c).²⁰

Technological requirements for increasing the c-Si solar cell efficiency are mainly based on an optimal usage of solar irradiation and on reducing electronic losses in solar cells. In Fig. 5 the world-record PERL c-Si solar cell is shown which nicely illustrates several technologies that can be used to maximize the solar cell efficiency.⁹ Optimal usage of incoming solar irradiation is guaranteed by a double layer antireflection coating, a pyramid surface texture at the front of the solar cell, and a SiO₂ reflector at the rear side

of the c-Si solar cell. The lightly P-doped front and the undiffused rear surface are passivated by thermal SiO₂. The bulk lifetime is maximized by the usage of relatively high resistivity float zone *p*-type c-Si. The metal contact fingers at the front side are optimized for an optimal electrical performance by a local heavy P-diffusion with a minimal surface coverage to minimize shading. The electrical contact at the rear side of the solar cell is optimized by a local heavy B-diffusion. It should be noted that the focus in the PERL solar cell was not on a cost-effective optimization of the solar cell efficiency. Similar, but more cost-effective, methods to optimize the solar cell efficiency are employed in innovative solar cell designs such as the emitter wrap through technology of Advent Solar and the back-contact solar cell design of SunPower.^{24,26}

More fundamental methods to increase the c-Si solar cell efficiency are photon up- and down-conversion.^{27,28} It is well known that the quantum efficiency (QE)^d of c-Si solar cells is not constant over the solar spectrum. Photons with an energy below the c-Si bandgap (1.12 eV) have an QE of zero, and even photons with an energy above the c-Si bandgap can have an QE less than unity. For example photons with a wavelength < 400 nm typically have an QE less than unity in industrial c-Si solar cells. In down-conversion process a high energy photon is transferred into one (photoluminescence), or preferentially two or more, photon(s) with a lower energy where the QE of the solar cell is higher. In the process of up-conversion two sub-bandgap photons are transferred into one photon with an energy above the c-Si bandgap. Both processes can, at least in theory, significantly improve the number of photo-generated electron-hole pairs, hence, increase the solar cell efficiency.^{27,28}

Some of the technological requirements summarized in Table I can be fulfilled by the application of functional thin films in c-Si solar cells, as will be discussed in detail in Section II. In this Ph.D. research work several of these functional thin films have been investigated that can fulfill at least one of the requirements summarized in Table I. The main focus has, however, been on thin films that can provide a good level of surface passivation on c-Si.

D. Framework and outline of this thesis

D.1 The EET-HRCEL project (Chapters 1 to 3)

The work described in this thesis was carried out in the Plasma & Materials Processing (PMP) group at the Eindhoven University of Technology. The PMP group has a strong background in fundamental plasma physics and chemistry and, in the last 15 years, in the field of thin film deposition. In the late 1980s the expanding thermal plasma (ETP) technique was developed and patented by the PMP group.^{29,30} The ETP technique,

^dThe quantum efficiency gives the ratio between the number of charge carriers collected by the solar cell to the number of photons of a given energy incident on the solar cell.

of which the operating principle is discussed in more detail in Frame I, is capable of high-rate deposition of various thin films including amorphous silicon (a-Si:H),³¹ silicon oxide (a-SiO_x),³² and silicon nitride (a-SiN_x:H).³³ The ETP technique is licensed and commercialized by OTB Solar. They employ the ETP technique in their DEP_x system for the deposition of a-SiN_x:H antireflection coatings.³⁴ Shortly after the market introduction of the DEP_x system in 2001, OTB Solar and the Eindhoven University of Technology started a joint project entitled “EET-HRCEL”. This project was funded by the Netherlands Ministry of Economic Affairs, the Ministry of Education, Culture and Science and the Ministry of Public Housing, Spatial Planning and the Environment.³⁵ The aim of the EET-HRCEL was to develop and optimize technologies that could be used for the production of high-efficiency c-Si solar cells.

Before the start of the EET-HRCEL project, the PMP group had already done a significant amount of work on a-SiN_x:H deposition by the ETP technique for c-Si solar cell applications. This work is reviewed in Chapter 2 of this thesis. Research on a-SiN_x:H deposition within the EET-HRCEL project was mainly focused on plasma chemistry and on optimization of the material properties of a-SiN_x:H films, deposited by the ETP technique. The plasma chemistry during a-SiN_x:H deposition was studied in detail in the Ph.D. research of Van den Oever.³⁶⁻³⁹ The reactive species emanating from the ETP plasma source operating on an Ar/NH₃ mixture were studied by a combination of advanced diagnostics. The absolute densities of the main radicals such as N, NH and NH₂ were determined by cavity ring-down absorption spectroscopy and mass spectrometry, whereas the ion densities were determined by Langmuir probe and mass spectroscopy.^{38,39} By similar studies on the influence of SiH₄ addition to the Ar-NH₃ plasma the a-SiN_x:H growth mechanism could be unraveled in significant detail. It was demonstrated that N and NH₂ radicals govern the N incorporation in the a-SiN_x:H film, while SiH_x ($x=0-3$) radicals determine the Si incorporation in the a-SiN_x:H film.³⁷ A fundamental insight in the a-SiN_x:H growth mechanism is not only interesting from an academic point of view but is in the long term also indispensable for the optimization of the a-SiN_x:H deposition process.

The second part of the EET-HRCEL project is described in Chapters 1 to 3 of this thesis. This part of the project focused on the functional properties of thin films for application in c-Si solar cells. As summarized in Table II, a-SiN_x:H, a-SiO₂ and a-Si:H deposited at high-rate (>1 nm/s) by the ETP technique were investigated as functional thin film for c-Si solar cells. Significant progress has been made in the level of bulk and surface passivation provided by ETP-deposited a-SiN_x:H films and simultaneously absorption in the a-SiN_x:H films was further reduced to improve its performance as antireflection coating.

Unfortunately a-SiN_x:H does not exhibit ideal properties for application at the rear side of *p*-type c-Si solar cells (see Section III (b) for more detail). Moreover, its level of surface passivation on a *p*-type emitter is inadequate.⁴⁰ For this reason a-SiO₂ and a-Si:H

deposited by the ETP technique were also studied in this Ph.D. research. A-SiO₂ is a good candidate to increase the rear surface reflection in c-Si solar cells, and can simultaneously reduce the electrical losses at the rear surface of solar cells (see Section II). A-Si:H is an excellent material to reduce the electrical losses at the c-Si surface of an arbitrary doping level, and hence, could be an interesting option for the passivation of *p*-type emitters. It was demonstrated that both a-SiO₂ and a-Si:H can be deposited at high-rates (>1 nm/s) by the ETP technique. Moreover, their deposition processes are compatible with the DEP_x system of OTB Solar. Consequently these experiments could serve as proof-of-principle for the industrial application of a-SiO₂ and a-Si:H in c-Si solar cells manufacturing. The a-SiO₂ process developed in this work was filed in a joint patent application by OTB Solar.⁴¹

D.2 *Al₂O₃ grown by atomic layer deposition (Chapters 4 to 8)*

In 2003 the PMP group started a new project funded by “Stichting voor de Technische Wetenschappen (STW)” on atomic layer deposition (ALD) entitled “Plasma-assisted atomic layer deposition for processing at the nano-scale”.⁴² ALD is a relatively new chemical vapor deposition (CVD) technique that is capable of depositing conformal and uniform thin films with monolayer growth control. One of the topics investigated in the project was plasma-assisted ALD of Al₂O₃ (see Frame 2). The first Al₂O₃ experiments for application for c-Si solar cells were conducted on a home-built lab-type ALD reactor (ALD-I). These experiments revealed that Al₂O₃ deposited by plasma-assisted ALD showed an excellent level of surface passivation on low resistivity *p*- and *n*-type c-Si (see Chapter 4).

In 2006 a beta version of the FlexAL reactor of Oxford Instruments (developed with contributions of our group) was installed in the cleanroom of the Eindhoven University of Technology. This commercial reactor is equipped for both thermal and plasma-assisted ALD processes. The level of surface passivation by the Al₂O₃ films deposited by plasma-assisted ALD at the commercial reactor was comparable to the results obtained on the lab-scale reactor, indicating the robustness of the plasma-assisted ALD Al₂O₃ process. The excellent level of surface passivation provided by plasma-assisted ALD Al₂O₃ as determined by in-house photoconductance was confirmed by techniques based on infrared absorption and photoluminescence in collaboration with ISFH in Germany and the University of New South Wales in Australia. Moreover, the level of c-Si surface passivation by Al₂O₃ deposited by thermal and plasma-assisted ALD could be compared at the FlexAL system. These experiments are described in Chapter 5 of this thesis.

In collaboration with the solar cell institute ISFH in Germany the performance of Al₂O₃ on *p*-type emitters and on the rear side of *p*-type c-Si solar cells was investigated as well. Al₂O₃ appeared to be a very promising new candidate for the passivation of *p*-type

emitters (see Chapter 6). Moreover, solar cells with a rear side Al_2O_3 passivation and a capping SiO_x film demonstrated a conversion efficiency of 20.6 % which was independently confirmed at Fraunhofer ISE in Germany (see Chapter 8).

D.3 Outline of this thesis

Most of the results of this Ph.D. research have been published in separate papers in peer-reviewed journals. These papers constitute Chapters 2 to 8 of this thesis. In Table II the topics addressed in Chapter 2 to 8 are summarized. The results obtained in Chapters 2 to 8 will be put into a broader perspective in Section III of this Introduction. Section III(c) will go into more detail on the results obtained with a-Si:H, as these results are not included in a separate chapter of this thesis. The results obtained for ETP deposited a-Si:H have been presented at two international conferences,^{43,44} and the results obtained for hot-wire chemical vapor (HWCVD) deposited a-Si:H will be published in detail by Gielis *et al.*⁴⁵

Table II: Summary of the materials investigated in this Ph.D. research with their functionality for c-Si solar cells.

Functional thin film	Deposition technique	Investigated topic	Chapter
a-Si:H	ETP HWCVD	Surface passivation of <i>n</i> - and <i>p</i> -type c-Si	1.III (c)
a-SiN _x :H	ETP	Antireflection performance	2
		Bulk passivation of mc-Si	
		<i>N</i> -type emitter passivation	
		Surface passivation of <i>p</i> -type c-Si	
a-SiO ₂	ETP	Surface passivation of <i>n</i> -type c-Si	3
		Rear surface reflection	
Al ₂ O ₃	ALD	Surface passivation of lightly doped <i>n</i> - and <i>p</i> -type c-Si	4,5
		Passivation of highly doped <i>p</i> -type c-Si ^a	5,6
		The c-Si surface passivation mechanism	7
		Application at rear side of <i>p</i> -type c-Si solar cells ^b	8

^a The surface passivation by Al₂O₃ on highly B-doped c-Si was compared experimentally to the level of surface passivation obtained by thermal SiO₂, as-deposited a-SiN_x:H and a-Si:H.

^b The performance of a *p*-type c-Si with an Al₂O₃ rear side passivation was directly compared to a reference solar cells with a state-of-the-art thermal SiO₂ rear side passivation.

FRAME 1: High-rate deposition by the ETP technique.

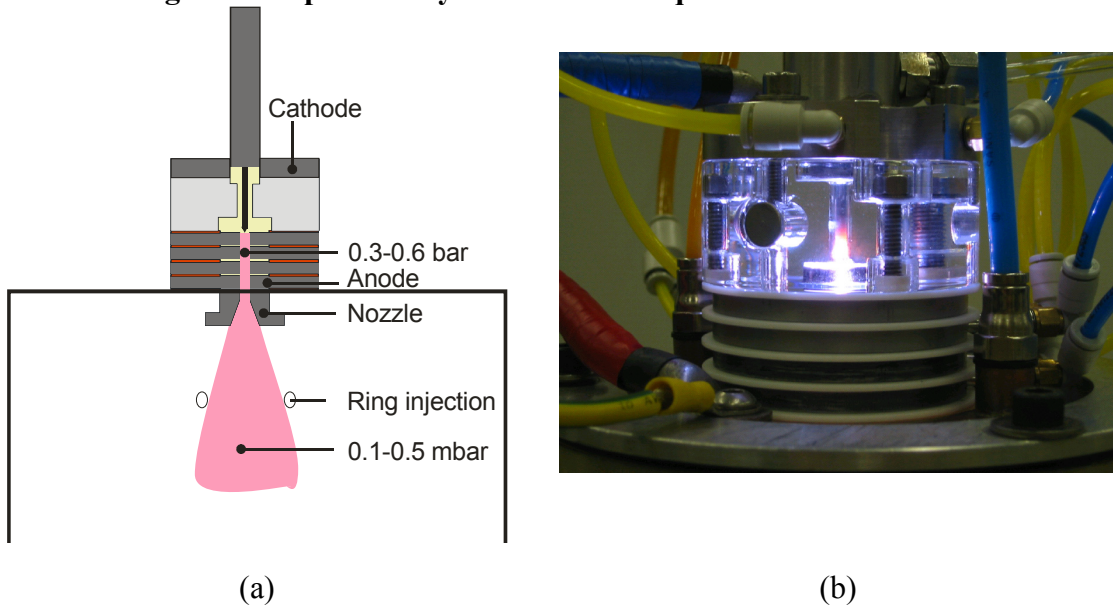


Figure 6: (a) Schematic illustration of the ETP plasma source used for the high-rate deposition of silicon nitride, silicon dioxide and amorphous silicon in this thesis. (b) The commercial cascaded arc source during the deposition of silicon nitride on the DEPx system developed by OTB Solar.³⁴

The expanding thermal plasma (ETP) technique is based on the geometric separation between plasma creation and deposition (i.e. a remote configuration). This allows separate optimization of the plasma creation and the deposition zone. As depicted schematically in Fig. 6 a thermal plasma is created at subatmospheric pressures by drawing a DC current (typically 45-75 A) through a narrow channel (typically 2-4 mm in diameter and a few cm in length) in which a gas is confined at relatively high pressures (0.3-0.6 bar). The thermal plasma subsequently supersonically expands into the reactor that is kept at low pressures (0.1-0.5 mbar) by means of roots pumping ($\sim 1500 \text{ m}^3/\text{hour}$). For the deposition of most materials the ETP source is operated on inert gas Ar. Up to 10-15 % of the Ar atoms are ionized in the ETP source and these Ar^+ ions are the foundation for the downstream precursor chemistry. This high density of reactive species allows high processing rates e.g. for thin film deposition or etching. The deposition precursor gasses (e.g. NH_3 and SiH_4 for a- $\text{SiN}_x\text{:H}$ deposition) are injected in the reactor by means of nozzle or ring injection, and react with the reactive species in the expanding plasma. The ETP technique has already been used for high-rate deposition of materials such as amorphous and microcrystalline silicon,^{31,46} amorphous and diamond-like carbon,^{47,48} aluminum doped zinc-oxide,⁴⁹ amorphous silicon nitride³³ and silicon-dioxide-like films.^{32,50}

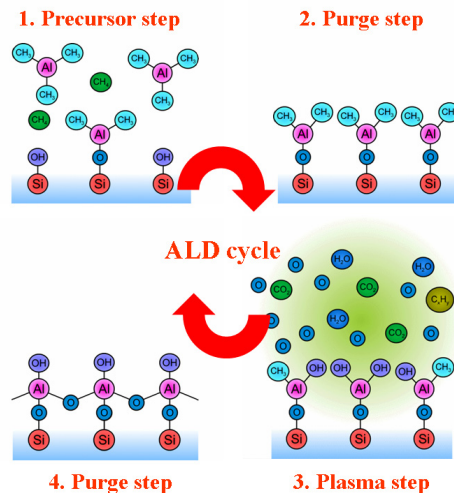
FRAME 2: Atomic layer deposition of Al₂O₃


Figure 7: Schematic representation of a plasma-assisted ALD cycle during the deposition of Al₂O₃. By alternating Al(CH₃)₃ dosing and an O₂ plasma exposure an Al₂O₃ film can be deposited with monolayer control.

Atomic layer deposition (ALD) is a chemical vapor deposition (CVD) method in which the deposition process is split up into two self limiting half-reactions. In the ALD deposition of Al₂O₃ the two half reactions consist of an Al(CH₃)₃ dosing and an oxidation step. Between the two self-limiting steps the reactor is purged and/or pumped down to remove the reactant and the reaction products from the ALD reactor. In Fig. 7 a schematic representation of a cycle for deposition of Al₂O₃ by plasma assisted ALD is shown. Starting from a c-Si surface the Al(CH₃)₃ is chemisorbed on the surface by splitting off volatile CH₄ and the surface is covered by Al(CH₃)_{3-n} groups. The excess Al(CH₃)₃ is subsequently removed from the reactor and an O₂ plasma is ignited. The O radicals from the plasma remove CH₃ ligands from the Al(CH₃)_{3-n} surface in a combustion like process, and an OH terminated surface is generated.⁵¹ Each ALD cycle one (sub)monolayer of Al₂O₃ is deposited. By repeating this ALD cycle multiple times, ultrathin films can be deposited with precise thickness control and high uniformity over large substrates. Due to the intrinsic self limiting nature of the ALD process even complex 3D structures can be conformally deposited and large scale uniformity is easily assured.

II. Physical principles of the electrical and optical improvement of c-Si solar cells by functional thin films

Functional thin films can be used to improve the electronic and optical quality at the front and the rear side of c-Si solar cells. In this Section we will briefly discuss the physical background of these improvements. The main focus in this Ph.D. research has been on the improvement of the electrical quality of the c-Si surface (i.e. surface passivation). Therefore this topic will be discussed in most detail.

A. Improving the optical quality at the front and the rear side of solar cells

In order to achieve an optimal conversion efficiency of c-Si solar cells a maximum amount of solar irradiation should be used to generate electron-hole pairs. Functional thin films can play an important role in reducing reflection losses at the front of solar cells and in improving light trapping properties of c-Si solar cells, for example by increasing reflection at the rear side. In combination with surface texturing techniques, such as the inverted pyramid structure in the PERL solar cell shown in Fig. 5, an optimal percentage of usable solar irradiation can be used for current generation in c-Si solar cells.

A.1 Reducing reflection losses at the front of solar cells by an antireflection coating

As shown in Fig. 8 a polished c-Si wafer reflects over 30 % of the light in the 300-1200 nm wavelength range. These reflection losses can significantly be reduced by application of a so-called antireflection coating (ARC). The working principle of an ARC is based on interference of solar light in a thin film on top of c-Si. From Fresnel's equations it can be calculated that minimum reflection under normal incidence from a single layer ARC is achieved when the refractive index of the ARC is equal to:⁵²

$$n_{ARC} = \sqrt{n_s n_0} , \quad (1)$$

with n_s and n_0 the refractive index of the substrate and of the surrounding medium respectively. In case of a single layer ARC on c-Si in air, Eq. 1 results in an ideal layer with a refractive index of $n=1.9$.^e The optical thickness of the single layer ARC should be equal to a quarter of the desired wavelength with minimum reflection. As shown in Fig. 8(a) a 80 nm thick a-SiN_x:H film with a refractive index of 1.9 indeed significantly reduces reflection losses compared to polished c-Si. Reflection is approximately

^e The refractive index of the materials is given at a photon energy of 2 eV throughout this section unless specified otherwise.

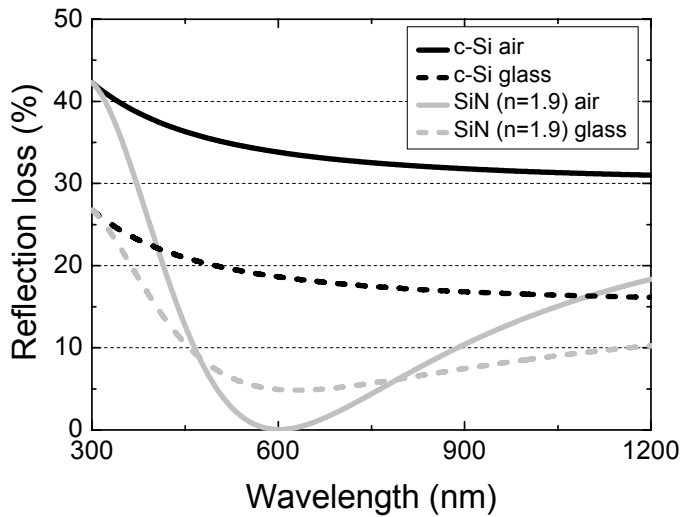


Figure 8: Reflection losses of a polished c-Si wafer with and without an ARC as a function of the wavelength. An a-SiN_x:H film with a refractive index of 1.9 is an excellent ARC when air is the surrounding medium. However, when applied in a solar cell module, the refractive index of the ARC should be higher to achieve minimum reflection losses.

zero for a photon wavelength of around 600 nm. This minimum coincides with the maximum photon count of the AM1.5 solar spectrum.

When a solar cell is placed in a module, the ideal refractive index of the single layer ARC increases up to 2.4 as the refractive index of the surrounding medium increases to $n_0=1.5$.⁵³ From Fig. 8 it can be seen that a single a-SiN_x:H film with refractive index of 1.9 would indeed not be a favorable ARC when a solar cell is placed in a module. It should, however, be noted that a-SiN_x:H with a refractive index > 2.0 has a significant absorption in the ultraviolet part of the solar spectrum due to band tail broadening. Hence, absorption losses in the ARC should be taken into account when choosing the optimum refractive index of the ARC.⁵³

A.2 Maximizing the internal reflection at the rear side of c-Si solar cells

Due to the ongoing reduction of the c-Si solar cell thickness the amount of usable light reaching the rear side of c-Si solar cells without being absorbed is increasing. From Fig. 9 (a) it can be seen that over 40 % of the > 1000 nm light is reaching the rear side of a 100 μm thick c-Si wafer under normal incidence. High reflection at the rear side of c-Si solar cells is therefore essential to make optimum usage of solar irradiation

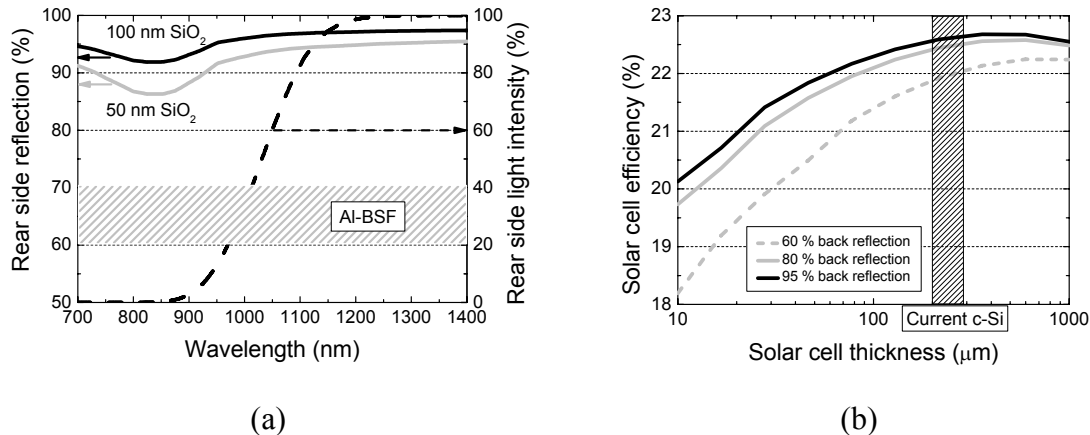


Figure 9: (a) Simulated rear reflection (left axes) as a function of the photon wavelength for c-Si solar cells with a conventional Al-BSF or a 50 and 100 nm SiO₂ film covered with Al. The dotted line indicates the amount of light (right axes) that is not absorbed in a single pass through a 100 μm thick intrinsic c-Si wafer. (b) The c-Si solar cell efficiency as a function of the solar cell thickness is shown for a 60, 80 and 95 % specular internal rear side reflection. Reflection and absorption spectra were obtained by model calculations in the software package WVASE supplied by J.A. Woollam.⁵⁴ Solar cell simulations were performed with the software package PC1D^f developed by the University of New South Wales.⁵⁵

and, hence, maximize the c-Si solar cell efficiency. The industry standard Al back contact only reflects ~60-70 % of the light as has been determined from direct measurements and from device performance.^{56,57} This low reflection is not attributed to the intrinsic poor reflectance of an Al film on c-Si, but is most probably related to parasitic absorption in the Al-Si intermixing region. Figure 9 clearly shows that reflection at the rear side has a significant impact on the efficiency of c-Si solar cells, even for the c-Si wafer thicknesses that are currently used in industry. For a 50 μm thick c-Si solar cell absolute solar cell efficiencies can even increase by 1.3 % when rear side reflection is increased from 65 % to 95 %.

Rear side reflection can be improved by application of a thin dielectric film between the c-Si and the Al back contact. In Fig. 9 (a) it is shown that rear side reflection of > 90 % can be obtained in the 700-1200 nm wavelength range by application of 50 or

^f In the PC1D simulations a high-efficiency c-Si solar cell design is used as basis throughout Section II. The base material of the solar cell is 1 Ω cm *p*-type c-Si with a bulk lifetime of 1.2 ms. The front of the solar cell consists of an high-efficiency emitter with a sheet resistance of 95 Ω/sq. passivated by a transparent film with a surface recombination velocity of 3×10^3 cm/s. The front surface is textured and has a wavelength independent reflection loss of 2 %. The rear side surface is characterized by a surface recombination velocity of 100 cm/s and an internal reflectance of 90 % unless indicated otherwise.

100 nm SiO₂ at the rear side of c-Si solar cells. In the study of Glunz *et al.* a rear surface reflection of 90 % has already been confirmed in the device performance of high-efficiency solar cells.⁵⁶

Apart from a low rear side reflection the Al-BSF has another more practical problem. Due to the significant difference in the thermal expansion coefficients of Al and Si the wafer experiences a bow after the co-firing process.^{g,58} This wafer bow is especially apparent for c-Si wafers with a thickness < 200 µm, which are currently used by various c-Si solar cell manufactures, and this severely troubles subsequent module fabrication. As a consequence it is expected that the Al-BSF has to be replaced in the near future.

B. Reducing recombination losses in the bulk and on the front and rear side of c-Si solar cells

After the photo-generation of an electron-hole pair, the charge carriers have to be collected at the front and the rear side of the solar cell. The *p-n* junction, typically at the front side of the solar cell, separates the photo-generated electron-hole pair and collects either the electron (for a diffused emitter *p*-type c-Si solar cell as shown in Fig. 5) or the hole (for a diffused emitter *n*-type c-Si solar cell). The remaining hole or electron has to reach to the rear side of the solar cell to be collected. Consequently the diffusion length, which is dependent on both the diffusion coefficient and the charge carrier lifetime, has a significant impact on the final solar cell efficiency. The charge carrier lifetime in c-Si is determined by recombination losses in the c-Si bulk and at the front and rear side surface. Both bulk and surface recombination losses can be reduced by the application of functional thin films.

B.1 Recombination in the bulk of c-Si

Recombination in the bulk of c-Si is determined by both *intrinsic* and *extrinsic* processes. Two *intrinsic*, hence unavoidable, recombination processes in the c-Si bulk are radiative recombination and Auger recombination as schematically depicted in Fig. 10. Radiative recombination in c-Si is a process with a relative low probability due to the indirect band gap of c-Si. Its probability is directly proportional with the product of the

^g The front and rear side electrical contacts of the c-Si solar cell are generally applied by screen-printing. At the front of a c-Si solar cell the contact grid is printed using an Ag containing paste. At the rear side of the solar cell a full coverage Al paste is applied. After printing and drying of the paste a high-temperature co-firing step (typically ~900 °C for a few seconds) is required to make electrical contact through the dielectric antireflection coating at the front of the solar cell (i.e. contact fire-through process). Moreover, the Al-back surface field at the rear side of the c-Si solar cell is also formed in this co-firing process as the *p*-dopant Al diffuses into the c-Si.

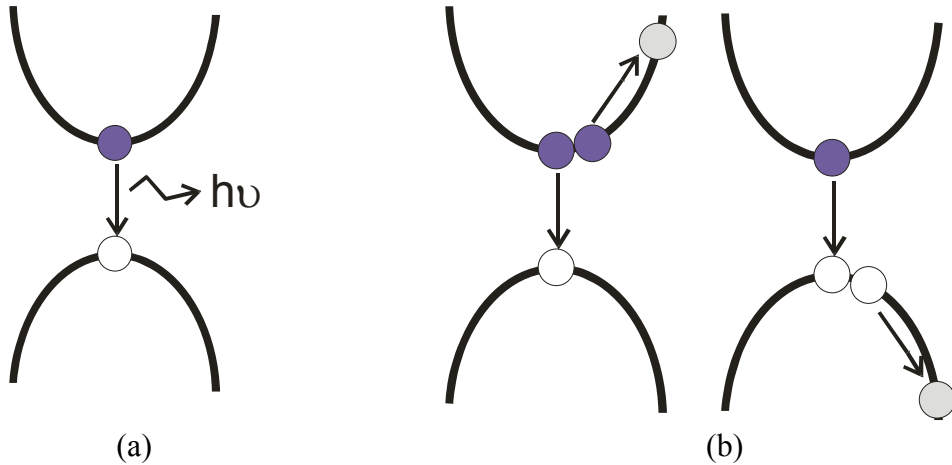


Figure 10: Schematic representation of intrinsic (a) radiative and (b) Auger recombination in the c-Si bulk. In radiative recombination the excess energy is transferred to an emitted photon and in Auger recombination to an excess electron or hole.

electron and the hole density. Although radiative recombination in c-Si is normally of minor importance for solar cell application it is the driving mechanism for light emitting diodes devices based on c-Si.⁵⁹ Auger recombination is normally the dominant intrinsic bulk recombination mechanism in c-Si solar cells. In this process an electron and a hole recombine in a three-particle process where momentum and energy conservation are assured by a third particle (either a hole or an electron). The probability of Auger

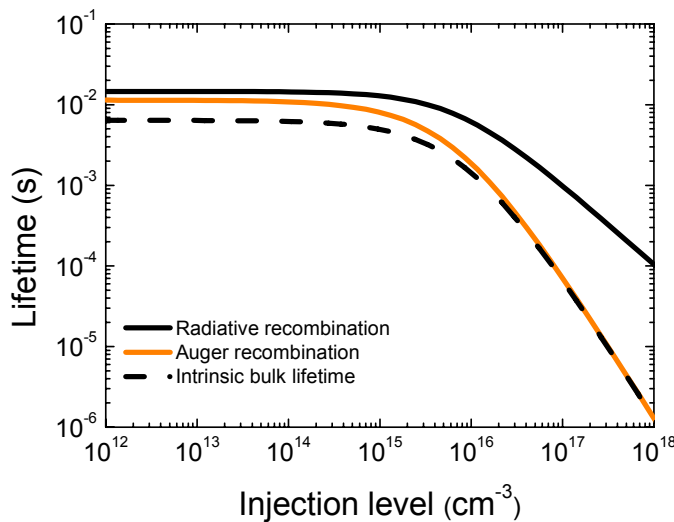


Figure 11: Injection level dependent lifetime determined by Auger and radiative recombination in the bulk of a 2.0 Ω cm p-type c-Si wafer.⁶⁰ The intrinsic bulk lifetime is than determined by the sum of Auger and radiative recombination.

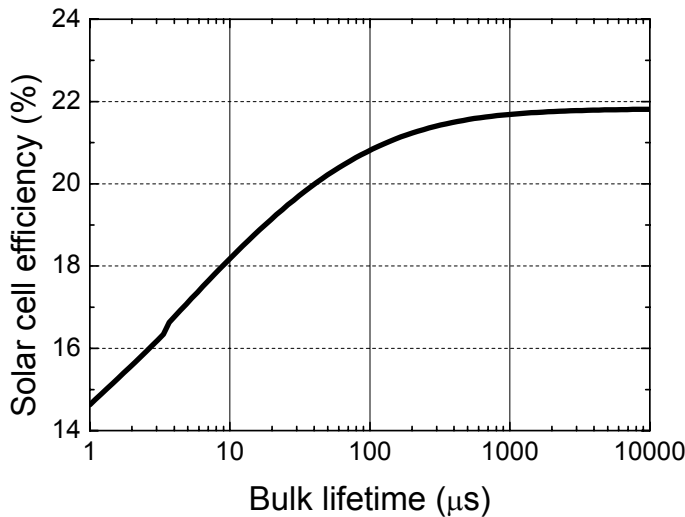


Figure 12: Simulated solar cell conversion efficiency for a 150 μm thick high-efficiency solar cell as a function of the effective bulk lifetime of charge carriers. The simulations were performed in the software package PC1D.⁵⁵

recombination therefore strongly depends on carrier concentration. Auger recombination is the dominant bulk loss mechanism in highly doped c-Si (e.g. as used in an emitter) and in concentrator solar cells. Both Auger recombination and radiative recombination are dependent on the c-Si doping level and charge carrier density.^{60,61} In Fig. 11 the bulk lifetime determined by Auger and radiative recombination are shown for a 2.0 $\Omega \text{ cm}$ *p*-type c-Si wafer as a function of the excess carrier density Δn (injection level). As expected the radiative lifetime shows a $1/\Delta n$ scaling and Auger recombination shows the $\sim 1/\Delta n^2$ scaling for high injection level. It can be seen that Auger recombination is even the dominant process for a moderately doped c-Si wafer, and that the intrinsic bulk lifetime due to Auger and radiative recombination is 6.4 ms at low injection level for a 2.0 $\Omega \text{ cm}$ *p*-type c-Si wafer.

The dominant bulk recombination mechanism for most c-Si wafers is, however, the *extrinsic* recombination via defect states, e.g. due to metallic impurities and Si dangling-bonds in the c-Si band gap. The bulk defect density is for example relatively high in multicrystalline (mc)-Si. Wafers of mc-Si consist of several large-grain (1-10 mm) crystals instead of one single crystal as in the case of c-Si grown by the float zone method. The mc-Si growth procedure is significantly faster compared to the float zone process and consequently the wafer production cost is lower.

The bulk recombination process was already described by Shockley, Read and Hall (SRH) in the 1950s.^{62,63} In recent years the recombination activity of various

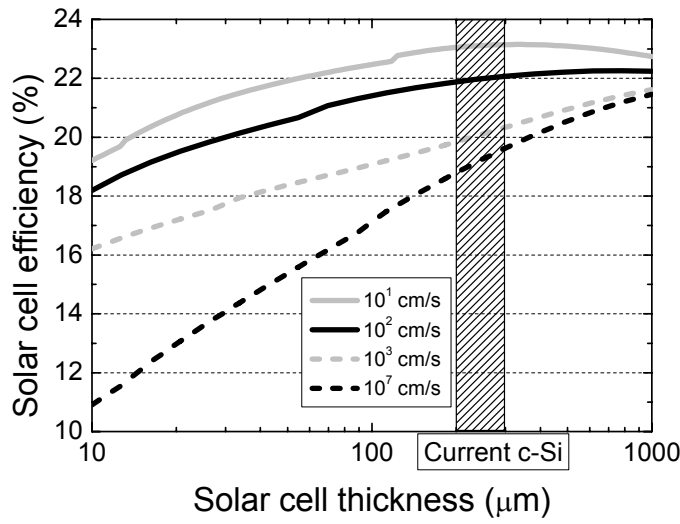


Figure 13: Simulated efficiency for a high-efficiency c-Si solar cell as a function of the solar cell thickness with an excellent rear side surface passivation (S_{eff} of 100 cm/s or less), industry standard rear side surface passivation (S_{eff} of 1000 cm/s) or no rear side surface passivation (S_{eff} of 10^7 cm/s). Simulations were performed in the software package PC1D.⁵⁵

metallic impurities such as Fe, Cr and Zn in the c-Si bulk has been investigated.⁶⁴ Moreover, the mechanism for the light induced degradation of c-Si solar cells based on Czochralski (Cz) grown *p*-type silicon has been attributed to the formation of recombination active B-O complexes in the bulk of the c-Si.⁶⁵

The impact of the bulk carrier lifetime on the c-Si solar cell conversion efficiency is shown in Fig. 12. It can be clearly seen that high bulk carrier lifetimes, and resulting bulk diffusion lengths, are prerequisite for high-efficiency c-Si solar cells. The typical bulk carrier lifetime of a mc-Si wafer is, however, typically $\sim 10 \mu\text{s}$.⁶⁶ Fortunately the bulk carrier lifetime can significantly be improved in the solar cell production process. During emitter formation significant amounts of recombination active impurities are gettered from the c-Si wafer and, consequently, the bulk lifetime can increase by more than one order of magnitude.^{25,66} Moreover some bulk defects can be passivated by atomic H e.g. supplied by a functional thin film such as a-SiN_x:H and released into mc-Si during the contact firing step.⁶⁷

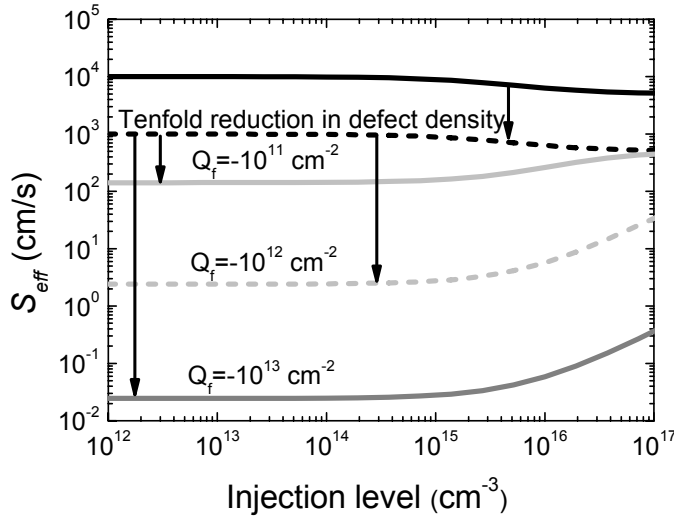


Figure 14: Injection level dependence of S_{eff} of a $2.0 \Omega \text{ cm}$ *p*-type c-Si wafer for various the fixed charge densities Q_f and interface defect densities. The simulations were performed in the lifetime simulation package developed by Martin and Garin.⁶⁸

B.2 Recombination at the c-Si surfaces

The surface of c-Si can be considered as a severe interruption from its crystallographic structure. A high amount of defect states are therefore present in the c-Si bandgap due to the presence of this surface. Recombination at a c-Si surface can be described similar as bulk SRH recombination, and is quantified by the so-called effective surface recombination velocity S_{eff} . As shown in Fig. 13 surface recombination on the rear side of a c-Si solar cell has a tremendous impact on the solar cell efficiency, especially when the solar cell thickness is further reduced from its present value of $\sim 200 \mu\text{m}$. The current industry standard Al-BSF only has a S_{eff} of $\sim 1000 \text{ cm/s}$ and it can be seen that by lowering this value to $10-100 \text{ cm/s}$ a significant gain in the solar cell conversion efficiency can be obtained. These values can actually be obtained in real c-Si solar cells as demonstrated by Glunz *et al.*⁵⁶

Recombination losses at semiconductor interfaces can be reduced by two different strategies. As the recombination rate is directly proportional to the interface defect density the first strategy is based on the reduction of the number of defects at the interface. The interface defect density can significantly be reduced by, for example, H passivation or the application of a functional thin film. The mid-gap interface defect density of c-Si can, for example, be as low as $1 \times 10^9 \text{ eV}^{-1} \text{ cm}^{-2}$ by growing a high quality thermal SiO₂ film, followed by an anneal in a H₂ containing gas (i.e. a forming gas anneal).⁶⁹ This strategy is illustrated in Fig. 14. The impact on S_{eff} of a tenfold reduction

in the interface defect density is shown, thereby assuming equal electron and hole capture cross-sections. The tenfold reduction in interface defect density results in a tenfold reduction in S_{eff} .

Apart from the amount of defects, the SRH recombination activity at the c-Si surface also depends on the electron and hole capture cross section of the dominant defect and the the electron and hole concentration at the c-Si surface. A maximum in surface recombination is obtained when:⁷⁰

$$n_s / p_s \approx \sigma_p / \sigma_n, \quad (2)$$

where n_s and p_s are the surface electron and hole density and σ_p and σ_n are the hole and electron capture cross section of the dominant surface defect, respectively. It was, for example, shown that for thermal SiO₂ on c-Si the hole capture cross section of the dominant defect is 1000 times smaller than the electron capture cross section and this partly explains the fact that especially *n*-type c-Si is effectively passivated by thermal SiO₂.⁷¹ If Eq. 2 is not met, the surface recombination rate $R_{surface}$ is limited by the capture of either electron or holes:

$$R_{surface} \sim n_s \text{ if } n_s \sigma_n < p_s \sigma_p, \quad (3)$$

$$R_{surface} \sim p_s \text{ if } n_s \sigma_n > p_s \sigma_p. \quad (4)$$

The second surface passivation strategy is therefore based on a significant reduction of the surface electron or hole concentration by an internal electric field below the interface. This internal electric field can be obtained by the application of a doping profile below the interface or by the presence of electrical charges at the semiconductor interface. This strategy is illustrated in Fig. 14 by showing the impact of a negative fixed charge density at the *p*-type c-Si surface on S_{eff} . By the negative fixed charge density at the c-Si the minority electron concentration is significantly reduced by electrostatical shielding, and S_{eff} decreases accordingly. A negative fixed charge density of 10¹³ cm⁻², which is within the range that can be reached in functional thin films, reduces S_{eff} over four orders of magnitude.

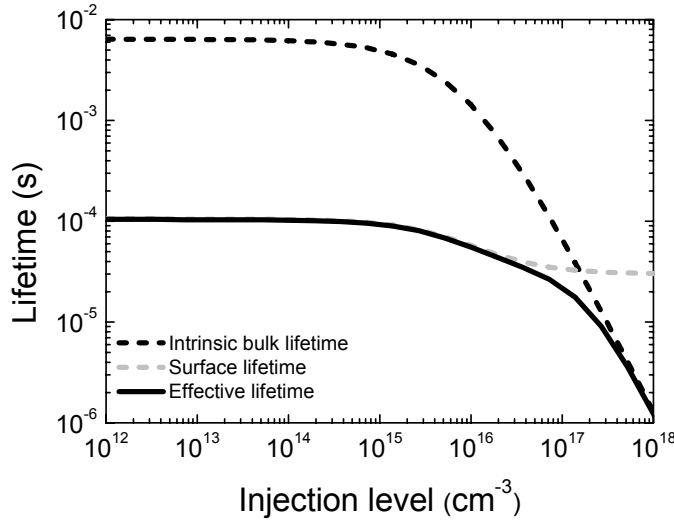


Figure 15: Effective lifetime of a $2.0 \Omega \text{ cm}$ *p*-type c-Si wafer with a thickness of $300 \mu\text{m}$ assuming only intrinsic recombination in the bulk and an identical surface passivation at both sides of the wafer. The S_{eff} values are taken from Fig. 14 assuming a negative fixed charge density of $1 \times 10^{11} \text{ cm}^{-2}$.

B.3 The effective lifetime of c-Si

The combined losses in the c-Si bulk and at the c-Si surfaces result in a so-called effective lifetime τ_{eff} of the minority charge carriers in a c-Si wafer which can be experimentally measured. In first approximation τ_{eff} of a symmetrically passivated c-Si wafer can be written as:⁷²

$$\frac{1}{\tau_{\text{eff}}} = \frac{1}{\tau_{\text{bulk}}} + \frac{1}{\tau_{\text{surface}}} = \frac{1}{\tau_{\text{bulk}}} + 2 \frac{S_{\text{eff}}}{d}, \quad (5)$$

with τ_{bulk} the bulk lifetime, τ_{surface} the surface lifetime, d the c-Si wafer thickness and S_{eff} the effective surface recombination velocity. By using c-Si grown by the float zone process, c-Si wafers with a high bulk lifetime are commercially available and consequently $\tau_{\text{effective}}$ is normally dominated by recombination losses at the c-Si surfaces. In Fig. 15 the effective lifetime is shown for a passivated $300 \mu\text{m}$ $2.0 \Omega \text{ cm}$ *p*-type c-Si wafer. The intrinsic bulk lifetime of the c-Si wafer is rather high with a lifetime of 6.4 ms at a low injection level, but strongly decreases for higher injection level due to Auger recombination. The surface lifetime is significantly lower with a lifetime of $\sim 100 \mu\text{s}$ using the SRV values from Fig. 15 assuming a negative fixed charge density of 10^{11} cm^{-2} . The effective lifetime is consequently dominated by surface recombination for a low injection level, and by bulk recombination for a high injection level.

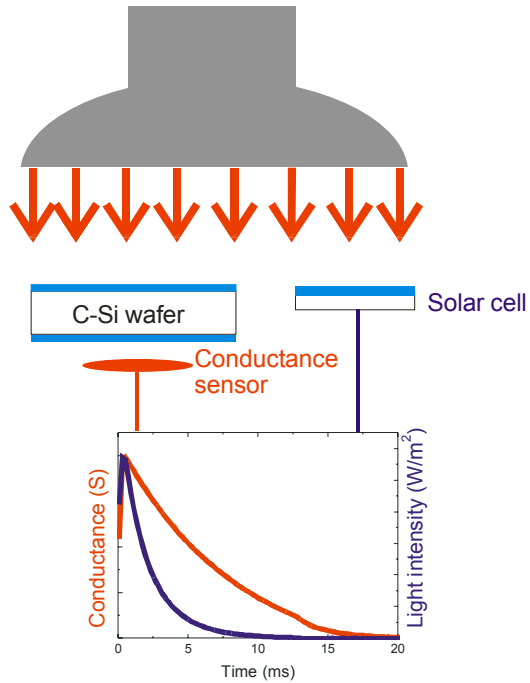


Figure 16: Schematic illustration of the principle of the photoconductance technique.⁷³ A high quality c-Si wafer is symmetrically coated by a passivating film and subsequently both wafer conductance and incident light intensity are monitored as a function of time during a short light pulse and used to extract the effective lifetime of the charge carriers in the wafer.⁷³

B.4 Determining the effective lifetime of c-Si

The standard technique to determine the effective lifetime of the charge carriers in a c-Si wafer is the photoconductance technique developed at Stanford University and commercialized by Sinton Consulting.⁷³ As schematically illustrated in Fig. 16 the conductance of a symmetrically passivated c-Si wafer is measured by an inductively coupled coil. By either a short [$\sim 15 \mu\text{s}$, photoconductance decay (PCD)] or a long [$\sim 2 \text{ ms}$, quasi-steady-state photoconductance (QSSPC)] light flash, excess electron-hole pairs are created in the c-Si wafer and as a result its conductance increases. The light has a wavelength $> 730 \text{ nm}$ (ensured by the presence of an infrared pass filter) to ensure a homogeneous carrier creation within the c-Si wafer. By simultaneously monitoring the excess conductance (i.e. photoconductance) and light intensity the effective lifetime can be determined as a function of the excess carrier density (i.e. injection level).⁷³

One major drawback of the photoconductance technique is its relatively large detection area of $\sim 6 \text{ cm}^2$, and consequently no spatially resolved information can be obtained. Recently two techniques have been developed that can provide spatially resolved lifetime information of a c-Si wafer. Infrared lifetime mapping, as developed at the Bavarian centre for Applied Energy Research in Germany, employs the free carrier

infrared absorption or emission to determine the effective lifetime under well-calibrated steady-state light illumination.^{74,75} Furthermore, photoluminescence has been applied to determine the effective lifetime of c-Si wafers.^{76,77} Photoluminescence employs the steady-state radiative recombination activity of excess carriers under steady-state light exposure to determine the effective lifetime in the c-Si wafer.⁷⁶ In addition to its unmatched measurement speed, techniques based on luminescence are not sensitive for carrier trapping and depletion region modulation and consequently the level of surface passivation can be measured for lower injection levels.^{78,79}

III. Functional thin films employed in c-Si solar cells

The first functional thin film that found widespread use in industrial solar cell manufacturing was TiO_2 , as it exhibited the ideal optical properties to serve as antireflection coating at the front of c-Si solar cells. However, as TiO_2 did not provide bulk and surface passivation it was gradually exchanged for a- $\text{SiN}_x\text{:H}$ from the year 2000. A- $\text{SiN}_x\text{:H}$ is currently used by almost every c-Si solar cell manufacturer as it simultaneously acts as ARC, and provides bulk and surface passivation. As new solar cell designs will emerge and the optical and electrical requirements will increase it is expected, however, that more functional thin films will find widespread usage in the field of c-Si PV. This has already become apparent in the highest efficiency commercial solar cells produced to date by Sanyo and SunPower in which thermal SiO_2 and a-Si:H are employed because of their excellent levels of c-Si surface passivation.^{24,80} In this section the most relevant functional thin films for c-Si will be discussed, and the results obtained for the various thin films in this Ph.D. research will be put into broader perspective.

A. Thermal and PECVD grown SiO_2

Thermally grown SiO_2 is the state-of-the-art surface passivation layer, and S_{eff} values as low as 2 cm/s and 12 cm/s have been reported on 1.5 $\Omega \text{ cm}$ *n*-type and 1 $\Omega \text{ cm}$ *p*-type c-Si, respectively.⁸¹ The excellent surface passivation by thermal SiO_2 is mainly attributed to its high quality of the c-Si/ SiO_2 interface. This high interface quality is assured by the fact that the thermal SiO_2 is grown into the silicon wafer by oxidation at elevated temperatures in the range of 1000-1100 °C. Hence, the final interface is almost unaffected by the initial c-Si surface condition. The electrical interface quality is further improved by extensive post-deposition processing that is mainly aimed at passivation of interface defect states by H. The most commonly used method to supply H to the c-Si/ SiO_2 interface for defect passivation is a post-deposition anneal in an H_2 containing atmosphere at a temperature of typically 400 °C. Another more elaborate method is the deposition of a sacrificial Al film on the SiO_2 followed by a subsequent anneal at typically 400 °C. In this so-called *alneal* process Al oxidizes due to the presence of residual H_2O , and during this process H is released for defect passivation at the c-Si/ SiO_2 interface. It was shown by Fussel *et al.* that the as-grown interface defect density could be lowered by one order of magnitude by a forming gas anneal and two orders of magnitude by an alneal.⁸² An alternative way to supply H to the c-Si/ SiO_2 interface is the deposition of an H-containing dielectric film such as a- $\text{SiN}_x\text{:H}$ on the c-Si/ SiO_2 stack as demonstrated by Schmidt *et al.*⁸³ Moreover, a small fixed positive fixed charge density (up to 10^{11} cm^{-2}) is present in the thermal SiO_2 layer as well. The positive fixed

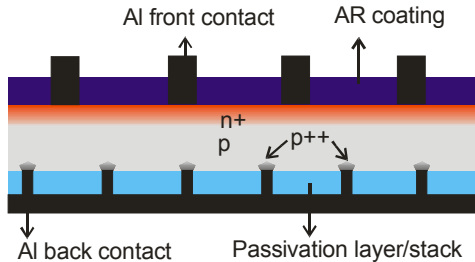


Figure 17: Industrial Passivated Emitter Rear Contact (*i*-PERC) c-Si solar cell design developed by IMEC.⁸⁴

charge density provides field-effect passivation by electrostatic shielding of holes from the c-Si surface.⁷¹ Thermally grown SiO₂ provides a state-of-the-art level of surface passivation on lightly doped *n*- and *p*-type c-Si.⁸¹ The level of surface passivation on highly doped *n*-type c-Si (e.g., an *n*⁺-emitter) is also reported to be excellent.⁸⁵ The level of passivation of *p*⁺-emitters on the other hand is still poorer and even degrades in time.⁴⁰

Due to the high processing temperatures only high purity c-Si (i.e. float zone or magnetically confined Cz grown c-Si) can be used without significant process induced bulk lifetime degradation.⁸⁶ Moreover, the refractive index of SiO₂ is 1.47, which is rather low for the application of SiO₂ as single layer antireflection coating on the front side of c-Si solar cells. Consequently, SiO₂ can only be applied in a stack structure, e.g. with a-SiN_x:H at the front side of c-Si solar cells. On the other hand, SiO₂ has an ideal refractive index to be applied as rear side surface reflector in combination with a full coverage Al film resulting in rear side surface reflectance of over 90 % as shown in Section II A.2.

The main barrier for the application of thermal SiO₂ is its high growth temperatures. Several low temperature approaches have therefore been pursued in recent years. It was shown by Schultz *et al.* that thermal SiO₂ with a good level of surface passivation could be grown at relative moderate temperatures of ~800 °C by wet oxidation involving H₂O.⁸⁷ This low temperature “wet” thermal SiO₂ film has resulted in the world record efficiency mc-Si solar cell with a conversion efficiency of 20.3 %.⁸⁷

An alternative approach is to grow the SiO₂ film by PECVD in a low temperature process (see, e.g. Leguit *et al.*).⁸⁸ As discussed in Chapter 3 of this thesis a low temperature PECVD SiO₂ process employing the ETP technique was developed in this Ph.D. research. These SiO₂ films were deposited at deposition rates in the range of 5-9 nm/s. They demonstrated a reasonably good level of surface passivation on low resistivity *n*-type c-Si with a *S_{eff}* of 54 cm/s on a 1.3 Ω cm *n*-type c-Si. The best level of surface passivation was obtained after a 15 min forming gas anneal at 600 °C.

These PECVD SiO₂ films were also applied as rear side surface passivation and reflection film in an *i*-PERC solar cell structure as shown in Fig. 17. The experiments were conducted in collaboration with IMEC in Belgium. The results of this experiment

Table III: One-sun parameters measured under standard testing conditions for ~200 μm *i*-PERC mc-Si (~1 $\Omega \text{ cm}$ *p*-type) solar cells with various rear side surface passivation schemes.

Rear surface		Efficiency (%)	Fill-Factor (%)	V_{oc} (mV)	I_{sc} (mA/cm ²)
Al-BSF	Best	15.6	77.1	607	33.4
	Average	15.3±0.2	76±1	604±3	33.3±0.2
ETP deposited 150 nm SiO ₂	Best	14.3	75.7	593	31.8
	Average	14.2±0.1	75.5±0.7	592±1	31.82±0.02
ETP deposited SiO ₂ capped by a-SiN _x :H ^a	Best	14.9	74.5	598	33.4
	Average	14.7±0.3	74.6±0.3	596±2	33.2±0.4

^a The thickness of the SiO₂ and a-SiN_x:H layers used in these experiments are part of a non-disclosure agreement and can therefore not be given.

are summarized in Table III. The performance of the *i*-PERC solar cells with a 150 nm SiO₂ layer at the rear side were, unfortunately, significantly poorer compared to Al back surface field (Al-BSF) reference solar cells. This low performance is most likely attributed to a poor thermal stability of SiO₂ under the high temperature contact firing step (~900 °C) used in the *i*-PERC process. It was also demonstrated by Schultz *et al.* that their “wet” thermal SiO₂ films showed a similar deterioration after a contact firing anneal.⁸⁹ The thermal stability of the SiO₂ film could significantly be improved by addition of a capping a-SiN_x:H film, as is clear from Table III. This improved performance can be attributed to supply of H from the a-SiN_x:H capping layer during the high temperature contact firing that partly recovers the surface passivating properties of SiO₂. A similar improvement of the thermal stability by addition of a capping a-SiN_x:H layer was also reported by Schultz *et al.*⁸⁹ More recently Hofman *et al.* have developed an all PECVD SiO_x:H/a-SiN_x:H/SiO_x:H stack that is firing stable on *p*-type c-Si.⁹⁰ This stack still demonstrated a $S_{\text{eff}} < 60$ cm/s after a contact firing step at 850 °C. Consequently, the results of Hofmann *et al.* and Agostinelli *et al.* indicate that a combination of PECVD SiO_x and a-SiN_x:H could be an interesting option for industrial solar cells.^{84,90}

B. A-SiN_x:H

A-SiN_x:H is currently the most widely applied functional thin film in the field of c-Si solar cells. A-SiN_x:H can act simultaneously as antireflection coating, bulk passivation and surface passivation layer. The advantages of a-SiN_x:H have already been

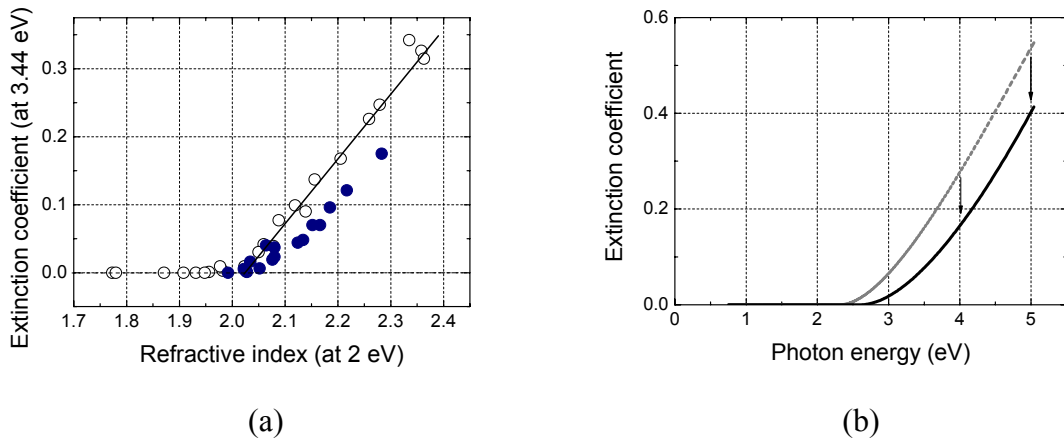


Figure 18:(a) The relation between the refractive index (at a photon energy of 2 eV) and the extinction coefficient (at a photon energy of 3.44 eV) of the ETP-deposited a-SiN_x:H films. A-SiN_x:H films with a lower mass density (open symbols) have a significantly lower refractive index compared to high mass density films (closed symbols) for a similar extinction coefficient. **(b)** The absorption is lower over the complete investigated photon energy range as shown for a low mass density silicon nitride film (dashed line) and an optimized high mass density silicon nitride film (solid line) with a refractive index of 2.15.

reported in the literature in the early 1980s by Hezel *et al.*,⁹¹ but the large scale implementation in c-Si solar cell manufacturing has started from 2000. From that moment high-throughput production equipment became available. One of the commercial tools for a-SiN_x:H deposition is the DEPx system developed by OTB Solar. In the DEPx system the ETP technology is employed for the high-rate deposition of a-SiN_x:H. The DEPx system has been used in the work described in Chapter 2 to study the bulk and surface passivation properties of a-SiN_x:H deposited by the ETP technique.

A-SiN_x:H is an interesting dielectric to serve as antireflection coating on c-Si solar cells. It is relatively easy to tune its refractive index in the 1.9-2.5 range. As mentioned in Section II.A.1 the ideal refractive index for a single layer ARC in a solar cell module would be around 2.4. An a-SiN_x:H film with a refractive index of 2.4, however, strongly absorbs in the ultraviolet part of the spectrum and would even *lower* the solar cell efficiency compared to an a-SiN_x:H film with a non ideal refractive index of 1.9.⁵³ In Fig. 18 (a) the absorption of an a-SiN_x:H film, expressed in the extinction coefficient at a photon energy of 3.44 eV, is shown as a function of the refractive index of the film.^h From Fig. 18 (a) we can see that a-SiN_x:H films with a higher mass density show a lower absorption for an identical refractive index. This is related to the fact that

^h The absorption coefficient can be calculated from the extinction coefficient via $\alpha(\lambda)=(4\pi k)/\lambda$, where α is the absorption coefficient, λ the wavelength, and k the extinction coefficient.

the refractive index of a-SiN_x:H is determined by both the Si/N ratio and the mass density and the extinction coefficient in first order only by the Si/N ratio. The refractive index can consequently be increased, to further reduce the reflection losses, by increasing the mass density while maintaining a similar level of (undesired) absorption in the a-SiN_x:H film. It was shown that for ETP deposited a-SiN_x:H, with a high mass density, a refractive index of 2.1 results in the lowest combined loss (reflection and absorption) in a solar cell module. In Fig. 18 (b) the extinction function of high and low mass density a-SiN_x:H film with a refractive index of 2.15 is shown. This clearly shows that the absorption of a high mass density a-SiN_x:H film is lower compared to a low mass density a-SiN_x:H film over the whole investigated photon energy range.

A high mass density has also been found to be important for the level of bulk passivation provided by the a-SiN_x:H film. In the study of our group published by Hong *et al.* it was clearly shown that higher mass densities result in a higher level of bulk passivation leading to a higher efficiency of mc-Si solar cells.⁹² This correlation, as proposed by Hong *et al.*, has been the driving force in the optimization of the level of bulk passivation by various deposition techniques,^{93,94} and was also confirmed in the work presented in Chapter 2 of this thesis. A high mass density is consequently found to be important for both the level of bulk passivation and the antireflection performance provided by an a-SiN_x:H film.

The surface passivation mechanism of a-SiN_x:H is mainly attributed to field-effect passivation provided by a high positive fixed charge density in the a-SiN_x:H film ($\sim 10^{12} \text{ cm}^{-2}$).⁹⁵ The positive fixed charge density is particularly beneficial in the passivation of *n*-type c-Si as the minority carriers (i.e. holes) are effectively shielded from the c-Si surface. S_{eff} values as low as 6 cm/s and 22 cm/s have been reported on $1.5 \Omega \text{ cm}$ *n*-type and $1 \Omega \text{ cm}$ *p*-type c-Si passivated by a-SiN_x:H, respectively.⁹⁶ The best results were obtained for nearly stoichiometric a-SiN_x:H while in earlier reports the best level of surface passivation was obtained for Si-rich a-SiN_x:H films with a refractive index > 2.3 .⁹⁷ The a-SiN_x:H deposited by the ETP technique demonstrate a constant level of surface passivation for a broad refractive index range of 1.9-2.4 with a S_{eff} of $\sim 50 \text{ cm/s}$ on $8.4 \Omega \text{ cm}$ *p*-type c-Si. Even though significantly lower S_{eff} values have been obtained on lower resistivity *p*-type c-Si for example by Kerr *et al.*⁹⁶ and Lauinger *et al.*⁹⁷ the ETP deposited a-SiN_x:H films were deposited at a significantly higher deposition rate of $\geq 4 \text{ nm/s}$. This is over one order of magnitude faster compared to other techniques. Moreover, these passivation results were obtained on the commercial DEP_x system instead of a lab-type reactor.

A-SiN_x:H has also demonstrated an excellent level of surface passivation on highly doped *n*-type c-Si with a comparable performance to thermal SiO₂.⁹⁸ As such, a-SiN_x:H can be effectively used as antireflection coating and emitter passivation film on diffused emitter *p*-type c-Si solar cells. A high positive fixed charge density can, on the

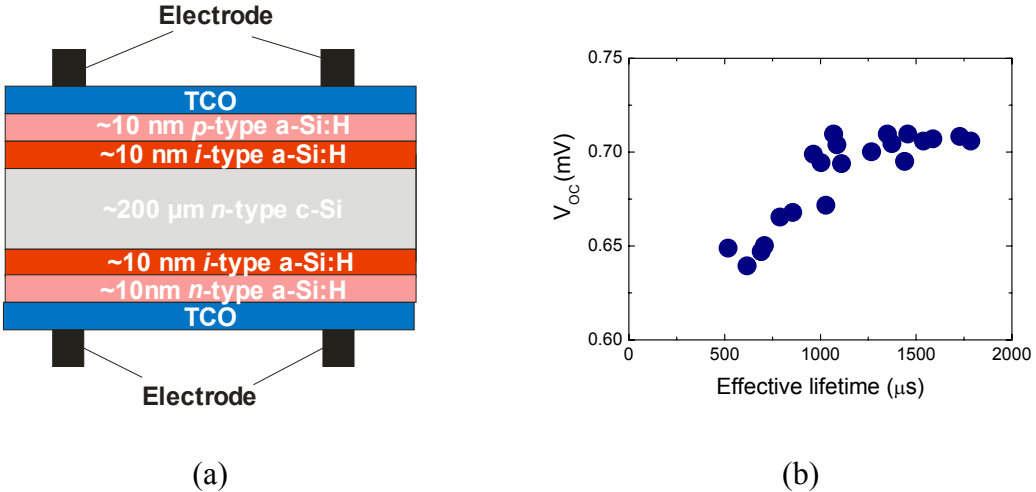


Figure 19: (a) Schematic illustration of the (bifacial) HIT c-Si solar cell design from Sanyo.⁸⁰ (b) The extraordinary high open-circuit voltage V_{oc} of the HIT solar cell design can largely be attributed to a high effective lifetime in the c-Si solar cell by an excellent surface passivation provided by the a-Si:H films.⁸⁰

other hand, be detrimental in the surface passivation of highly doped *p*-type c-Si surfaces (as shown in Chapter 7). It was, however, recently reported that Si-rich a-SiN_x:H can effectively passivate highly doped *p*-type c-Si surfaces after a four hour post-deposition anneal at 400 °C, although the mechanism is not yet understood.⁹⁹ Moreover, the fixed positive charge density can induce a parasitic shunting when applied at the backside of *p*-type solar cells.¹⁰⁰ This parasitic shunting lowers the short-circuit current of the solar cell, and hence lowers the solar cell efficiency.

C. A-Si:H

A-Si:H has recently gained significant interest in the field of c-Si PV. A-Si:H has demonstrated an excellent level of c-Si surface passivation that is effectively exploited in the HIT c-Si solar cell developed by Sanyo.²⁰ The HIT solar cell design is schematically depicted in Fig. 19 (a). As can be seen the solar cell structure is formed by a lightly doped *n*-type c-Si wafer symmetrically passivated by a 10 nm intrinsic a-Si:H film. On the front of the solar cell a 10 nm B-doped a-Si:H is applied to form the front emitter, and on the rear side of the solar cell a 10 nm P-doped a-Si:H film is applied to form the back surface field. In this way the high temperature steps involved with dopant diffusion can be omitted. This avoids bulk lifetime degradation during high temperature processing when using lower quality c-Si. The HIT solar cell currently has a record efficiency of 22.3 % in the lab, and an average efficiency of 20.2 % in industrial manufacturing.⁸⁰ The high conversion efficiency of the HIT solar cell design can largely be attributed to an excellent surface passivation by the stack of the intrinsic and doped a-Si:H. As shown in Fig. 19 (b) the effective lifetime of the HIT solar cell structure strongly correlates with the open

circuit voltage V_{oc} of the solar cell.²⁰ A remarkable aspect of the HIT solar cell design is the fact that, up to this moment, the excellent results of Sanyo were not reproduced by others, despite the fact that the HIT solar cell concept is investigated in numerous groups all over the world. Consequently, the c-Si surface passivation by a-Si:H is still a very active research area.

It was shown by Dauwe *et al.* that a-Si:H deposited by conventional rf-PECVD demonstrated an excellent level of surface passivation on low resistivity p - and n -type c-Si on a similar level as in the HIT solar cell.¹⁰¹ Moreover, a-Si:H has demonstrated a good level of surface passivation on highly doped p^+ - and n^+ -type c-Si as is shown by Plagwitz *et al.*¹⁰² The results obtained in the study of Dauwe *et al.* on low resistivity p -type c-Si are shown in Fig. 20 combined with the best results obtained in this Ph.D. research for a-Si:H deposited by hot-wire chemical vapor deposition (HWCVD) and the ETP technique on n -type c-Si. From Fig. 20 we can learn that the initial study of Dauwe indicated that deposition temperatures of 200-300 °C are required for a good level of surface passivation by an a-Si:H film. An excellent level of surface passivation is however also obtained for a-Si:H films grown at 135 °C by HWCVD and for a-Si:H films deposited at 400 °C by the ETP technique. Results obtained with rf-PECVD and hot-wire CVD indicate that the level of surface passivation provided by the a-Si:H film improves for increasing deposition temperatures up to a certain transition temperature, and subsequently the level of surface passivation deteriorates when going to even higher deposition temperatures. This transition temperature is higher if the a-Si:H films are deposited with higher deposition rates. For the high-rate ETP technique a-Si:H films with an excellent level of surface passivation can even be deposited at 400 °C.⁴³ For the a-Si:H films grown by HWCVD it was detected by high-resolution transmission electron microscopy (HR-TEM) that some epitaxial growth took place when the deposition temperature was ≥ 150 °C.¹⁰³ It was shown by Fujiwara *et al.* and Yan *et al.* that an abrupt interface is essential for the level of surface passivation provided by a-Si:H.^{104,105} By increasing the deposition rate it appears that an abrupt interface can be obtained for higher deposition temperatures.

In this respect it is interesting to note that in recent work of our group it was shown that epitaxial growth, even for the first few nanometers, could be detected *in situ* during a-Si:H film growth by the interface and surface sensitive second harmonic generation (SHG) technique.¹⁰³ The SHG technique was also applied during the deposition of the HWCVD a-Si:H films presented in Fig. 20. The detection of initial epitaxial growth, as expected, strongly correlated with the obtained level of surface passivation.⁴⁵

The main challenge in the application of a-Si:H in a solar cell device is related to its relatively low thermal stability. It was, for example, demonstrated that the level of surface passivation provided by ETP grown a-Si:H degraded by a factor of three by a

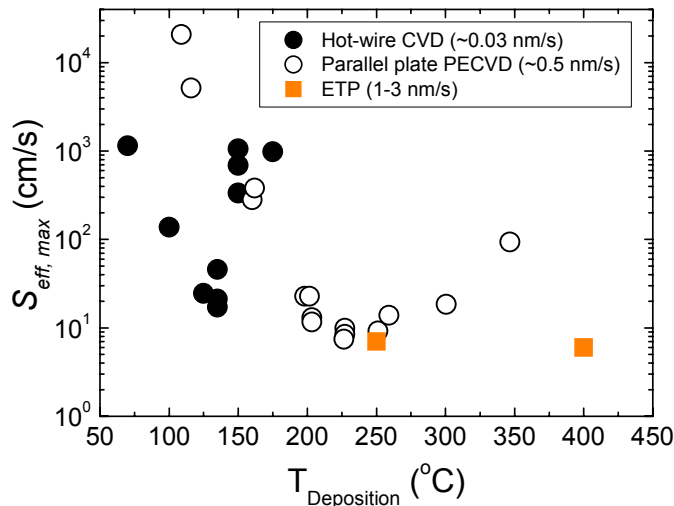


Figure 20: Upper limit of the S_{eff} for $<100>$ c-Si passivated by a-Si:H deposited by various deposition techniques and deposition rates. The values for the a-Si:H films deposited by rf-PECVD were taken from the study published by Dauwe *et al.*¹⁰¹ on 1.6 Ω cm *p*-type c-Si, while the values for HWCVD and ETP deposited a-Si:H were obtained in this Ph.D. research on 1.9 Ω cm *n*-type c-Si.

30 min anneal at the deposition temperature of 400 °C. Moreover, no selective etch chemistry for a-Si:H versus c-Si is available. Hence, conventional photolithography, such as applied in high-efficiency lab c-Si solar cells, cannot be applied. The electrical contact through the a-Si:H film can fortunately be formed by the so-called COSIMA (contacts to a-Si:H passivated wafers by means of annealing) process.¹⁰⁶ In the COSIMA process an Al film dissolves in a-Si:H in an ~1 hour anneal at ~210 °C, and an electrical contact is formed through the a-Si:H film. Using the COSIMA process a-Si:H has already been successfully applied as rear surface passivating film in a *p*-type c-Si solar cell by Schaper *et al.*, resulting in a 20.1 % efficient solar cell.¹⁰⁷ Another disadvantage of a-Si:H is its high absorption in the UV part of the solar spectrum. The a-Si:H film thickness should consequently be kept as low as possible when applied at the front of c-Si solar cells. Moreover, its optical properties are not optimal for the application at the rear side of c-Si solar cells. Reflectance at the rear side of c-Si solar cells is not optimum as the dielectric contrast with c-Si is relatively small.

D. Al_2O_3

Amorphous Al_2O_3 is a material that has recently gained considerable interest for application in the field of c-Si solar cells. In the late eighties Al_2O_3 was already applied for c-Si surface passivation in metal-insulator-semiconductor (MIS) solar cells by Hezel and Jaeger.⁹⁵ They demonstrated that Al_2O_3 could provide a reasonable level of surface passivation with an effective surface recombination velocity of $\sim 200 \text{ cm/s}$ on $2 \Omega \text{ cm}$ *p*-type c-Si. The c-Si surface passivation was explained by a relatively low mid-gap interface defect density ($\sim 1 \times 10^{11} \text{ eV}^{-1} \text{ cm}^{-2}$) and a *negative* fixed charge density of $\sim 3 \times 10^{12} \text{ cm}^{-2}$. More recently Agostinelli *et al.* demonstrated that Al_2O_3 grown by thermal ALD demonstrated an excellent level of surface passivation on *p*-type c-Si.¹⁰⁸

As described in detail in Chapters 4 to 8 significant progress has been made in the characterization of c-Si surface passivation by Al_2O_3 . Al_2O_3 has demonstrated a similar level of surface passivation compared to thermal SiO_2 on low resistivity c-Si and even a better level of surface passivation on heavily B-doped c-Si surfaces. The excellent surface passivation by Al_2O_3 on c-Si can largely be attributed to a high negative fixed charge density in the Al_2O_3 film. Moreover, Al_2O_3 was also successfully applied at the rear side of *p*-type c-Si solar cells. This was the first high-efficiency c-Si solar cell to our knowledge with a negative-charge-dielectric at the rear side of c-Si solar cells.

E. Comparison between various functional thin films for c-Si PV

Apart from the materials discussed above AlF_3 and a- $\text{SiC}_x:\text{H}$ are, or have been, considered as well for the application as functional thin films for c-Si solar cells. AlF_3 is a negative-charge dielectric that was investigated by Konig *et al.*¹⁰⁹⁻¹¹² The level of c-Si surface passivation provided by AlF_3 was reasonable with an effective surface recombination velocity of 122 cm/s on $1 \Omega \text{ cm}$ *p*-type c-Si.¹¹¹ The AlF_3 films contained a negative fixed charge density up to $7 \times 10^{12} \text{ cm}^{-2}$, which is comparable to the negative fixed charge density found in Al_2O_3 deposited by plasma-assisted ALD. AlF_3 has already been applied in a *p*-inversion type solar cell as well. Due to non-optimized processing, however, the solar cell efficiencies were below 1 %.¹¹¹ Films of a- $\text{SiC}_x:\text{H}$ have demonstrated a reasonably good level of surface passivation on low resistivity *p*- and *n*-type c-Si as shown by Martin *et al.*^{113,114} A- $\text{SiC}_x:\text{H}$ has already been successfully applied at the rear side of *p*-type c-Si solar cells.⁵⁶ The best a- $\text{SiC}_x:\text{H}$ passivated solar cell demonstrated an efficiency of 20.2 % compared to 21.0 % for a solar cell passivated by thermal SiO_2 .⁵⁶

In Table IV all functional thin films discussed in this section are compared for application in c-Si solar cells. At the front side TiO_2 , a- $\text{SiC}_x:\text{H}$ and a- $\text{SiN}_x:\text{H}$ are the materials of choice for an optimal single layer ARC as their refractive index can be tuned around the optimal value of 2.1-2.4. However, if simultaneously bulk and/or surface

Table IV: Functional thin films that are, or have been, considered for application in c-Si solar cells. The highlighted materials and material properties have been investigated in this Ph.D. research.

Material	Optical properties		Surface passivation			
	Front	Rear	<i>p</i> -type	<i>p</i> ⁺ -type	<i>n</i> -type	<i>n</i> ⁺ -type
TiO ₂	++	++	-- ¹¹⁵	-- ^{116a}	?	?
Thermal SiO ₂	+	++	++ ⁸¹	+ ⁴⁰	++ ⁸¹	++ ⁹⁸
PECVD SiO ₂	+	++	+/- ⁸⁸	?	+/- ⁸⁸	?
a-SiN _x :H	++	++	+ ⁹⁶	- ^{40,b}	++ ⁹⁶	++ ⁹⁸
a-Si:H	-	-	++ ¹⁰¹	+ ⁴⁰	++ ¹⁰¹	++ ¹⁰²
a-SiC _x :H	++ ^c	++	+/- ¹¹³	- ¹¹⁷	+ ¹¹⁴	+/- ¹¹⁸
AlF ₃	+	++	+/-	?	?	?
Al ₂ O ₃	+	++	++	++	++	?

^a In combination with a ~6 nm SiO₂ film a reasonable level of surface passivation can be obtained as reported by Richards *et al.*¹¹⁶

^b Recently it was reported that by prolonged (up to 4 hours) annealing at 400 °C Si-rich a-SiN_x:H can passivate highly B-doped c-Si surfaces.

^c The best surface passivation is obtained by Si-rich films (up to 90 at.%) with a corresponding high absorption in the visible part of the solar spectrum.

passivation is desired, a-SiN_x:H is by far the best choice, especially on diffused emitter *p*-type c-Si solar cells. The level of surface passivation provided by a-SiN_x:H is generally not affected by the high-temperature co-firing step that is applied in current industrial solar cell manufacturing. Moreover, a-SiN_x:H releases atomic H during this co-firing step and this atomic H can improve the bulk lifetime by passivating bulk defects. Apart from the HIT solar cell, currently all industrial solar cell designs employ an a-SiN_x:H layer as antireflection coating.

As can be seen, all dielectric films in Table IV can be used to increase reflection at the rear side of c-Si solar cells. On the other hand, a-Si:H does not exhibit the ideal optical properties for application at the rear side of c-Si solar cells. The a-Si:H thickness at this side of the solar cell consequently needs to be as low as possible. The choice for the functional thin film at the rear side will depend on the level of surface passivation that can be obtained on the c-Si surface of interest, as some functional thin films show a better level of surface passivation on *n*-type c-Si compared to *p*-type c-Si and vice versa. Moreover, the functional thin film should be compatible with the solar cell production process. As the materials summarized in Table IV are all non-conducting, the films have to be locally opened for electrical contacting at the rear side. As mentioned previously,

the co-firing process using metal containing firing-paste could potentially be used for this purpose. In order to avoid the high-temperatures required for the co-firing process, however, alternative processes are being developed. Using high intensity lasers the functional thin film can be locally ablated or alloyed with a contacting metal in the so-called laser fired contact approach.^{119,120} Photolithography is another alternative to locally remove the functional thin film for metal contacting. Not all films summarized in Table IV are, however, compatible with standard photo-lithography as they are difficult to etch selectively. Moreover, photo-lithography is quite elaborate and expensive and involves a few additional process steps. Consequently, the laser fired contact approach is probably most suitable for large scale industrial production.

As summarized in Table IV only a few materials give a good level of surface passivation on heavily doped *p*-type c-Si such as *p*-type emitters in diffused emitter *n*-type c-Si solar cells. Moreover the high processing temperatures required to obtain a high quality thermal SiO₂ are not desired for a B-diffused surface. Consequently a-Si:H and Al₂O₃ seem to be the most interesting option at this moment for the passivation of heavily *p*-doped c-Si surfaces as is explained further in Chapter 6.

V Recommendations and future outlook

Even though c-Si wafer solar cells have been perceived to be far too expensive in the past, they currently still dominate the PV market. It is expected that the cost reduction potential of c-Si wafer solar cells is sufficient to continue this dominance for at least one decade. As explained in this thesis, part of the cost reduction for c-Si solar cells can be achieved by the application of functional thin films at the front and the rear side of c-Si solar cells. It is expected that after the successful wide-scale introduction of a-SiN_x:H as first multifunctional thin film in the field of c-Si solar cells more functional thin films will be applied at an industrial scale. As the c-Si PV industry is growing towards maturity and is currently attracting significant amounts of (venture) capital, it is expected that new technologies have the potential to enter the PV market relatively fast, especially when compared to the more mature (and conservative) semiconductor industry. The moderate electrical and optical performance of the Al-BSF will become unacceptable for c-Si solar cell manufacturers, and consequently functional thin films are expected to be applied at the rear side of c-Si solar cells within a few years.

Most of the functional thin films investigated for application in c-Si solar cells are grown by means of plasma (enhanced) processes. A plasma can, however, also be used for other steps in the c-Si solar cell manufacturing. It has for example been demonstrated that c-Si can be etched at very high rates by the ETP techniques which could for example be applied for surface texturing.¹²¹ Moreover, it has been demonstrated that SiO₂ could selectively be etched over c-Si, indicating that also the conventional HF chemistry could be mimicked by a plasma.¹²² This approach is currently also under investigation in the

PMP group employing the ETP technique. Consequently, the c-Si surface etching, phosphorus glass removal step and the deposition of functional thin films could be combined in one plasma reactor. This could reduce the number of process steps in the solar cell manufacturing and this could reduce costs and increase the manufacturing yield.

Moreover the PV industry is now clearly moving towards a dedicated c-Si production as it is now consuming over half of the total c-Si feedstock supply. This dedicated PV c-Si production could potentially result in a dominance of *n*-type c-Si as it is significantly more tolerant to various metallic impurities. It has been shown in this Ph.D. research that even the *p*⁺-type c-Si surface could effectively be passivated by Al₂O₃. As a result all industrially relevant c-Si surfaces can now effectively be passivated by thin films, which allows more freedom in designing the solar cell structure.

Si-based solar cells, based on a-Si:H and μ c-Si, currently have a large share in the second generation PV market. It is therefore expected that the results presented in this Ph.D. thesis for application in first generation c-Si solar cells could also be relevant for the next generation solar cells. Thin film solar cells intrinsically exhibit a high surface-to-volume ratio and, consequently, benefit from an adequate surface passivation and enhanced light trapping. Moreover, various concepts proposed in the third generation PV, such as quantum-dot solar cells, will also require an excellent level of surface passivation.¹²³ Consequently the results presented in this thesis are expected to be relevant also in a “beyond c-Si” stage of PV.

REFERENCES:

- 1 International Panel on Climate Change, <http://www.ipcc.ch/>
2 United nations Secretary General Ban Ki-moon,
3 <http://www.un.org/News/Press/docs/2007/sgsm11175.doc.htm>
4 <http://www.climatecrisis.net/>
5 http://nobelprize.org/nobel_prizes/peace/laureates/2007/
6 German Advisory Council on Global Change, World in Transition, Towards Sustainable Energy Systems, available from www.wbgu.de
7 EPIA, Annual report 2006, available from available from www.epia.org
8 E. Becquerel, Compt. Rend. **9**, 561 (1839).
9 D. M. Chapin, C. S. Fuller, and G. L. Pearson, J. Appl. Phys. **25**, 676 (1954).
10 J. H. Zhao, A. H. Wang, and M. A. Green, Prog. Photovoltaics **7**, 471 (1999).
11 www.epia.org
12 M. A. Green, Prog. Photovoltaics **9**, 123 (2001).
13 R. M. Swanson, Prog. Photovoltaics **14**, 443 (2006).
14 EPIA and Greenpeace, Solar Generation IV, available from www.epia.org
15 J. I. Hanoka, Sol. Energ. Mat. Sol. C. **65**, 231 (2001).
16 P. J. Verlinden, A. W. Blakers, K. J. Weber, J. Babaei, V. Everett, M. J. Kerr, M. F. Stuckings, D. Gordeev, and M. J. Stocks, Sol. Energ. Mat. Sol. C. **90**, 3422 (2006).
17 K. D. Smith, R. J. Nielsen, H. K. Gummel, D. B. Cuttriss, W. Rosenzweig, and J. D. Bode, Bell Syst. Tech. J. **42**, 1765 (1963).
18 J. E. Cotter, J. H. Guo, P. J. Cousins, M. D. Abbott, F. W. Chen, and K. C. Fisher, IEEE Trans. Electron. Dev. **53**, 1893 (2006).
19 R. M. Swanson (Moderator), Proc. of the 12th NREL Silicon Workshop, Breckenridge, CO, 2002), p. 16.
20 P. M. Mulligan, D. H. Rose, M. J. Cudzinovic, and D. M. de Ceuster, Proc. of the 19th EU-PVSEC, Paris, (WIP Renewable Energies, Munich, 2004), p. 387.
21 M. Taguchi, K. Kawamoto, S. Tsuge, T. Baba, H. Sakata, M. Morizane, K. Uchihashi, N. Nakamura, S. Kiyama, and O. Oota, Prog. Photovoltaics **8**, 503 (2000).
22 N. Yuge, M. Abe, K. Hanazawa, H. Baba, N. Nakamura, Y. Kato, Y. Sakaguchi, S. Hiwasa, and F. Aratani, Prog. Photovoltaics **9**, 203 (2001).
23 www.sunpowercorp.com
24 <http://www.qcells.com/>
25 D. de Ceuster, P. J. Cousins, D. Rose, M. Cudzinovic, and W. Mulligan, Proc. of the 22nd EU-PVSEC, Milan, (WIP Renewable Energies, Munich, 2007), p. 816.
S. M. Myers, M. Seibt, and W. Schroter, J. Appl. Phys. **88**, 3795 (2000).

- 26 P. Hacke, J.M. Gee, M. Hilali, J. Dominguez, H. Dundas, A. Jain, G. Lopez, B.
Fischer, and B. L. Soppori, Proc. of the 21th EU-PVSEC, Dresden, (WIP
Renewable Energies, Munich, 2006), p. 761.
- 27 T. Trupke, M. A. Green, and P. Wurfel, *J. Appl. Phys.* **92**, 4117 (2002).
- 28 T. Trupke, M. A. Green, and P. Wurfel, *J. Appl. Phys.* **92**, 1668 (2002).
- 29 D. C. Schram and G. M. W. Kroesen, US Patent No. 4,871,580 (1989).
- 30 D. C. Schram and G. M. W. Kroesen, European Patent No. 0297637 (1992).
- 31 W. M. M. Kessels, R. J. Severens, A. H. M. Smets, B. A. Korevaar, G. J.
Adriaenssens, D. C. Schram, and M. C. M. van de Sanden, *J Appl Phys* **89**, 2404
(2001).
- 32 M. Creatore, F. Palumbo, R. d'Agostino, and P. Fayet, *Surface Coatings Technol.*
142, 163 (2001).
- 33 W. M. M. Kessels, J. Hong, F. J. H. van Assche, J. D. Moschner, T. Lauinger, W.
J. Soppe, A. W. Weeber, D. C. Schram, and M. C. M. van de Sanden, *J. Vac. Sci.
Technol. A* **20**, 1704 (2002).
- 34 http://www.otb-solar.com/solar/products/products_depx.html
- 35 http://www.senternovem.nl/eet/projecten/hr_cel.asp
- 36 P. J. van den Oever, Ph.D. thesis, Eindhoven University of Technology, 2007.
- 37 P. J. van den Oever, J. H. van Helden, J. L. van Hemmen, R. Engeln, D. C.
Schram, M. C. M. van de Sanden, and W. M. M. Kessels, *J. Appl. Phys.* **100**,
093303 (2006).
- 38 P. J. van den Oever, J. L. van Hemmen, J. H. van Helden, D. C. Schram, R.
Engeln, M. C. M. van de Sanden, and W. M. M. Kessels, *J. Appl. Phys.* **15**, 546
(2006).
- 39 P. J. van den Oever, J. H. van Helden, C. C. H. Lamers, R. Engeln, D. C. Schram,
M. C. M. van de Sanden, and W. M. M. Kessels, *J. Appl. Phys.* **98**, 093301
(2005).
- 40 P. P. Altermatt, H. Plagwitz, R. Bock, J. Schmidt, R. Brendel, M. J. Kerr, and A.
Cuevas, Proc. of the 21st EU-PVSEC, Dresden, (WIP Renewable Energies,
Munich, 2006), p. 647.
- 41 M.D. Bijker, B. Hoex, W. M. M. Kessels, and M. C. M. van de Sanden,
Nederland Patent No. 1029647 (2007).
- 42 <http://www.stw.nl/Projecten/E/emm/emm6174.htm>
- 43 B. Hoex, W. M. M. Kessels, M.D. Bijker, and M. C. M. van de Sanden, Proc. of
the 21st European PVSEC, Dresden, (WIP Renewable Energies, Munich, 2006), p.
435.
- 44 B. Hoex, F. J. J. Peeters, A. J. M. van Erven, M. D. Bijker, W. M. M. Kessels, and
M. C. M. van de Sanden, Proc. of the 4th WCPEC, Hawaii, 2006), p. 1036.
- 45 J. J. H. Gielis, P. J. Van den Oever, B. Hoex, M. C. M. van de Sanden, and W. M.
M. Kessels, (to be published).

-
- ⁴⁶ C. Smit, R. A. C. M. M. van Swaaij, H. Donker, A. M. H. N. Petit, W. M. M. Kessels, and M. C. M. van de Sanden, *J. Appl. Phys.* **94**, 3582 (2003).
- ⁴⁷ J. W. A. M. Gielen, M. C. M. van de Sanden, and D. C. Schram, *Thin Solid Films* **271**, 56 (1995).
- ⁴⁸ J. Benedikt, M. Wisse, R. V. Woen, R. Engeln, and M. C. M. van de Sanden, *J. Appl. Phys.* **94**, 6932 (2003).
- ⁴⁹ R. Groenen, J. L. Linden, H. R. M. van Lierop, D. C. Schram, A. D. Kuypers, and M. C. M. van de Sanden, *Appl. Surf. Sci.* **173**, 40 (2001).
- ⁵⁰ B. Hoex, F. J. J. Peeters, M. Creatore, M. A. Blauw, W. M. M. Kessels, and M. C. M. van de Sanden, *J. Vac. Sci. Techn. A* **24**, 1823 (2006).
- ⁵¹ S. B. S. Heil, P. Kudlacek, E. Langereis, R. Engeln, M. C. M. van de Sanden, and W. M. M. Kessels, *Appl. Phys. Lett.* **89**, 131505 (2006).
- ⁵² F. Pedrotti and L. Pedrotti, *Introduction into optics*. (Prentice-Hall, Englewood Cliffs, N.J., 1996).
- ⁵³ P. Doshi, G. E. Jellison, and A. Rohatgi, *Appl. Optics* **36**, 7826 (1997).
- ⁵⁴ <http://www.jawoollam.com/>
- ⁵⁵ P. A. Basore, *IEEE Trans. Electron. Dev.* **37**, 337 (1990).
- ⁵⁶ S. W. Glunz, A. Grohe, M. Hermle, M. Hofmann, S. Janz, T. Roth, O. Schultz, M. Vetter, I. Martin, R. Ferré, S. Bermejo, W. Wolke, W. Warta, R. Preu, and G. P. Willeke, Proc. of the 20th EU-PVSEC, Barcelona, (WIP Renewable Energies, Munich, 2005), p. 572.
- ⁵⁷ D. Kray, M. Hermle, and S.W. Glunz, *Prog. Photovoltaics* **16**, 1 (2007).
- ⁵⁸ F. Huster, Proc. of the 20th EU-PVSEC, Barcelona, (WIP Renewable Energies, Munich, 2005), p. 635.
- ⁵⁹ M. A. Green, J. H. Zhao, A. H. Wang, P. J. Reece, and M. Gal, *Nature* **412**, 805 (2001).
- ⁶⁰ M. J. Kerr and A. Cuevas, *J. Appl. Phys.* **91**, 2473 (2002).
- ⁶¹ P. P. Altermatt, F. Geelhaar, T. Trupke, X. Dai, A. Neisser, and E. Daub, *Appl. Phys. Lett.* **88**, 261901 (2006).
- ⁶² R. N. Hall, *Phys. Rev.* **87**, 387 (1952).
- ⁶³ W. Shockley and W. T. Read, *Phys. Rev.* **87**, 835 (1952).
- ⁶⁴ D. Macdonald and L. J. Geerligs, *Appl. Phys. Lett.* **85**, 4061 (2004).
- ⁶⁵ J. Schmidt, C. Berge, and A. G. Aberle, *Appl. Phys. Lett.* **73**, 2167 (1998).
- ⁶⁶ A. Cuevas, M. Stocks, S. Armand, M. Stuckings, A. Blakers, and F. Ferrazza, *Appl. Phys. Lett.* **70**, 1017 (1997).
- ⁶⁷ J. Tan, A. Cuevas, D. Macdonald, T. Trupke, R. Bardos, and K. Roth, *Prog. Photovoltaics*, 10.1002/PIP (2007).
- ⁶⁸ I. Martin, M. Vetter, M. Garin, A. Orpella, C. Voz, J. Puigdollers, and R. Alcubilla, *J. Appl. Phys.* **98**, 114912 (2005).

- 69 H. Jin, K. J. Weber, N. C. Dang, and W. E. Jellett, *Appl. Phys. Lett.* **90**, 262109
(2007).
- 70 A. G. Aberle, S. Glunz, and W. Warta, *Sol. Energ. Mat. Sol. C.* **29**, 175 (1993).
- 71 A. G. Aberle, S. Glunz, and W. Warta, *J. Appl. Phys.* **71**, 4422 (1992).
- 72 A. G. Aberle, *Crystalline silicon solar cells: Advanced Surface Passivation and Analysis*. (UNSW Publishing and Printing Services, Sydney, 1999).
- 73 R. A. Sinton and A. Cuevas, *Appl. Phys. Lett.* **69**, 2510 (1996).
- 74 M. Bail, J. Kentsch, R. Brendel, and M. Schultz, Proc. of the 28th IEEE Photovoltaic Specialist Conference, New York, (IEEE, Piscataway, NJ, 2000), p. 99.
- 75 P. Pohl and R. Brendel, Proc. of the 19th European PVSEC, Paris, (WIP Renewable Energies, Munich, 2004), p. 46.
- 76 T. Trupke and R. A. Bardos, Proc. of the IEEE PVSEC, Lake Buena Vista, FL, (IEEE, Piscataway, NJ, 2005), p. 903.
- 77 T. Trupke, R. A. Bardos, M. C. Schubert, and W. Warta, *Appl. Phys. Lett.* **89**, 044107 (2006).
- 78 M. Bail, M. Schulz, and R. Brendel, *Appl. Phys. Lett.* **82**, 757 (2003).
- 79 D. Macdonald and A. Cuevas, *Appl. Phys. Lett.* **74**, 1710 (1999).
- 80 S. Taira, Y. Yoshimine, T. Baba, M. Taguchi, H. Kanno, T. Kinoshita, H. Sakata, E. Maruyama, and M. Tanaka, Proc. of the 22nd European PVSEC Milan, (WIP Renewable Energies, Munich, 2007), p. 932.
- 81 M. J. Kerr and A. Cuevas, *Semicond. Sci. Tech.* **17**, 35 (2002).
- 82 W. Fussel, M. Schmidt, H. Angermann, G. Mende, and H. Flietner, *Nucl. Instrum. Methods Phys. Res. A* **377**, 177 (1996).
- 83 J. Schmidt, M. Kerr, and A. Cuevas, *Semicon. Sci. Technol.* **16**, 164 (2001).
- 84 G. Agostinelli, P. Choulat, H. F. W. Dekkers, Y. Ma, and G. Beaucarne, Proc. of the 21st EU-PVSEC, Dresden, (WIP Renewable Energies, Munich, 2006), p. 601.
- 85 P. P. Altermatt, J. O. Schumacher, A. Cuevas, M. J. Kerr, S. W. Glunz, R. R. King, G. Heiser, and A. Schenk, *J. Appl. Phys.* **92**, 3187 (2002).
- 86 J. Zhao, A. H. Wang, and M. A. Green, *Sol. Energ. Mat. Sol. C.* **66**, 27 (2001).
- 87 O. Schultz, S. W. Glunz, and G. P. Willeke, *Prog. Photovoltaics* **12**, 553 (2004).
- 88 C. Leguijt, P. Lolgen, J. A. Eikelboom, A. W. Weeber, F. M. Schuurmans, W. C. Sinke, P. F. A. Alkemade, P. M. Sarro, C. H. M. Maree, and L. A. Verhoef, *Sol. Energ. Mat. Sol. Cells* **40**, 297 (1996).
- 89 O. Schultz, M. Hofmann, S. W. Glunz, and G. P. Willeke, Proc. of the IEEE PVSEC, Lake Buena Vista, FL, (IEEE, Piscataway, NJ, 2005), p. 872.
- 90 M. Hofmann, S. Kambor, C. Schmidt, D. Grambole, J. Rentsch, S. Glunz, and R. Preu, Proc. of the 22nd EU-PVSEC, Milan, (WIP Renewable Energies, Munich, 2007), p. 1030.
- 91 R. Hezel and R. Schorner, *J. Appl. Phys.* **52**, 3076 (1981).

-
- ⁹² J. Hong, W. M. M. Kessels, F. J. H. van Assche, H. C. Rieffe, W. J. Soppe, A. W. Weeber, and M. C. M. van de Sanden, *Prog. Photovoltaics* **11**, 125 (2003).
- ⁹³ H. F. W. Dekkers, S. De Wolf, G. Agostinelli, F. Duerinckx, and G. Beaucarne, *Sol. Energ. Mat. Sol. C.* **90**, 3244 (2006).
- ⁹⁴ A. W. Weeber, H. C. Rieffe, W. C. Sinke, and W. J. Soppe, Proc. of the 19th EU-PVSEC, Paris, (WIP Renewable Energies, Munich, 2004), p. 1005.
- ⁹⁵ R. Hezel and K. Jaeger, *J. Electrochem. Soc.* **136**, 518 (1989).
- ⁹⁶ M. J. Kerr and A. Cuevas, *Semicond. Sci. Tech.* **17**, 166 (2002).
- ⁹⁷ T. Lauinger, J. Schmidt, A. G. Aberle, and R. Hezel, *Appl. Phys. Lett.* **68**, 1232 (1996).
- ⁹⁸ M. J. Kerr, J. Schmidt, A. Cuevas, and J. H. Bultman, *J. Appl. Phys.* **89**, 3821 (2001).
- ⁹⁹ F. W. Chen, T. T. A. Li, and J. E. Cotter, *Appl. Phys. Lett.* **88**, 263514 (2006).
- ¹⁰⁰ S. Dauwe, L. Mittelstadt, A. Metz, and R. Hezel, *Prog. Photovoltaics* **10**, 271 (2002).
- ¹⁰¹ S. Dauwe, J. Schmidt, and R. Hezel, Proc. of the 29th IEEE Photovoltaic Specialist Conference, New Orleans, (IEEE, Piscataway, NJ, 2002), p. 1246.
- ¹⁰² H. Plagwitz, Y. Takahashi, B. Terheiden, and R. Brendel, Proc. of the 21st EU-PVSEC, Dresden, (WIP Renewable Energies, Munich, 2006), p. 688.
- ¹⁰³ J. J. H. Gielis, P. J. van den Oever, M. C. M. van de Sanden, and W. M. M. Kessels, *Appl. Phys. Lett.* **90**, 202108 (2007).
- ¹⁰⁴ H. Fujiwara and M. Kondo, *Appl. Phys. Lett.* **90**, 013503 (2007).
- ¹⁰⁵ Y. F. Yan, M. Page, T. H. Wang, M. M. Al-Jassim, H. M. Branz, and Q. Wang, *Appl. Phys. Lett.* **88**, 121925 (2006).
- ¹⁰⁶ H. Plagwitz, M. Nerding, N. Ott, H. P. Strunk, and R. Brendel, *Prog. Photovoltaics* **12**, 47 (2004).
- ¹⁰⁷ M. Schaper, J. Schmidt, H. Plagwitz, and R. Brendel, *Prog. Photovoltaics* **13**, 381 (2005).
- ¹⁰⁸ G. Agostinelli, A. Delabie, P. Vitanov, Z. Alexieva, H. F. W. Dekkers, S. De Wolf, and G. Beaucarne, *Sol. Energ. Mat. Sol. C.* **90**, 3438 (2006).
- ¹⁰⁹ D. Konig, G. Ebest, R. Scholz, S. Gemming, I. Thurzo, T. U. Kampen, and D. R. T. Zahn, *Physica E* **14**, 259 (2002).
- ¹¹⁰ D. Konig, R. Scholz, D. R. T. Zahn, and G. Ebest, *J. Appl. Phys.* **97**, 093707 (2005).
- ¹¹¹ D. Konig, D. R. T. Zahn, and G. Ebest, *Appl. Surf. Sci.* **234**, 222 (2004).
- ¹¹² D. Konig, D. R. T. Zahn, R. Reich, K. Gottfried, and G. Ebest, Proc. of the 3rd WCPEC, Osaka, Japan, (IEEE, Piscataway, NJ, 2003), p. 232.
- ¹¹³ I. Martin, M. Vetter, A. Orpella, J. Puigdollers, A. Cuevas, and R. Alcubilla, *Appl. Phys. Lett.* **79**, 2199 (2001).

- ¹¹⁴ I. Martin, M. Vetter, A. Orpella, C. Voz, J. Puigdollers, and R. Alcubilla, *Appl. Phys. Lett.* **81**, 4461 (2002).
- ¹¹⁵ L. M. Doeswijk, H. H. C. de Moor, D. H. A. Blank, and H. Rogalla, *Appl. Phys. A* **69**, S409 (1999).
- ¹¹⁶ B. S. Richards, J. E. Cotter, and C. B. Honsberg, *Appl. Phys. Lett.* **80**, 1123 (2002).
- ¹¹⁷ M. Vetter, R. Ferre, I. Martin, P. Ortega, R. Alcubilla, R. Petres, J. Libal, and R. Kopecek, Proc. of the 4th WCPEC, Hawaii, (IEEE, Piscataway, NJ, 2006), p. 1271.
- ¹¹⁸ R. Ferre, I. Martin, P. Ortega, M. Vetter, I. Torres, and R. Alcubilla, *J. Appl. Phys.* **100**, 073703 (2006).
- ¹¹⁹ E. Schneiderlochner, R. Preu, R. Ludemann, and S. W. Glunz, *Prog. Photovoltaics* **10**, 29 (2002).
- ¹²⁰ P. Engelhart, N. P. Harder, R. Grischke, A. Merkle, R. Meyer, and R. Brendel, *Prog. Photovoltaics* **15**, 237 (2007).
- ¹²¹ M. A. Blauw, P. J. W. van Lankvelt, F. Roozeboom, M. C. M. van de Sanden, and W. M. M. Kessels, *Electrochem. Sol. State Lett.* **10**, H309 (2007).
- ¹²² J. Rentsch, C. Schetter, H. Schlemm, K. Roth, and R. Preu, Proc. of the 20th European PVSEC, Barcelona, (WIP Renewable Energies, Munich, 2005), p. 639.
- ¹²³ D. Jurbergs, E. Rogojina, L. Mangolini, and U. Kortshagen, *Appl. Phys. Lett.* **88**, 233116 (2006).

Chapter 2^{*}

Industrial High-Rate (~5 nm/s) Deposited Silicon Nitride Yielding High-Quality Bulk and Surface Passivation under Optimum Antireflection Coating Conditions

High-quality surface and bulk passivation of crystalline silicon solar cells has been obtained under optimum antireflection coating properties by silicon nitride ($a\text{-SiN}_x\text{:H}$) deposited at very high deposition rates of ~5 nm/s. These $a\text{-SiN}_x\text{:H}$ films were deposited using the expanding thermal plasma (ETP) technology under regular processing conditions in an inline industrial-type reactor with a nominal throughput of 960 solar cells/hour. The low surface recombination velocities (50-70 cm/s) were obtained on *p*-type silicon substrates (8.4 Ωcm resistivity) for as-deposited and annealed films within the broad refractive index range of 1.9-2.4, which covers the optimum bulk passivation and antireflection coating performance reached at a refractive index of ~2.1.

* Published as: B. Hoex, A.J.M. van Erven, R.C.M. Bosch, W.T.M. Stals, M.D. Bijker, P.J. van den Oever, W.M.M. Kessels, M.C.M. van de Sanden, Progr. Photovoltaics **13**, 705 (2005).

I. Introduction

Silicon nitride ($\text{a-SiN}_x\text{:H}$) has become the state-of-the-art antireflection coating for crystalline silicon solar cells as, ideally, this coating does not only reduce reflection losses, but simultaneously provides surface and bulk passivation. The current challenges are, however, reaching an optimum level of both surface and bulk passivation under optimum antireflection coating performance as well as depositing the $\text{a-SiN}_x\text{:H}$ at high deposition rates.

The combination of lowering the reflection losses and passivating bulk defects by the $\text{a-SiN}_x\text{:H}$ is already inevitable for reaching state-of-the-art, optimized efficiencies for multicrystalline silicon solar cells, which are dominating today's solar cell market.¹ However, within the current trend towards thinner silicon solar cell substrates and high-efficiency solar cell schemes,² passivation of the (front and back) surface will also become important for multicrystalline silicon solar cells. Surface passivation can be reached by $\text{a-SiN}_x\text{:H}$ films,³ but optimal levels of surface passivation are generally achieved for films with a refractive index $n \geq 2.4$, which, as a consequence, show considerable absorption in the ultraviolet part of the solar spectrum. For this reason, present surface passivation schemes used in industry for monocrystalline silicon solar cells still often involve thermal oxides (requiring a long processing time), possibly combined with an $\text{a-SiN}_x\text{:H}$ antireflection coating to reduce reflection losses.^{4,5} Therefore it is obvious that the photovoltaic community is persistent in their efforts to combine high-quality bulk and surface passivation and optimized antireflection properties in one single $\text{a-SiN}_x\text{:H}$ film.

The second challenge, i.e., depositing the $\text{a-SiN}_x\text{:H}$ films at high deposition rates, is probably as important from a cost-perspective. To reach economy-of-scale, high production throughputs are required for solar cell manufacturing, while these should be obtained with minimal investments in production equipment. Improving throughput by simply duplicating the number of production lines is, consequently, not a preferable option. Instead, by employing a technique with a high deposition rate, high production volumes can be achieved using equipment with a relatively small footprint and decreased (costly) vacuum volume.

In this present work, the main focus will be on obtaining a high-quality surface passivation by depositing $\text{a-SiN}_x\text{:H}$ in an industrial reactor under conditions applicable for "standard" industrial-type solar cells such as, e.g., screen-printed multicrystalline silicon solar cells. The level of surface passivation is usually expressed in terms of effective surface recombination velocity S_{eff} as reached on low-resistivity float zone silicon wafers (generally p -type). In lab-scale experiments, values of S_{eff} as low as 4 cm/s have been obtained for Si-rich films ($n=2.3\text{-}2.4$),⁶ while higher S_{eff} values are found when going to a lower refractive index.^{7,8} An exception to this trend has been found by Schmidt *et al.* who reached the lowest S_{eff} for stoichiometric films (<10 cm/s for $n=1.9$) in a

standard lab reactor.⁹ This different passivation behavior was attributed to the admixing of a significant amount of nitrogen gas to the commonly used reactant mixture of silane and ammonia. For industrial(-like) inline reactors, the general trend of a decreasing S_{eff} with increasing refractive index is also observed. However, recently fairly high levels of surface passivation have also been reported for a-SiN_x:H films with a commercially interesting refractive index (~ 50 cm/s for $n = 2.0\text{-}2.1$) deposited in a reactor with a microwave plasma source.^{10,11} In a similar reactor, Winderbaum *et al.* found the highest level of surface passivation for a-SiN_x:H with a low refractive index ($n=1.9$) but only after thermal treatment.¹² Their as-deposited a-SiN_x:H showed almost no surface passivation irrespective of the refractive index of the films. It is important to note that these aforementioned results were all obtained for a-SiN_x:H films deposited at deposition rates well below 1 nm/s.⁹⁻¹²

In this article we will show that a-SiN_x:H films deposited in an *industrial* inline PECVD system employing the expanding thermal plasma (ETP) technique can achieve good surface passivation as well as excellent bulk passivation and reduction of reflection losses with a *single* a-SiN_x:H film deposited at very high deposition rates of ~ 5 nm/s.

II. High-Rate Deposition with the Expanding Thermal Plasma Technique

The expanding thermal plasma (ETP) technique is renowned for the high deposition rates that can be achieved for films of various materials including a-SiN_x:H.^{13,14} The reason that these high deposition rates can be achieved is due to the fact that plasma production takes place in an upstream plasma source operated at subatmospheric pressure. At this high pressure, plasma production is very effective (with ionization degrees up to 10% and dissociation degrees up to 100% when molecular gases are used). This results in large flows of reactive ions and/or neutrals once the plasma expands into a downstream, low-pressure region. In this region, the large “amount of reactivity” can be used to dissociate large flows of deposition precursor gases such as NH₃ and SiH₄ for a-SiN_x:H. The downstream pressure is typically 20 Pa (comparable to other plasma techniques) and is sufficiently low to avoid heavy gas phase polymerization. Besides the high deposition rates, the ETP technique has also other advantages: due to the pressure difference, the plasma source is not affected by the downstream conditions, which prevents drift in operation. Also the fact that the source is dc operated is beneficial in this respect. The “remote” nature of the ETP technique also allows for easier optimization of processing conditions and more freedom in reactor and substrate design and size. Finally, ion bombardment of the substrate is virtually absent as there is no electrical power coupling into the downstream plasma.

The application of the ETP technology for depositing antireflection coatings on

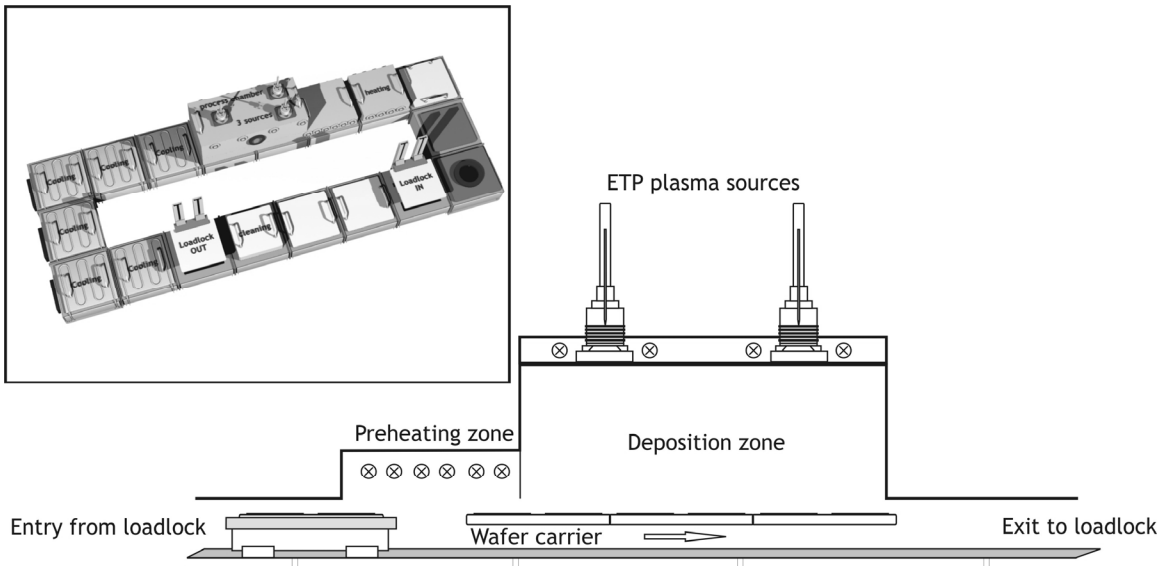


Figure 1: Schematic cross-section of the DEPx inline a-Si_x:H deposition system showing the pre-heating zone, deposition zone with expanding thermal plasma sources, and cooling zone. As indicated in the figure, the wafer carriers are propelled individually but in the depositing zone the carriers are lined up such that deposition on the carriers takes place in a continuous process. The inset shows a schematic overview of the DEPx system.

silicon solar cells has been investigated for N₂-SiH₄ and NH₃-SiH₄ reactant mixtures. Initial studies revealed that the technique was capable of reducing reflection losses¹³ and inducing bulk passivation.¹⁴ Evidence for bulk passivation was obtained by local internal-quantum-efficiency (IQE) measurements, however, the level of bulk passivation still lagged behind compared to state-of-the-art a-SiN_x:H films used as a reference. Apart from a poor uniformity (caused by the use of only one plasma source in a not-optimized lab-reactor), the mass density of the films turned out to be a critical parameter as a clear correlation was observed between the level of bulk passivation reached and the mass density of the a-SiN_x:H.¹⁵ Although increasing the mass density of a-SiN_x:H films is not trivial for high deposition rates, high mass densities (up to 2.5 g/cm³) have finally been reached after elaborate optimization studies and by implementing the ETP technique in an industrial inline PECVD reactor. This is the so-called DEPx system (OTB Solar)¹⁶ that is also used in this study.

As schematically depicted in Fig. 1, in the DEPx silicon solar cell wafers are placed on carriers which are propelled electromagnetically through different reactor zones. The carriers, which can hold 2×2 solar cell wafers with a size of 15.7×15.7 cm² each, are first heated to the desired deposition temperature (typically 400-450 °C) by infrared radiation in the pre-heating zone. Subsequently, the solar cell wafers enter the deposition zone containing three ETP plasma sources operated on pure Ar and a typical DC current of 40-70 A.¹⁶ The process gases NH₃ and SiH₄ are injected into the plasma jet emanating

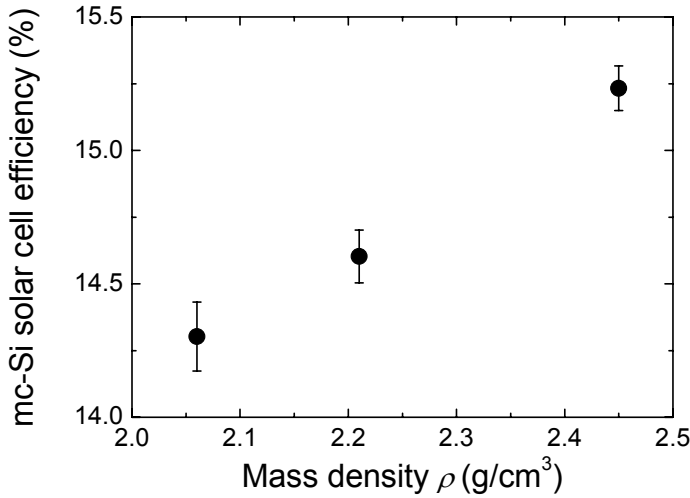


Figure 2: Efficiency of multicrystalline silicon solar cells (averaged over 10 cells) as a function of the mass density ρ of the a-SiN_x:H antireflection coating.¹⁷ The mass density of the a-SiN_x:H films, measured by Rutherford backscattering analysis, is varied by changing the deposition temperature of the solar cells from 300 to 425 °C. The thickness of the films was tuned such that the reflectivity of the solar cells was minimized for small changes in refractive index.

from the ETP source and are cracked down into reactive growth precursors leading to an a-SiN_x:H film with a uniformity of $\pm 2.5\%$ over the total carrier width. The deposition zone is kept at a pressure of ~ 20 Pa by a two-stage rootsblower system with a high pumping capacity. The deposition temperature is maintained constant by infrared radiation until the solar cell wafers enter the cooling zone. The throughput of the system is 960 solar cell wafers/hr corresponding with a typical a-SiN_x:H deposition rate of ~ 5 nm/s.

III. Bulk and Surface Passivation under Optimum Antireflection Coating Conditions

With the DEPx system, multicrystalline silicon solar cells with an a-SiN_x:H antireflection coating have been produced using a standard industrial process involving contact-screenprinting, an aluminum back surface field, and surface texturing. In Fig. 2 the efficiency of the solar cells is shown for the high mass density a-SiN_x:H films deposited at deposition temperatures in the range of 300-425 °C. This figure shows that efficiencies up to 15.3% have been obtained (as averaged over 10 solar cells) when a-SiN_x:H with a mass density of 2.45 g/cm³ is used.¹⁷ These solar cells results show that

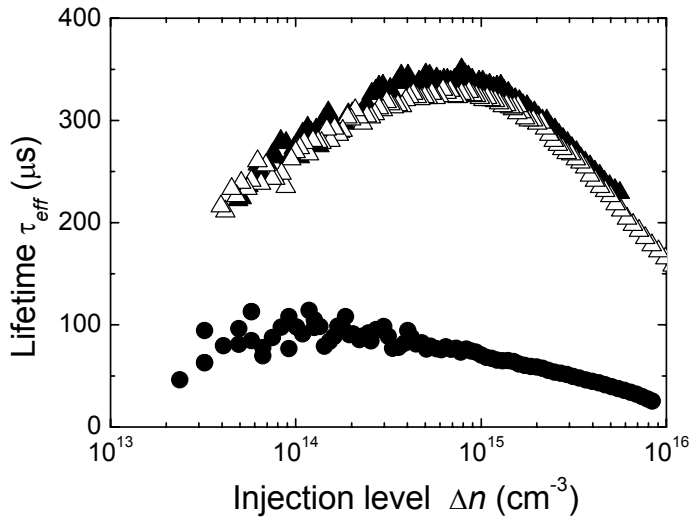


Figure 3: The effective carrier lifetime τ_{eff} as a function of the injection level Δn of a-SiNx:H passivated p-type float zone Si wafers ($8.4 \Omega\text{cm}$ resistivity). Results are given for an a-SiN_x:H film deposited at a temperature of ~ 350 °C (closed circles) and for an a-SiN_x:H film deposited at a temperature of ~ 425 °C before (closed triangles) and after (open triangles) a standard industrial firing process. The refractive index of both films is ~ 2.2 .

the very high-rate deposited a-SiN_x:H films can compete with low-rate ($\ll 1$ nm/s) a-SiN_x:H films yielding a top solar cell efficiency of 15.5% in a reference experiment. Furthermore, Fig. 2 again confirms our previous proposition that high mass densities are essential for obtaining a high level of bulk passivation and, therefore, for obtaining high-efficiency multicrystalline silicon solar cells.^{15,18}

The surface passivation induced by the a-SiN_x:H films deposited by the DEPx system has been investigated without further optimization of the deposition process. To this end, the carrier lifetime was measured in double-polished *p*-type float zone silicon wafers with (100) surface orientation, a resistivity of $8.4 \Omega\text{cm}$, and a thickness of 380 μm . The wafers were cleaned using a standard RCA clean followed by a HF-dip and were coated on both sides with an identical a-SiN_x:H film of 50-80 nm thickness. The carrier lifetime was measured using a contactless inductively coupled photoconductance tester (Sinton Consulting, WCT100) that was used in both photoconductance decay mode (PCD) as well as in quasi-steady-state photoconductance (QSSPC) mode in which the reflectivity of the wafers was taken into account.¹⁹ A typical lifetime measurement as a function of the injection level is shown in Fig. 3, which reveals that lifetimes up to 350 μs can be reached for the high-rate deposited a-SiN_x:H. In this figure also data is given for the

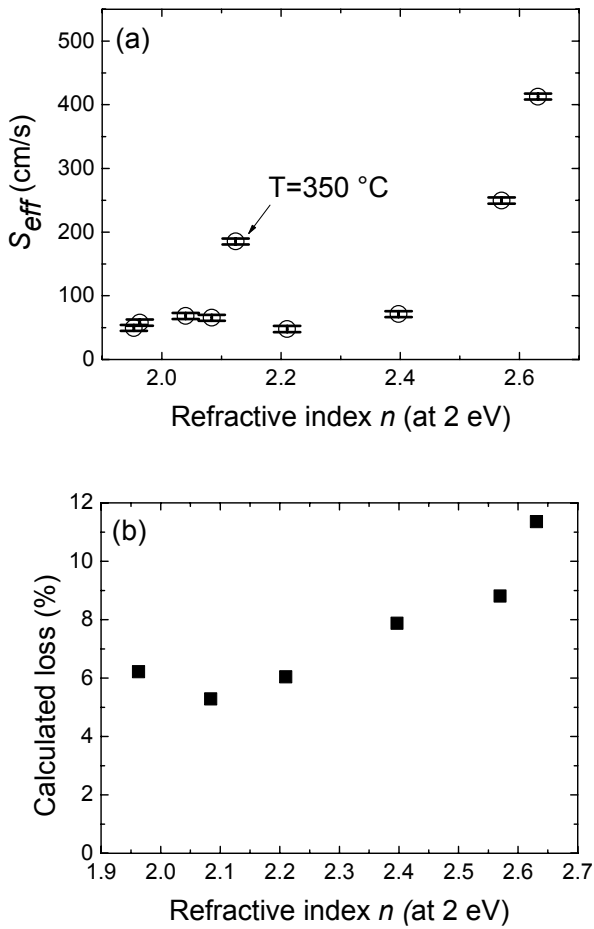


Figure 4: (a) The effective surface recombination velocity S_{eff} at an injection level of $2\text{--}5 \times 10^{14}$ cm⁻³ and (b) the calculated photon loss by reflection and absorption of the a-SiN_x:H under glass, using the method of Doshi *et al.*²⁰ as a function of the refractive index n of the a-SiN_x:H at a photon energy of 2 eV. Due to the small size the error bars are omitted. All a-SiN_x:H films have been deposited at ~425 °C apart from the film for which the temperature is indicated.

lifetimes obtained after a high-temperature (>750 °C) firing step of the a-SiN_x:H in a standard metallization firing furnace revealing the thermal stability of the material. From the lifetime measurements the effective surface recombination velocity S_{eff} was calculated for a typical injection level of $2\text{--}5 \times 10^{14}$ cm⁻³ by assuming a realistic bulk lifetime of 4 ms.²¹ Upper and lower error margins for S_{eff} were evaluated assuming an infinite bulk lifetime and the lower lifetime limit of 2 ms for the Si material, respectively. The surface recombination velocity has been determined for as-deposited a-SiN_x:H films with a refractive index ranging from 1.9 to 2.7 obtained by changing the NH₃/SiH₄ ratio in the

plasma. The refractive index as well as the absorption coefficient and film thickness were determined by means of spectroscopic ellipsometry (Woollam M2000) over a photon energy range of 0.7 – 5.0 eV. The ellipsometry data were analyzed by a simple two-layer optical model (bulk film with surface roughness) and using the Tauc-Lorentz formalism.²² In Fig. 4(a) the values of S_{eff} are shown as a function of the refractive index of the films at a photon energy of 2 eV. The corresponding antireflection coating performance for optimized film thickness was determined from the films' optical properties by calculating the absorption and reflection losses weighted over the air mass global 1.5 solar spectrum range (360-1100 nm).²⁰ These results are shown in Fig. 4(b).

The surface recombination velocities S_{eff} obtained range from ~50 to ~425 cm/s and are more than one order of magnitude lower compared to the best reported values for ETP deposited a-SiN_x:H so far.¹³ Interestingly, the lowest S_{eff} values are reached for the refractive index range of $n = 1.95\text{--}2.4$ in which S_{eff} is basically constant. This range is the most appropriate for solar cell applications while for the widely applied refractive index of $n=2.1$ S_{eff} is comparable to the state-of-the-art S_{eff} values obtained in other industrial-type reactors for somewhat lower resistivity wafers.¹⁰⁻¹² An important difference between the a-SiN_x:H films is, however, that the films deposited by the ETP technique in the DEPx reactor are deposited at significant higher deposition rate of ~5 nm/s. Figure 4(a) shows also directly the impact of the deposition temperature on the level of surface passivation obtained. S_{eff} increases significantly (from 60 cm/s to 180 cm/s) when the deposition temperature is decreased from 425 °C to 350 °C. As mentioned earlier, such a large effect was also observed for the level of bulk passivation (see Fig. 2)¹⁴ and it possibly indicates that a high mass density is also important for surface passivation. Furthermore, it has to be mentioned that the unexpected increase in S_{eff} when going to a refractive index $n > 2.4$ can possibly be attributed to the fact that no process optimization for the deposition of these high index a-SiN_x:H films has taken place.

When combining the data on the surface recombination velocity with the reflection and absorption losses induced by the a-SiN_x:H films under glass, it is clear that a good level of surface passivation can be obtained under conditions where simultaneously optimum antireflection coating performance can be reached ($n = \sim 2.1$). These conditions also yield a high level of bulk passivation for multicrystalline silicon solar cells as recently reported in a separate study.¹⁷

IV. Conclusions

It has been shown that a-SiN_x:H films deposited with an industrial inline PECVD reactor employing the Expanding Thermal Plasma technique lead to relatively low surface recombination velocities of 50-70 cm/s on 8.4 Ωcm p-type c-Si wafers. These results are achieved for a broad refractive index range of $n=1.95\text{--}2.4$ and are not affected by a standard industrial firing process. The combination of these results with the optical

properties of the films and with the results on multicrystalline silicon solar cells shows that a good level of surface and bulk passivation can be reached simultaneously under optimal antireflection coating conditions and even for very high deposition rates of ~5 nm/s. Furthermore, the results show once again that a high a-SiN_x:H film density is key for solar cell applications.

ACKNOWLEDGMENTS

This study has been carried out within the E.E.T.-program “HR-CEL” funded by the Netherlands Ministry of Economic Affairs, the Ministry of Education, Culture and Science and the Ministry of Public Housing, Physical Planning and Environment. The research of W.K. has been made possible by a fellowship of the Royal Netherlands Academy of Arts and Sciences (KNAW).

REFERENCES:

- ¹ G.P. Willeke, Proc. of the 19th EU-PVSEC, Paris, (WIP Renewable Energies, Munich, 2004), p. 383.
- ² O. Schultz, S. W. Glunz, and G. P. Willeke, Prog. Photovoltaics **12**, 553 (2004).
- ³ A. G. Aberle, Prog. Photovoltaics **8**, 473 (2000).
- ⁴ J. H. Zhao, A. H. Wang, M. A. Green, and F. Ferrazza, Appl. Phys. Lett. **73**, 1991 (1998).
- ⁵ P. M. Mulligan, D. H. Rose, M. J. Cudzinovic, and D. M. de Ceuster, Proc. of the 19th EU-PVSEC, Paris, (WIP Renewable Energies, Munich, 2004), p. 387.
- ⁶ T. Lauinger, J. Schmidt, A. G. Aberle, and R. Hezel, Appl. Phys. Lett. **68**, 1232 (1996).
- ⁷ T. Lauinger, J. Moschner, A. G. Aberle, and R. Hezel, J. Vac. Sci. Technol. A **16**, 530 (1998).
- ⁸ J. Schmidt, IEEE Trans. Electron. Dev. **46**, 2018 (1999).
- ⁹ J. Schmidt and M. Kerr, Sol. Energy Mater. Sol. Cells **65**, 585 (2001).
- ¹⁰ A. W. Weeber, H. C. Rieffe, W. C. Sinke, and W. J. Soppe, Proc. of the 19th EU-PVSEC, Paris, (WIP Renewable Energies, Munich, 2004), p. 1005.
- ¹¹ J. D. Moschner, J. Henze, J. Schmidt, and R. Hezel, Prog. Photovoltaics **12**, 21 (2004).
- ¹² S. Winderbaum, A. Cuevas, F. Chen, J. Tan, K. Hanton, D. Macdonald, and K. Roth, Proc. of the 19th EU-PVSEC, Paris, (WIP Renewable Energies, Munich, 2004), p. 576.
- ¹³ W. M. M. Kessels, J. Hong, F. J. H. van Assche, J. D. Moschner, T. Lauinger, W. J. Soppe, A. W. Weeber, D. C. Schram, and M. C. M. van de Sanden, J. Vac. Sci. Technol. A **20**, 1704 (2002).
- ¹⁴ J. Hong, W. M. M. Kessels, F. J. H. van Assche, H. C. Rieffe, W. J. Soppe, A. W. Weeber, and M. C. M. van de Sanden, Prog. Photovoltaics **11**, 125 (2003).
- ¹⁵ J. Hong, W. M. M. Kessels, W. J. Soppe, A. W. Weeber, W. M. Arnoldbik, and M. C. M. van de Sanden, J Vac Sci Technol B **21**, 2123 (2003).
- ¹⁶ R.C.M Bosch, W.T.M. Stals, A.J.M. Van Erven, R.L.J.R. Pennings, and M.D. Bijker, Proc. of the 19th EU-PVSEC, Paris, (WIP Renewable Energies, Munich, 2004), p. 1098.
- ¹⁷ A.J.M. Van Erven, R.C.M. Bosch, R. Toelle, O. Voigt, S. Petri, and M.D. Bijker, Proc. of the 31st IEEE PVSEC, Lake Buena Vista, (IEEE, Piscataway, NJ, 2005), p. 945.
- ¹⁸ W. M. M. Kessels, P.J. Oever, B. Hoex, R.C.M Bosch, A.J.M. Van Erven, M.D. Bijker, and M. C. M. van de Sanden, Proc. of the 31st IEEE PVSEC, Lake Buena Vista, FL, (IEEE, Piscataway, NJ, 2005), p. 1253.
- ¹⁹ R. A. Sinton and A. Cuevas, Appl. Phys. Lett. **69**, 2510 (1996).

-
- ²⁰ P. Doshi, G. E. Jellison, and A. Rohatgi, *Appl. Optics* **36**, 7826 (1997).
- ²¹ J. Schmidt and A. G. Aberle, *J. Appl. Phys.* **81**, 6186 (1997).
- ²² G. E. Jellison and F. A. Modine, *Appl. Phys. Lett.* **69**, 371 (1996).

Chapter 3^{*}

High-Rate Plasma Deposited SiO₂ Films for Surface Passivation of Crystalline Silicon

SiO₂ films were deposited by means of the expanding thermal plasma technique at rates in the range of 0.4-1.4 μm/min using an argon/oxygen/octamethylcyclotetrasiloxane (OMCTS) gas mixture. The film composition was studied by means of various optical and nuclear profiling techniques. The films deposited with a low OMCTS to oxygen ratio showed no residual carbon and a low hydrogen content of ~2% with a refractive index close to thermal oxide. For a higher OMCTS to oxygen ratio a carbon content of ~4% was detected in the films and the refractive index increased to 1.67. The surface passivation of the SiO₂ films was tested on high quality crystalline silicon. The films yielded an excellent level of surface passivation for plasma-deposited SiO₂ films with an effective surface recombination velocity of 54 cm/s on 1.3 Ω cm *n*-type float zone crystalline silicon substrates after a 15 min forming gas anneal at 600 °C.

* Published as: B. Hoex, F.J.J. Peeters, M. Creatore, M.A. Blauw, W.M.M. Kessels, M.C.M. van de Sanden, J. Vac. Sci. Technol. A **24**, 1823 (2006).

I. Introduction

To further decrease the cost of energy from crystalline silicon (c-Si) solar cells, the c-Si solar cell wafer thickness is reduced and higher conversion efficiencies schemes are explored. For this purpose, both the optical and electrical quality of the c-Si solar cell wafer have to be optimized. SiO₂ is the material of choice to meet these requirements and is already effectively used in the world-record efficiency c-Si solar cell produced by the University of New South Wales.¹ Thermally grown SiO₂ has an ideal refractive index to maximize internal reflection at the back of the solar cell. The surface passivation of the as-grown SiO₂ is rather poor due to a relative high interface defect density, but is significantly improved by a postdeposition anneal in a hydrogen containing gas (forming gas anneal). The best level of surface passivation is, however, obtained by evaporating a sacrificial high quality aluminum film (0.1-1 μm) on the SiO₂ and subsequently annealing the Si substrate at 350-400 °C. In this so-called *alneal* step, atomic hydrogen resulting from the aluminum oxidation process passivates defects states at the interface between c-Si and SiO₂.² Application-wise, the main disadvantages in obtaining a passivating thermal SiO₂ are the long and elaborate processing and the high temperatures in the range of 1000-1100 °C that can deteriorate the wafer bulk quality, especially for lower quality substrate material [e.g. Czochalski c-Si or multi-c-Si(mc-Si)]. Recently, these disadvantages were partly solved by using a wet oxidation process at 800 °C that resulted in the world-record mc-Si solar cell.³ However, the processing times were still in the order of hours due to the requirement of a rather thick SiO₂ film of ~100 nm for optimal optical performance at the back of the solar cell. The application of a plasma-deposited SiO₂ film, obtained in a low temperature process and with a good level of surface passivation, might form a solution to reduce the processing time needed.

SiO₂ films synthesized by plasma enhanced chemical vapor deposition (PECVD) already have numerous technological applications. They are used as a dielectric in complementary metal-oxide-semiconductor CMOS devices,⁴ as an oxygen and water permeation barrier on polymers,^{5,6} as a scratch resistant coating for, e.g., car glazing and as protective layer for semiconductor devices.^{7,8} In the field of microelectronics a lot of effort is put in the development of plasma-deposited SiO₂ films with a low interface defect density. This has led to plasma-deposited SiO₂ films with an interface defect density of $\sim 5 \times 10^{10} \text{ cm}^{-2} \text{ eV}^{-1}$ after an *alneal* at 400 °C.⁹ These SiO₂ films also showed excellent surface passivation on nearly intrinsic ($> 500 \Omega \text{ cm}$) *n*-type c-Si.¹⁰ However, for the production of solar cells generally lower resistivity wafers are used and it is well known that the level of surface passivation is strongly dependent on the substrate doping level. The effective surface recombination velocity on the commonly used *p*-type c-Si substrates with a resistivity of 1 Ω cm was only in the range of 700 cm/s.¹¹ Leguit *et al.* and Sivoththaman *et al.* were able to reach minimal effective surface recombination velocities of ~100 cm/s on moderately doped *p*- or *n*-type c-Si.^{12,13} However, for higher

doping levels the effective surface recombination velocity strongly increases.^{12,13} It should be noted that the surface passivation of the as-deposited SiO₂ films in all these studies was rather poor and a 20 min or 15 h anneal at 350-400 °C in a forming gas (commonly 10% H₂ in nitrogen) was required to achieve the reported level of surface passivation.¹¹⁻¹³ Furthermore, a forming gas anneal or *anneal* is also essential to obtain a good level of surface passivation for both wet or dry thermal oxide.^{3,14}

In the aforementioned studies of the surface passivation of plasma deposited SiO₂ films, SiH₄-O₂ or SiH₄-N₂O gas mixtures were used to deposit the SiO₂ films.¹¹⁻¹³ However, also organosilicons such as tetraethoxysilane (TEOS), hexamethyldisiloxane (HMDSO) or octamethylcyclotetrasiloxane (OMCTS) can be used for the deposition of SiO₂ films. Organosilicons are relatively inexpensive, nonflammable and have a low toxicity rating; hence, no special safety installation is required as in the case of SiH₄. Films deposited using organosilicons also give a better step coverage compared to films deposited with SiH₄.¹⁵ A possible disadvantage of using organosilicons for SiO₂ deposition is that carbon and water related impurities can be built into the film that can influence the electrical performance.¹⁶

In this study we used OMCTS in combination with an Ar-O₂ mixture as SiO₂ growth precursor. OMCTS is an inexpensive, relatively nonhazardous liquid and has four cyclic Si-O groups and eight methyl groups. The desired Si-O-Si groups are already present in the molecule and OMCTS has a higher Si-O to carbon ratio than, e.g., TEOS. OMCTS was, for example, already used for the deposition of low-*k* (*k*=2.8-3.2) carbon doped silicon oxide films by Ross *et al.*¹⁷ Rau *et al.*¹⁸ and Qi *et al.*¹⁹ used several organosilicons to deposit SiO₂-like films and found that films deposited using OMCTS showed the lowest carbon content. Nearly stoichiometric SiO₂-like films could be deposited using an O₂/OMCTS ratio of eight.¹⁹ An extensive material characterization of SiO₂-like films deposited by using OMCTS was reported by Zajickova *et al.*, where the impact of an additional substrate bias on the SiO₂ material quality was studied in detail.²⁰ In this article we will show that SiO₂ films with a low impurity content and a high level of surface passivation can be deposited by means of the expanding thermal plasma technique using an Ar-O₂-OMCTS mixture. First the SiO₂ films deposited for a varying OMCTS/O₂ ratio will be considered and their film properties studied by various optical and nuclear profiling techniques will be reported. Subsequently, the level of surface passivation of the SiO₂ films will be addressed on low resistivity *n*-type substrates. Finally, the effect of a post thermal treatment in a forming gas on the level of surface passivation and the composition of the films will be reported.

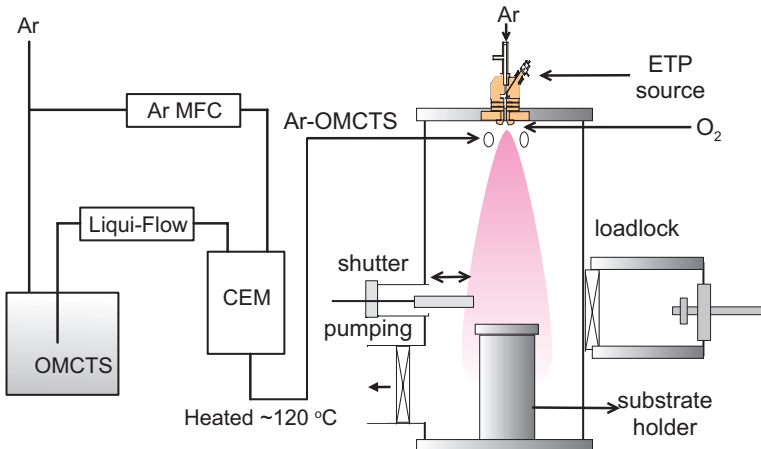


Figure 1: Schematic top view of the expanding thermal plasma (ETP) setup used for the deposition of SiO_2 films from $\text{Ar}/\text{O}_2/\text{octamethyltetrcyclosiloxane}$ (OMCTS) mixtures.

II. Experimental Details

A. Expanding thermal plasma setup

The SiO_2 films were deposited using a laboratory-scale reactor employing the expanding thermal plasma (ETP) technique, as shown in Fig. 1. This setup is already described extensively in the literature (see, e.g., van Hest *et al.*²¹) and will, therefore, only be addressed briefly here. An Ar plasma is created at subatmospheric pressures (typically 0.5-0.7 bar) in the ETP source and then expands supersonically through a nozzle into the deposition chamber, which is kept at a low pressure of 0.3-0.5 mbar by a two-stage roots blower system. Overnight the system is evacuated by a turbo molecular pump to a base pressure of $< 10^{-5}$ mbar. Via the nozzle O_2 [0-200 sccm (sccm denotes standard cubic centimeter per minute at STP)] is injected into the plasma expansion. Finally an Ar-OMCTS mixture is fed into the plasma at ~5 cm from the plasma source by an injection ring. The OMCTS flow rate (4-200 g/h, 6-280 sccm) is set by means of a Bronkhorst liquid flow meter (L2) and is thereafter evaporated (boiling point 176 °C at 1 bar) and mixed with Ar (0-500 sccm) in a controlled evaporation module (CEM, Bronkhorst W-202A) operating at 95 °C. The Ar-OMCTS mixture is transported to the reaction chamber in a heated line (~120 °C) to prevent condensation. The substrates are placed in the deposition chamber via a load-lock system with a base pressure of $< 10^{-5}$ mbar. The substrate holder can be heated up to 400 °C by means of resistive heating element. Good thermal contact between the substrate and the chuck is ensured by a He back flow (~100 sccm) allowing a temperature control within < 10 °C during plasma deposition as confirmed by means of infrared interferometry.²²

B. Film analysis

The films analyzed in this study were deposited on single side polished 10-20 Ω cm *p*-type Cz c-Si substrates with a <100> orientation. The substrates were ultrasonically cleaned in ethanol for 40 min and blown dry with N₂ prior to deposition. In case of the Rutherford backscattering (RBS) measurements, the substrates were immersed in a diluted HF solution (5%) prior to deposition to remove the native oxide. The films were measured both *in situ* and *ex situ* by spectroscopic ellipsometry (Woollam M2000) in the 250-1000 nm wavelength range. The data was analyzed by a three layer model consisting of the c-Si substrate with native oxide, the SiO₂ layer with the dielectric function described with the Tauc-Lorentz formalism,²³ and a surface roughness layer described by the Bruggeman effective medium approximation assuming a mixture of 50% bulk layer and 50% voids. More information about the surface roughness was obtained by atomic force microscopy (NT-MDT Solver P49 pro). Infrared absorption spectra were measured by Fourier transform infrared (FTIR) spectroscopy (Bruker Vector 22) in the 370-8000 cm⁻¹ range with a resolution of 4 cm⁻¹. The measurements were taken at normal incidence both prior to and after deposition to obtain a reliable background of the transmission spectrum. At least 20 spectra were averaged to obtain a sufficiently high signal-to-noise ratio. The absorption spectrum of the SiO₂ film was deduced by taken into account interference effects in the films.²⁴ The atomic composition of the films was obtained from RBS and elastic recoil detection (ERD) measurements. For the RBS/ERD measurement a monoenergetic beam of high energy He⁺ ions (2 MeV) was directed at the sample at normal incidence in the case of RBS or at 75° with respect to the normal for ERD.²⁵ The impurity content of the SiO₂ films was further investigated by dynamic secondary ion mass spectrometry (SIMS) using a 3 keV O₂⁺ primary beam with a current of 180 nA on a 180 μm^2 spot size.²⁶

C. Surface passivation

The surface passivation of the SiO₂ films was tested on double-side polished float zone 1.3 Ω cm *n*-type FZ c-Si substrates with a thickness of 380 μm . The c-Si substrates were cleaned using a conventional radio corporation America (RCA) clean and received a final cleaning step in diluted HF (5%) prior to the deposition.⁸ A SiO₂ film was deposited on both sides of the c-Si wafer and the effective lifetime of the charge carriers in the lifetime sample was determined by means of the photoconductance decay method (Sinton WCT100). These measurements were performed both in transient and quasi-steady-state mode taking the reflectivity of the wafer into account.²⁷ The effective surface recombination velocity was calculated by assuming an infinite bulk lifetime in the float zone c-Si substrates.

Table I: Spectroscopic ellipsometry results for SiO₂ films obtained at different OMCTS flow rates. The Ar (2000 sccm) and O₂ flows (200 sccm) were set to their maximum value, while the plasma source current was 75 A. The deposition temperature was 400 °C and the deposition time was 12 s for all samples.

OMCTS flow (sccm)	Reactor pressure (mbar)	Refractive index (at 2 eV)	Extinction coefficient (at 5 eV)	Film thickness (nm)	Deposition rate (μm/min)
6.3	0.41	1.46	-	76	0.38
9.2	0.42	1.47	-	110	0.54
13.5	0.44	1.47	-	158	0.77
16.6	0.45	1.49	-	196	0.98
19.5	0.46	1.52	0.02	224	1.12
28.3	0.49	1.67	0.15	286	1.35

The impact of a post thermal anneal on the level of surface passivation of the SiO₂ films was studied by annealing the lifetime samples in a forming gas (10% H₂ in N₂) environment in the temperature range of 400-700 °C using a rapid thermal anneal oven (AST SHS-100). The impact of a forming gas anneal (FGA) on the SiO₂ film properties was also investigated by means of FTIR and RBS.

III. Film Properties

A. Optical analysis

From our previous depositions using HMDSO as the main growth precursor, we know that a high amount of Ar⁺ ions and atomic oxygen is needed to remove the methyl groups from the organosilicon growth precursor.²⁸ For this reason the highest Ar flow rate (2000 sccm), highest plasma current (75 A) and O₂ flow rate (200 sccm) were chosen in this experiment and the OMCTS flow was varied in the range of 6-30 sccm at a substrate temperature of 400 °C. The resulting refractive index (at 2 eV), extinction coefficient (at a photon energy of 5 eV), film thickness, and deposition rates obtained at different OMCTS flows are summarized in Table I. The deposition rate of the SiO₂ films, as determined by dividing the film thickness by the deposition time, increased linearly with the OMCTS flow up to ~1.12 μm/min for an OMCTS flow of 20 sccm, as shown in Fig. 2(a). For the highest investigated OMCTS flow of 28 sccm, the deposition rate of ~1.4 μm/min was lower than expected from this linear relation. The deposition rates are comparable with the values reported by Qi *et al.* for a electron cyclotron resonance (ECR) plasma,¹⁹ although they used a higher OMCTS flow of 50 sccm. As shown in

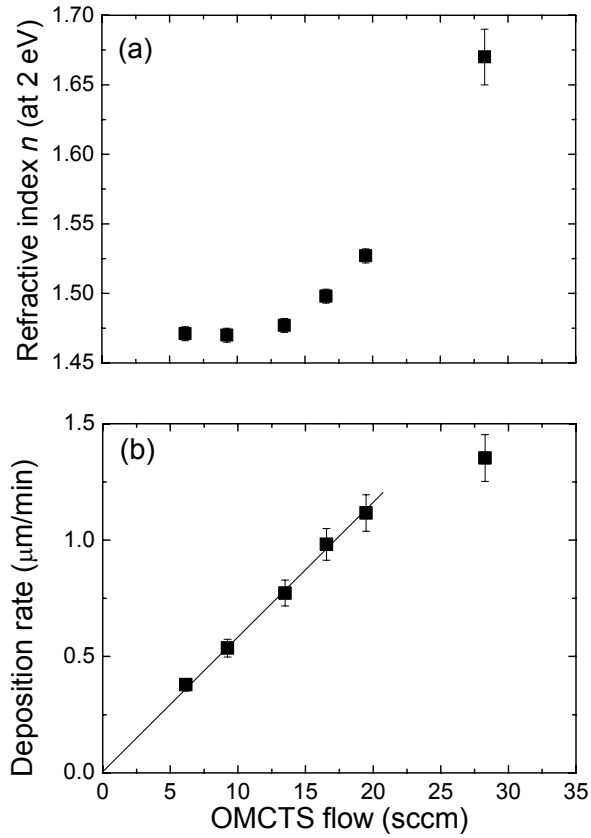


Figure 2: (a) Refractive index at a photon energy of 2 eV and (b) the deposition rate as a function of the OMCTS flow. The error bars are an indication in the variation in the obtained values. The line serves as a guide to the eye.

Fig. 2(a) the refractive index of the SiO_2 films was constant at 1.46-1.47 for a OMCTS flow up to 13 sccm and nearly equal to the refractive index of thermally grown SiO_2 ($n=1.46$ at 2 eV). When the OMCTS flow rate was increased from 13 to 28 sccm, the refractive index of the deposited SiO_2 -like film gradually increased up to 1.67 for a film deposited with an OMCTS flow of 28 sccm. This change can be explained by an change in the O/Si ratio to values below 2 and the incorporation of carbon in the film, as determined by means of RBS and summarized in Table II.²⁹ For the SiO_2 -like films deposited at the highest OMCTS flow rates, also absorption in the UV part of the spectrum had to be taken into account. However, the extinction coefficient was very moderate with a value of 0.15 at a photon energy of 5 eV for the film deposited with an OMCTS flow of 28 sccm. This also indicates a change in atomic composition of the films. No significant difference between the refractive index measured *in situ* and *ex situ* was observed, indicating no observable water uptake after exposure to air.³⁰

Table II: Atomic composition of three SiO₂ films deposited for various OMCTS flows as determined by RBS and ERD.

OMCTS flow (sccm)	[Si] (at.%)	[O] (at.%)	[H] (at.%)	[C] (at.%)	Atomic density (10 ²² at./cm ³)	Mass density (g/cm ³)
6.3	32.2	65.7	2.1	<3	6.6	2.15
9.2	32.4	65.5	2.1	<3	6.1	2.00
28.3	35.1	42.9	17.8	4±2	6.5	1.83

From the spectroscopic ellipsometry analysis the SiO₂ layers appeared to be very smooth with no significant surface roughness for low OMCTS flows. For higher OMCTS flows the surface roughness was estimated to increase up to ~4 nm. This was verified by AFM measurements. Samples with a thickness of ~200 nm were deposited for three OMCTS flows. The root mean square surface roughness of a SiO₂ film deposited with a low OMCTS flow of 6 sccm and 9 sccm was found to be ~0.5 nm. However, for a SiO₂ film deposited with an OMCTS flow of 28 sccm the RMS surface roughness increased up to ~2.4 nm.

B. Compositional analysis

To get more insight in the composition and atomic density of the SiO₂ films three samples were analyzed by means of RBS/ERD and SIMS. For this reason SiO₂ films were deposited for three OMCTS flows of 6.3, 9.2 and 28.3 sccm on HF dipped c-Si substrates keeping the other deposition conditions equal to those used in the optical analysis. The deposition time was chosen such that the resulting film thickness for all films was approximately 200 nm.

From the RBS/ERD measurements, as summarized in Table II, it is observed that the SiO₂ films deposited with a low OMCTS flow are nearly stoichiometric in composition and have a small residual hydrogen content of ~2%. The residual carbon content is below the detection limit of RBS (< 3 at.%). For the highest OMCTS flow studied, the SiO₂-like films are Si-rich and also higher levels of C (4.5 at.%) and H (17.8 at.%) are incorporated in the film. These results are comparable to the results published by Qi *et al.*¹⁹

For a more quantitative analysis of the carbon content the SiO₂ films were analyzed by means of the SIMS technique. The carbon concentration in the films deposited with a low OMCTS flow (6.3 and 9.2 sccm) was determined to be below the detection limit of 0.03 at.%. The carbon content of the SiO₂-like film deposited with an

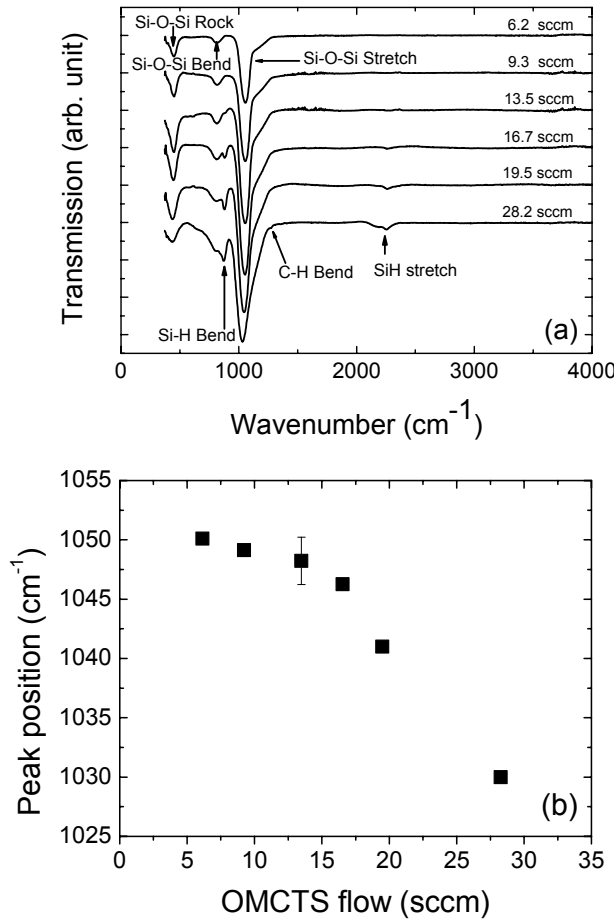


Figure 3: (a) Infrared transmission spectra of SiO_2 films deposited with various OMCTS flows. The spectra have been offset vertically for clarity. (b) Si-O-Si in plane asymmetric stretch (AS1) peak position as a function of the OMCTS flow. The typical error in the peak position is indicated for an OMCTS flow of 13 sccm.

OMCTS flow of 28.3 sccm was easily detectable and in agreement with the results obtained by RBS. Therefore, we can conclude that the SiO_2 films deposited with a low OMCTS flow do not contain a significant amount of residual carbon. However, when using higher OMCTS flow carbon is incorporated into the film.

C. Infrared analysis

Figure 3 (a) shows the infrared transmission spectra in the range of $370\text{-}4000 \text{ cm}^{-1}$ of SiO_2 films deposited for various OMCTS flows. The characteristic vibrational rocking, bending and stretching bands of Si-O-Si (as summarized in Table III) were detected in all SiO_2 films. The various absorption peaks were fitted using a Gaussian distribution and the

Table III: Infrared peak positions for the Si-O-Si, and silicon and carbon hydrides as reported in literature (AS1=asymmetric in-phase and AS2=asymmetric out-phase).

Configuration	Mode peak position (cm ⁻¹)		
	Rocking	Bending	Stretching
Si-O-Si	457 ^a	810 ^a	1076 ^a (AS1) 1200 ^a (AS2)
H-Si(O ₃)	-	860 ^b	2260 ^{b,c}
H-Si(SiO ₂)	-	835 ^b	2195 ^{b,c}
H-Si(Si ₂ O)	-	775 ^b	2108 ^{b,c}
H-Si(Si ₃)	485 ^d	630 ^b	2000 ^{b,c}
Si-CH ₃	-	1260 ^f	-
CH ₃	-	-	2960 ^e

^a Kirk, Phys. Rev. B **38**, 1255 (1988).^b L. He, Y. Kurata, T. Inokuma, and S. Hasegawa, Appl. Phys. Lett. **63** 162 (1993).^c G. Lucovsky, J. Yang, S.S. Chao, J.E. Tyler, and W. Czubatyj, Phys. Rev. B **28**, 3225 (1983).^d G. Lucovsky, S.S. Chao, J. Yang, J.E. Tyler, and W. Czubatyj, J. Vac. Sci. Technol. A **2**, 353 (1984).^e C. Rau and W. Kulisch, Thin Solid Films **249**, 28 (1994).^f N. Inagaki and M. Taki, J. Appl. Polymer Sci. **27**, 4337 (1982).

peak position of the in-phase asymmetric stretching mode (AS1 mode) is shown as a function of the OMCTS flow in Fig. 4. The AS1 mode is known to shift as a function of the composition or density of the SiO₂ films.³¹⁻³³ From Fig. 3 (b) we can learn that the peak position of the AS1 mode is approximately constant for OMCTS flows up to 13 sccm, and then continuously decreases when increasing the OMCTS flow up to 28 sccm. This is in agreement with the observed increase in the refractive index of the SiO₂ film due to the change in atomic composition as observed by RBS and summarized in Table II. The total normalized absorption in the Si-O stretch mode decreased by approximately 30% when the OMCTS flow was increased from 6 to 28 sccm, in agreement with the decrease in oxygen content as measured by RBS.

When increasing the OMCTS flow above 13 sccm also residual carbon and hydrogen was detected in the FTIR spectrum at the peak positions summarized in Table III. The hydrogen and carbon related absorptions increased as a function of the OMCTS flow rate. No O-H related absorptions (infrared absorption peak position around 3600 cm⁻¹)³⁴ were detected in the films for the FTIR measurement with 20 averages. Using a proportionality constant of 1.8×10^{20} cm⁻² for the Si-H stretching mode,³⁴ a bonded hydrogen concentration of $\sim 8 \times 10^{21}$ cm⁻³ can be calculated for the SiO₂-like film

deposited with a OMCTS flow of 28 sccm. Combining the RBS and FTIR data we can learn that most hydrogen is bonded to silicon for the SiO₂-like film deposited with the highest OMCTS flow. This is remarkable because no Si-H bonds are present in the growth precursor itself.

IV. Surface Passivation and the Impact of Annealing

A. Surface passivation by SiO₂ films

SiO₂ films deposited with OMCTS flows of 6.6 and 9.2 sccm were selected to test the surface passivation on low resistivity *n*-type c-Si. The level of surface passivation was measured prior to and after a thermal posttreatment, as shown in Fig. 4. For both deposition conditions, the surface passivation of the as-deposited SiO₂ films was rather poor with an effective surface recombination velocity of 4×10^3 cm/s. This is comparable to the values reported for SiO₂ prepared by wet oxidation,³ but higher compared to thermal SiO₂.² However, a 30 min forming gas anneal (10% H₂ in N₂) at 400 °C already improved the surface passivation to an effective surface recombination velocity of 7×10^2 cm/s and 3×10^2 cm/s for SiO₂ films deposited with a OMCTS flow 6.2 and 9.2 sccm, respectively. A similar improvement was reported on *p*-type c-Si for SiO₂ grown by wet oxidation.³ By adopting even higher annealing temperatures, the level of surface passivation kept improving. The best results were obtained by performing a 15 min forming gas anneal at 600°C leading to an optimal effective surface recombination velocity of 54 cm/s for a SiO₂ film deposited with a OMCTS flow of 9.2 sccm. For higher annealing temperatures the effective surface recombination velocity increased again, for example for a 15 min FGA at 700 °C, an effective surface recombination velocity of ~100 cm/s was obtained for a SiO₂ film deposited with a OMCTS flow of 9.2 sccm.

The obtained level of surface passivation of plasma-deposited SiO₂ films on low resistivity *n*-type substrates is significantly higher compared to the results previously reported. To the best of our knowledge, the best values reported on low resistivity *n*-type substrates were in the 100-400 cm/s range obtained on slightly higher resistivity substrates ($3\text{-}6 \Omega$),^{12,13} and it is generally found that the effective surface recombination velocity decreases for increasing wafer resistivity. The surface recombination velocity shows only a limited injection level dependence, similar to what is observed for silicon carbide, amorphous silicon and silicon nitride on low resistivity *n*-type crystalline silicon.³⁵⁻³⁷ The improvement of the surface passivation with increasing annealing temperature up to 600 °C is not in agreement with results obtained by Chen *et al.*¹⁰ They found that the optimal annealing temperature was 350 °C for their plasma-deposited SiO₂,

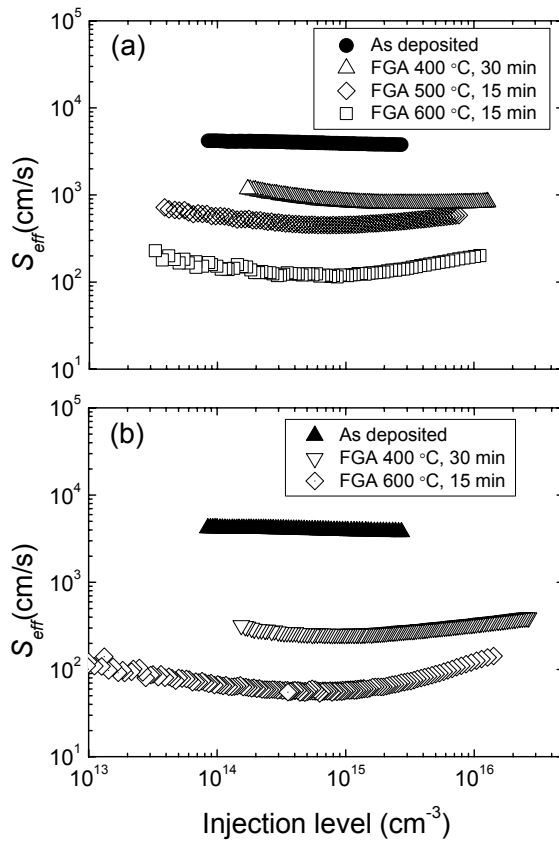


Figure 4: Effective surface recombination velocity S_{eff} as a function of the injection level for SiO_2 films deposited with OMCTS flow of (a) 6.3 sccm and (b) 9.2 sccm prior and after the forming gas anneals at the temperature indicated.

while for annealing temperatures above 350 °C the level of surface passivation significantly deteriorated. The stability of the surface passivation by plasma deposited SiO_2 is generally a concern.^{10,12,13} The level of surface passivation of our samples did not deteriorate over time and was tested to remain constant over a period of more than half a year.

For SiO_2 grown by wet or dry thermal oxidation, an anneal in forming gas or anneal is essential to maximize the level of surface passivation.^{2,3} This improvement is related to a significant reduction of the interface defect density by atomic hydrogen. In our SiO_2 films, however, already 2 at.% hydrogen is present in the films, which can diffuse during the anneal and passivate interface defect states. For this reason, some lifetime samples were annealed in a *nitrogen only* environment to investigate the impact of the presence of H_2 during the forming gas anneal. As shown in Fig. 5, no significant improvement in the effective surface recombination velocity can be observed when the

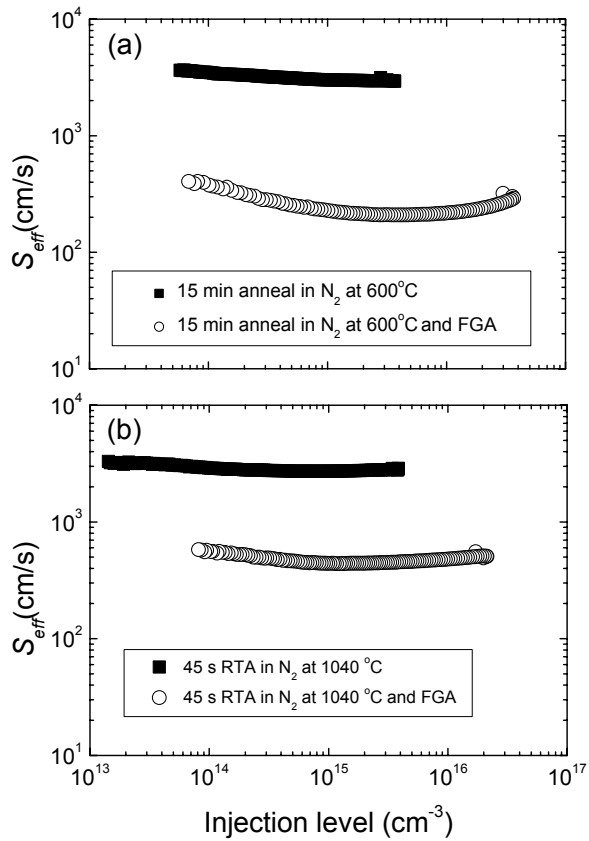


Figure 5: Effective surface recombination velocity S_{eff} as a function of the injection level for SiO₂ films deposited with 9.2 secm after an anneal in a N₂ environment (closed symbols) for (a) 15 min at 600 °C and (b) 15 s at 1040 °C (rapid thermal anneal). Subsequently the samples received a standard forming gas anneal (10% H₂ in N₂) for 30 min at 400 °C (open symbols).

most successful anneal, 15 min at 600 °C, is applied in a nitrogen environment. However, by a subsequent forming gas anneal at 400 °C, similar effective surface recombination velocities were found as before, hence, without the additional anneal at 600 °C. Also the scheme applied by Sivoththaman *et al.*,¹³ a 45 s rapid thermal anneal at 1040 °C, did not yield any improvement in the level of surface passivation compared to the as-deposited film. A subsequent forming gas anneal for 30 min at 400 °C resulted in a surface recombination velocity of ~500 cm/s, hence, no improvement was observed by the additional anneal. It seems that the presence of hydrogen in the annealing environment is essential to improve the level of surface passivation for our SiO₂ film, despite the presence of hydrogen in the film.

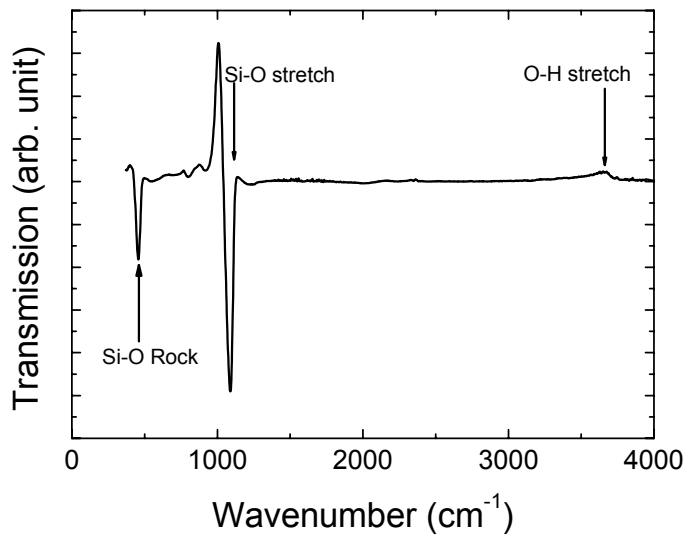


Figure 6: Differential infrared transmission spectrum of a SiO_2 film with a thickness of ~ 200 nm after a 15 min FGA at 600 °C. The differential spectrum was obtained by dividing the infrared spectrum after the forming gas anneal by the infrared spectrum before the forming gas anneal.

Preliminary experiments showed that a 30 min *alneal* at 400 °C after a forming gas anneal at 600 °C did not yield any improvement in the level of surface passivation. This is in contrast to the results published for thermal oxide where an *alneal* after a forming gas anneal resulted in a large improvement in the level of surface passivation.²

B. Compositional changes due to annealing

The compositional changes of the SiO_2 film due to the forming gas anneal at 600 °C were investigated by means of FTIR and RBS. For this reason 200 nm-thick SiO_2 films were deposited on single side polished 10-20 $\Omega \text{ cm}$ Cz c-Si substrates that had received a HF dip of 1 min prior to deposition. The RBS sample was divided into two parts and one part was treated by a forming gas anneal at 600 °C.

The FTIR spectrum (averaged over 800 scans to increase the signal-to-noise ratio) of the substrate with the SiO_2 film was taken after a FGA at 600 °C and divided by the spectrum taken prior to the forming gas anneal. The resulting differential infrared transmission spectrum is shown in Fig. 6. From this figure it is clear that both the intensities of the Si-O-Si rocking and stretching modes increased after annealing. Also a peak shift of the asymmetric Si-O-Si stretching mode from 1048 to 1060 cm^{-1} can be observed. Furthermore, by fitting the absorption spectrum by means of multiple Gaussian peaks, we observe a decrease in the peak widths of all the Si-O-Si related absorption peaks. The

increased sensitivity (800 instead of 20 averages) also allows detecting an O-H related absorption in the as-deposited SiO₂ film. This O-H related absorption peak is completely removed during annealing and it was not detected in the FTIR spectrum of the sample after the forming gas anneal. The amount of O-H in the deposited film is estimated to be $\sim 1.1 \times 10^{21} \text{ cm}^{-3}$ (1.8 at.%) using a O-H proportionality constant of $0.44 \times 10^{20} \text{ cm}^{-2}$.³⁴ This is in good agreement with RBS analysis, summarized in Table II, where $1.2 \times 10^{21} \text{ cm}^{-3}$ (2 at.%) of hydrogen was detected in the SiO₂ film deposited with an OMCTS flow of 9.2 sccm. The removal of hydrogen during the forming gas anneal was also confirmed by RBS, the hydrogen concentration decreased from 2.1 down to 0.7 at.% after the forming gas anneal. From spectroscopic ellipsometry measurements a decrease of ~4% in film thickness was observed, indicating a significant densification of the SiO₂ film during the forming gas anneal.

V. Conclusions

In this Chapter we have shown that SiO₂ films with a low impurity content and a high level of surface passivation can be deposited by the ETP technique at a high rate from an argon/oxygen/OMCTS mixture. From the material analysis we can conclude that SiO₂ films deposited with a low OMCTS to oxygen ratio have a carbon content below 0.03% and a low hydrogen (~2at.%) content mainly present in the form of O-H groups. When increasing the OMCTS to oxygen ratio the O/Si ratio of the films changes to below 2 and a significant amount of carbon (up to 4.5 at.%) is incorporated into the film. The amount of hydrogen in the film also significantly increases (up to 17 at.%) and the hydrogen is mainly bonded to silicon for the SiO₂-like films deposited with a high OMCTS flow.

The level of surface passivation of the SiO₂ films is significantly improved by a FGA and the best results are obtained with a 15 min FGA at 600 °C. The FGA densifies the SiO₂ film and the bulk hydrogen content of the film is reduced by a factor of three. The presence of H₂ during the post-deposition anneal is shown to be essential to improve the level of surface passivation. To the best of our knowledge, the obtained effective surface recombination velocity of 54 cm/s on 1.3 Ω cm *n*-type c-Si is the best reported value so far for PECVD SiO₂ films on low resistivity c-Si.

ACKNOWLEDGMENTS

The authors thank M.J.F. van de Sande and J.F.C. Jansen for their skillful technical assistance. Dr. Y. Tamminga and T. Dao (Philips Research) are thanked for the RBS analysis and Dr. P. van Hal (Philips Research) for the SIMS measurements. I. Volintiru is acknowledged for her help with the plasma reactor. Dr. M.D. Bijker (OTB Solar) is thanked for the fruitful discussions. This study has been carried out within the

EET-program “HR-CEL” funded by the Netherlands Ministry of Economic Affairs, the Ministry of Education, Culture and Science and the Ministry of Public Housing, Physical Planning and Environment. The research of one of the authors (WK) has been made possible by a fellowship of the Royal Netherlands Academy of Arts and Sciences (KNAW).

REFERENCES:

- ¹ J. H. Zhao, A. H. Wang, M. A. Green, and F. Ferrazza, *Appl. Phys. Lett.* **73**, 1991 (1998).
- ² A. G. Aberle, *Crystalline silicon solar cells: Advanced Surface Passivation and Analysis*. (UNSW Publishing and Printing Services, Sydney, 1999).
- ³ O. Schultz, S. W. Glunz, and G. P. Willeke, *Prog. Photovoltaics* **12**, 553 (2004).
- ⁴ A. A. Bright, *J. Vac. Sci. Technol.* **9**, 1088 (1991).
- ⁵ M. Creatore, F. Palumbo, R. d'Agostino, and P. Fayet, *Surface Coatings Technol.* **142**, 163 (2001).
- ⁶ A. S. D. Sobrinho, M. Latreche, G. Czeremuszkin, J. E. Kleemberg-Sapieha, and M. R. Wertheimer, *J. Vac. Sci. Technol. A* **16**, 3190 (1998).
- ⁷ Y. Barrell, M. Creatore, M. Schaepkens, C. D. Iacovangelo, T. Miebach, and M. C. M. van de Sanden, *Surface Coatings Tech.* **180-81**, 367 (2004).
- ⁸ W. Kern and R.S. Rosler, *J. Vac. Sci. Technol.* **5**, 1082 (1977).
- ⁹ Z. Chen, K. Yasutake, A. Doolittle, and A. Rohatgi, *Appl. Phys. Lett.* **63**, 2117 (1993).
- ¹⁰ Z. Chen, S. K. Pang, K. Yasutake, and A. Rohatgi, *J. Appl. Phys.* **74**, 2856 (1993).
- ¹¹ A. Ebong, P. Doshi, S. Narasimha, A. Rohatgi, J. Wang, and M. A. El-Sayed, *J. Electrochem. Soc.* **146**, 1921 (1999).
- ¹² C. Leguijt, P. Lolgen, J. A. Eikelboom, A. W. Weeber, F. M. Schuurmans, W. C. Sinke, P. F. A. Alkemade, P. M. Sarro, C. H. M. Maree, and L. A. Verhoef, *Sol. Energ. Mat .Sol. Cells* **40**, 297 (1996).
- ¹³ S. Sivoththaman, P. De Schepper, W. Laureys, J. F. Nijs, and R. P. Mertens, *IEEE Electron Device Lett.* **19**, 505 (1998).
- ¹⁴ M. J. Kerr and A. Cuevas, *Semicond. Sci. Tech.* **17**, 35 (2002).
- ¹⁵ C. S. Pai and C. P. Chang, *J. Appl. Phys.* **68**, 793 (1990).
- ¹⁶ Keisuke Ishii, Yoshimichi Ohki, and Hiroyuki Nishikawa, *J. Appl. Phys.* **76**, 5418 (1994).
- ¹⁷ A. D. Ross and K. K. Gleason, *J. Appl. Phys.* **97**, 113707 (2005).
- ¹⁸ C. Rau and W. Kulisch, *Thin Solid Films* **249**, 28 (1994).
- ¹⁹ Y. Qi, Z. G. Xiao, and T. D. Mantei, *J. Vac. Sci. Technol. A* **21**, 1064 (2003).
- ²⁰ L. Zajickova, J. Janca, and V. Perina, *Thin Solid Films* **338**, 49 (1999).
- ²¹ M. F. A. M. van Hest, B. Mitu, D. C. Schram, and M. C. M. van de Sanden, *Thin Solid Films* **449**, 52 (2004).
- ²² J. W. A. M. Gielen, W. M. M. Kessels, M. C. M. van de Sanden, and D. C. Schram, *J. Appl. Phys.* **82**, 2643 (1997).
- ²³ G. E. Jellison and F. A. Modine, *Appl. Phys. Lett.* **69**, 371 (1996).

- ²⁴ J. W. A. M. Gielen, M. C. M. van de Sanden, and D. C. Schram, Thin Solid Films **271**, 56 (1995).
- ²⁵ Y. Tamminga, F.H.P.M. Willemse, F. H. P. M. Habraken, and A. E. T. Kuiper, Nucl. Instr. and Meth. **200**, 499 (1982).
- ²⁶ P. C. Zalm, Mikrochimica Acta **132**, 243 (2000).
- ²⁷ R. A. Sinton and A. Cuevas, Appl. Phys. Lett. **69**, 2510 (1996).
- ²⁸ M. Creatore, W. M. M. Kessels, Y. Barrell, J. Benedikt, and M. C. M. van de Sanden, Mat. Sci. Semicond. Process. **7**, 283 (2004).
- ²⁹ A. Sassella, A. Borghesi, F. Corni, A. Monelli, G. Ottaviani, R. Tonini, B. Pivac, M. Bacchetta, and L. Zanotti, J. Vac. Sci. Technol. A **15**, 377 (1997).
- ³⁰ M. Creatore, J. C. Cigal, G. M. W. Kroesen, and M. C. M. van de Sanden, Thin Solid Films **484**, 104 (2005).
- ³¹ Y. H. Kim, M. S. Hwang, H. J. Kim, J. Y. Kim, and Y. Lee, J. Appl. Phys. **90**, 3367 (2001).
- ³² D. V. Tsu, G. Lucovsky, and B. N. Davidson, Phys. Rev. B **40**, 1795 (1989).
- ³³ G. Lucovsky, J. Manitini, J.K. Srivastava, and E.A. Irene, J. Vac. Sci. Technol. B **5**, 530 (1983).
- ³⁴ A. Ermolieff, T. Sindzingre, S. Marthon, P. Martin, F. Pierre, and L. Peccoud, Appl. Surface Sci. **64**, 175 (1993).
- ³⁵ M. J. Kerr and A. Cuevas, Semicond. Sci. Tech. **17**, 166 (2002).
- ³⁶ I. Martin, M. Vetter, A. Orpella, C. Voz, J. Puigdollers, and R. Alcubilla, Appl. Phys. Lett. **81**, 4461 (2002).
- ³⁷ M. Schaper, J. Schmidt, H. Plagwitz, and R. Brendel, Prog. Photovoltaics **13**, 381 (2005).

Chapter 4^{*}

Ultralow Surface Recombination of c-Si Substrates Passivated by Plasma-Assisted Atomic Layer Deposited Al₂O₃

Excellent surface passivation of c-Si has been achieved by Al₂O₃ films prepared by plasma-assisted atomic layer deposition, yielding effective surface recombination velocities of 2 and 13 cm/s on low resistivity *n*- and *p*-type c-Si, respectively. These results obtained for ~30 nm thick Al₂O₃ films are comparable to state-of-the-art results when employing thermal oxide as used in record-efficiency c-Si solar cells. A 7 nm thin Al₂O₃ film still yields an effective surface recombination velocity of 5 cm/s on *n*-type silicon.

^{*} Published as: B. Hoex, S.B.S. Heil, E. Langereis, M.C.M. van de Sanden, W.M.M. Kessels, Appl. Phys. Lett. **89**, 0412112 (2006).

Surface passivation of crystalline silicon (c-Si) is of key importance for the performance of high efficiency industrial solar cells. The surface to volume ratio is increasing due to the cost-driven reduction of the solar cell thickness, which makes surface passivation a decisive factor for the final solar cell efficiency. Hydrogenated amorphous silicon nitride ($a\text{-SiN}_x\text{:H}$) is routinely applied in solar cell production as an anti-reflection coating on the front side and provides good surface passivation of low resistivity n - and p -type c-Si. However, the surface passivation of $a\text{-SiN}_x\text{:H}$ on highly doped p -type silicon (e.g. p -type emitters) is rather poor. When $a\text{-SiN}_x\text{:H}$ is applied on the back of a p -type solar cell the high positive built-in charge induces a parasitic junction, limiting the solar cell efficiency.¹ Thermally grown oxide is the state-of-the-art surface passivation layer for n - and p -type c-Si of arbitrary doping level and is used in the record-efficiency passivated emitter and rear locally-diffused (PERL) c-Si solar cell.² The surface passivation of the as-grown thermal oxide is moderate, but is significantly improved by a subsequent annealing in a forming gas (H_2 in N_2). The best results are obtained by the so-called *alneal* scheme, where a sacrificial layer of Al is evaporated on the film prior to annealing. The oxidation of the Al film during the annealing releases atomic hydrogen that strongly reduces the number of interface defect states. However, the high processing temperatures ($\sim 950\text{--}1100^\circ\text{C}$) and elaborate processing necessary to obtain such a high quality thermal oxide are not always desirable. Therefore considerable effort is put in the development of low temperature surface passivation schemes that do not show the limitations of thermal oxide and $a\text{-SiN}_x\text{:H}$. Materials such as amorphous silicon carbide ($a\text{-SiC}_x\text{:H}$) and hydrogenated amorphous silicon ($a\text{-Si:H}$) have recently demonstrated a good level of surface passivation on both n - and p -type c-Si.^{3\text{--}5} However, both materials have significant absorption in the visible part of the solar spectrum. These films are also thermally unstable, hence, only steps with a low thermal budget can be used after deposition of these films.

Another interesting option is the use of the high band-gap dielectric Al_2O_3 as a surface passivation layer. With a refractive index of ~ 1.65 and no significant absorption in the visible part of the solar spectrum, Al_2O_3 is well suited to improve the optical quality at the front or the back of the solar cell. Hezel and Jeaeger already demonstrated that Al_2O_3 grown by the pyrolysis of aluminium-tri-isopropoxide can show a reasonable level of surface passivation.⁶ More recently, Agostinelli *et al.* have shown that Al_2O_3 films grown by thermal atomic layer deposition provide a good level of surface passivation on p -type c-Si.⁷

In this Letter we will show that ultrathin films of Al_2O_3 exhibit a similar level of surface passivation as *alnealed* thermal silicon oxide on both n - and p -type silicon. These films were prepared by plasma-assisted atomic layer deposition (PA-ALD) allowing monolayer growth control of high quality thin films, while the plasma step enables the use of relatively short purging times and low deposition temperatures.

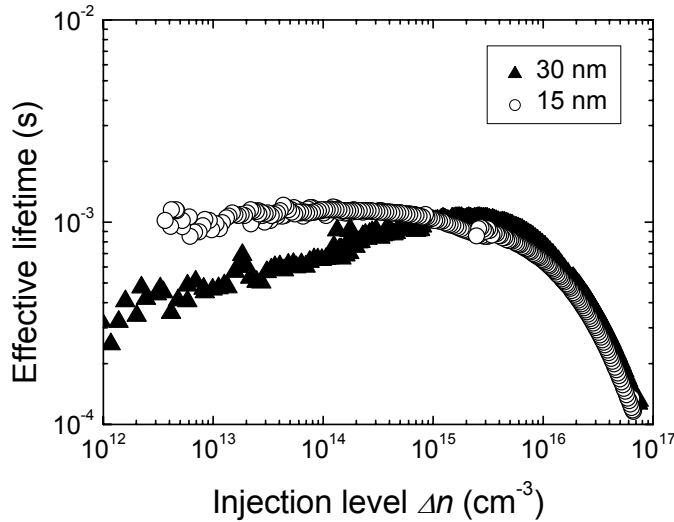


Figure 1: Effective lifetime as a function of the excess carrier density for low resistivity *p*-type (300 μm , $<111>$, 2.0 $\Omega\text{ cm}$) float zone c-Si substrate passivated with a 30 and 15 nm thick Al_2O_3 film.

Al_2O_3 films with a thickness of 7-30 nm were grown in a homebuilt PA-ALD reactor at a substrate temperature of 200 $^{\circ}\text{C}$.⁸ The films were prepared by alternating trimethylaluminium (TMA) exposure and a remote O_2 plasma with a total cycle time of ~30 s. The film growth was monitored by means of *in situ* spectroscopic ellipsometry (250-1000 nm range) and revealed a growth rate in the 1.2 \AA range per cycle. The atomic composition of the films was determined by means of Rutherford backscattering (RBS) and elastic recoil detection (ERD). The films were oxygen rich ($\text{Al}:\text{O}=2:3.14$) and a small amount of hydrogen (~3 at.%) was detected in the films. The carbon content was below the detection limit of RBS (<2 at.%). The surface passivation was tested by depositing identical Al_2O_3 films on both sides of low resistivity *p*-type (300 μm , $<111>$, 2.0 $\Omega\text{ cm}$) and *n*-type (275 μm , $<100>$, 1.9 $\Omega\text{ cm}$) float zone (FZ) c-Si substrates. The substrates received a standard RCA clean with final HF dip prior to deposition to remove the native oxide. After deposition, the lifetime samples were annealed in a N_2 environment for 30 min at 425 $^{\circ}\text{C}$ in a rapid thermal annealing furnace. The effective lifetime τ_{eff} was measured using a lifetime tester (Sinton WCT-100) in both the quasi steady state and transient mode.⁹ The level of surface passivation is quantified by the effective surface recombination velocity. Assuming an infinite bulk lifetime, the upper limit of the effective surface recombination velocity S_{eff} can be calculated by:

$$S_{\text{eff}} \leq \frac{W}{2 \cdot \tau_{\text{eff}}}, \quad (1)$$

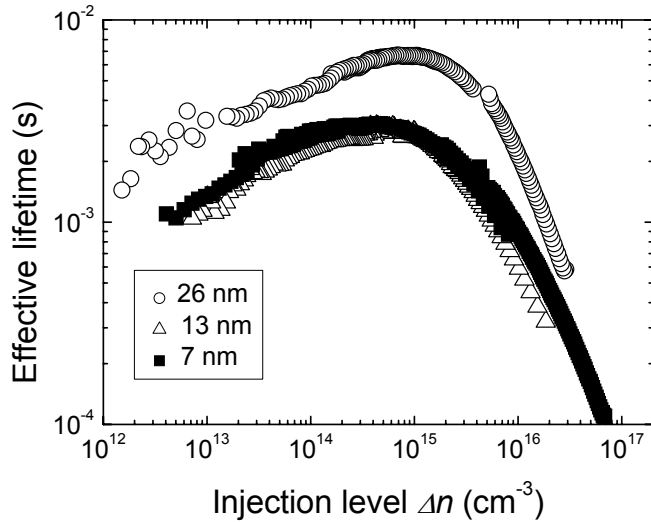


Figure 2: Effective lifetime as a function of the excess carrier density for low resistivity *n*-type ($275 \mu\text{m}$, $<100>$, $1.9 \Omega \text{ cm}$) float zone c-Si substrate passivated with a 30, 15, and 7 nm thick Al_2O_3 film.

with W the substrate thickness.

In Fig. 1 the effective lifetime as a function of the injection level is shown for the low resistivity *p*-type substrates passivated by 15 and 30 nm thin Al_2O_3 films. The post-deposition anneal was necessary to obtain the reported effective lifetimes, as the effective lifetime of the samples with the *as-deposited* Al_2O_3 films was only in the range of 2-8 μs . Effective lifetimes up to 1.2 ms were measured for a *p*-type substrate passivated by 30 nm Al_2O_3 film corresponding to a $S_{\text{eff}} \leq 13 \text{ cm/s}$. No difference in effective lifetime is observed when a 15 nm Al_2O_3 film is used instead of a 30 nm Al_2O_3 film, except for the behavior for lower injection levels.

The surface passivation of Al_2O_3 was also tested on *n*-type c-Si. In Fig. 2 the effective lifetime for $1.9 \Omega \text{ cm}$ *n*-type silicon passivated by 7, 14 and 26 nm Al_2O_3 is shown. A maximum lifetime of 6.6 ms was measured for a *n*-type substrate passivated by a 26 nm Al_2O_3 film corresponding to a $S_{\text{eff}} \leq 2 \text{ cm/s}$. For an Al_2O_3 film thickness of 7 and 15 nm comparable results were obtained and effective lifetimes up to 3.0 ms were measured, corresponding to a $S_{\text{eff}} \leq 5 \text{ cm/s}$.

The postdeposition annealing was essential for a good level of surface passivation, however, from RBS/ERD no significant changes could be detected in the atomic composition of the annealed Al_2O_3 films. From high resolution transmission electron microscopy (HR-TEM) it was found that both the *as-deposited* and annealed Al_2O_3 film are amorphous of composition, as shown in Fig. 3 for the annealed film. An

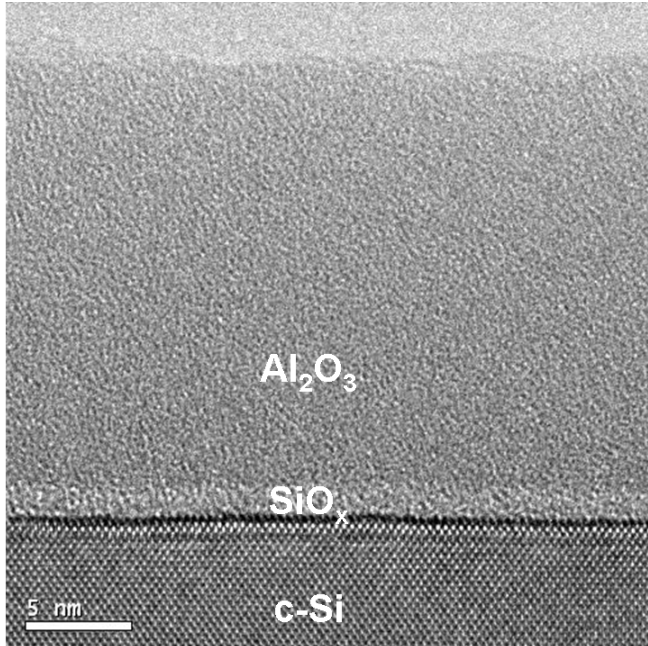


Figure 4: High resolution-TEM image showing a 20 nm thick Al_2O_3 film on c-Si after a 30 min anneal at 425°C in a N_2 environment.

interfacial oxide layer of ~ 1.5 nm (~ 1.2 nm prior to anneal) is present between the c-Si and Al_2O_3 as a result of the deposition process, possibly from the exposure of the substrate to the O_2 plasma in the first ALD cycles. In a separate experiment it was verified that the oxide layer formed during the O_2 plasma exposure on itself does not yield any surface passivation, also not after annealing.

The effective lifetimes measured for a *p*-type c-Si substrate passivated by a 15 nm Al_2O_3 film in this study are significantly higher compared to the results reported for substrates passivated by an Al_2O_3 film grown by thermal ALD and by a- $\text{SiC}_x:\text{H}$ grown by plasma-enhanced chemical vapor deposition (PECVD).^{4,7} The results are comparable to the best results obtained for *annealed* thermal SiO_2 and nearly stoichiometric a- $\text{SiN}_x:\text{H}$ and approach the results obtained for a- $\text{Si}:\text{H}$.^{3,10-12} It should be noted that the reported literature values were obtained for films with thicknesses in the range of 20-100 nm and that the level of surface passivation of a- $\text{SiC}_x:\text{H}$ and a- $\text{SiN}_x:\text{H}$ is reported to deteriorate for films with thicknesses below 40 nm and 20 nm, respectively.^{13,14} On the other hand, the effective lifetimes for *n*-type c-Si passivated with a 26 nm Al_2O_3 film are comparable to the best results obtained for *annealed* thermal SiO_2 , a- $\text{SiN}_x:\text{H}$ and a- $\text{Si}:\text{H}$ films and significantly higher than reported for a- $\text{SiC}_x:\text{H}$ films.^{3,5,10,11}

All lifetime curves in Figs. 1 and 2 show the expected decrease in effective lifetime at higher injection levels due to Auger recombination. For the *p*-type wafer in Fig. 1 passivated with a 30 nm Al_2O_3 , the effective lifetime shows the typical injection level dependence also reported for *p*-type wafers passivated by a- $\text{SiN}_x:\text{H}$, a- $\text{SiC}_x:\text{H}$ or thermal oxide,^{4,10,11} probably caused by Shockley-Read-Hall (SRH) recombination in the

bulk or at the surface through a midgap defect.^{15,16} Remarkably, the lifetime curve for the *p*-type wafer passivated by a 15 nm film is constant for lower injection level. For the *n* type wafers passivated by 7-26 nm Al₂O₃, the effective lifetime slightly decreases for lower injection level comparable to results obtained for *n*-type wafers passivated by a-SiC_x:H and a-Si:H.^{3,5} This decrease can again be attributed to SRH recombination in the bulk or at the surface.

The excellent surface passivation by the Al₂O₃ film is mainly determined by the field effect passivation due to a large ($\sim 10^{13}$ cm⁻²) built-in *negative* charge as indicated by C-V measurements. This negative built-in charge for Al₂O₃ was also reported by Hezel *et al.*⁶ and Agostinelli *et al.*^{6,7} The negative charge in Al₂O₃ is suggested to be present at the unique tetrahedrally coordinated Al site present at the interface that has a net negative charge, in contrast to the octahedrally coordination site where Al has a charge of 3+.¹⁷ For the commonly used thermal oxide and a-SiN:H *positive* built-in charges in the range of 10^{10} - 10^{12} cm⁻² are reported,^{6,18} and for a-SiC:H the sign of the built-in charge is reported to depend on the wafer doping type.^{4,5} A negative built-in charge is especially beneficial for passivation of highly doped *p*-type silicon.

The fact that the high level of surface passivation could only be obtained by a post-deposition anneal of the Al₂O₃ films (deposited at 200 °C) could be caused by a local reconstruction of the Al₂O₃ at the interface, consequently increasing the negative built-in charge.¹⁹ In addition, hydrogen from the Al₂O₃ bulk could diffuse and provide chemical passivation at the c-Si/Al₂O₃ interface thereby reducing defect related recombination. A factor 10 reduction of the interface defect density was reported for a metal-insulator-semiconductor structure with Al₂O₃ as the insulator after a 15 min annealing at 500 °C.⁶

In conclusion, we have shown that excellent surface passivation, similar to *annealed* thermal oxide, can be obtained on *n*- and *p*-type c-Si by thin Al₂O₃ films prepared by the PA-ALD technique. An ultrathin film of 7 nm thick Al₂O₃ yields a $S_{eff} \leq 5$ cm/s on *n*-type c-Si. By process optimization, cycle times could be reduced to a (sub) second level and the total process, growth, and annealing would be significantly faster compared to the state-of-the-art passivation schemes applied presently.

ACKNOWLEDGMENTS

The authors thank M.J.F. van de Sande, J.F.C. Jansen and J.J.A. Zeebregts for their skillful technical assistance, H.C.M. Knoops and P. Kudláček for their help with the depositions and Dr. F. Roozeboom and Dr. J. Klootwijk from Philips Research for the HR-TEM measurements. Dr. J. Schmidt from ISFH is thanked for the insightful discussions. This work is supported by the Netherlands Technology Foundation STW. The work of one of the authors (BH) is financially supported by OTB Solar. The research of another author (WK) has been made possible by a fellowship of the Royal Netherlands Academy of Arts and Sciences (KNAW).

REFERENCES:

- ¹ S. Dauwe, L. Mittelstadt, A. Metz, and R. Hezel, *Prog. Photovoltaics* **10**, 271 (2002).
- ² J. H. Zhao, A. H. Wang, M. A. Green, and F. Ferrazza, *Appl. Phys. Lett.* **73**, 1991 (1998).
- ³ S. Dauwe, J. Schmidt, and R. Hezel, Proc. of the 29th IEEE Photovoltaic Specialist Conference, New Orleans, (IEEE, Piscataway, NJ, 2002), p. 1246.
- ⁴ I. Martin, M. Vetter, A. Orpella, J. Puigdollers, A. Cuevas, and R. Alcubilla, *Appl. Phys. Lett.* **79**, 2199 (2001).
- ⁵ I. Martin, M. Vetter, A. Orpella, C. Voz, J. Puigdollers, and R. Alcubilla, *Appl. Phys. Lett.* **81**, 4461 (2002).
- ⁶ R. Hezel and K. Jaeger, *J. Electrochem. Soc.* **136**, 518 (1989).
- ⁷ G. Agostinelli, P. Vitanov, Z. Alexieva, A. Harizanova, H.F.W. Dekkers, S. De Wolf, and G. Beaucarne, Proc. of the 19th EU-PVSEC, Paris, (WIP Renewable Energies, Munich, 2004), p. 132.
- ⁸ S. B. S. Heil, E. Langereis, A. Kemmeren, F. Roozeboom, M. C. M. van de Sanden, and W. M. M. Kessels, *J. Vac. Sci. Technol. A* **23**, L5 (2005).
- ⁹ R. A. Sinton and A. Cuevas, *Appl. Phys. Lett.* **69**, 2510 (1996).
- ¹⁰ M. J. Kerr and A. Cuevas, *Semicond. Sci. Tech.* **17**, 166 (2002).
- ¹¹ M. J. Kerr and A. Cuevas, *Semicond. Sci. Tech.* **17**, 35 (2002).
- ¹² J. Schmidt and M. Kerr, *Sol. Energy Mater. Sol. Cells* **65**, 585 (2001).
- ¹³ R. Ferre, I. Martin, M. Vetter, M. Garin, and R. Alcubilla, *Appl. Phys. Lett.* **87**, 202109 (2005).
- ¹⁴ T. Lauinger, J. Moschner, A. G. Aberle, and R. Hezel, *J. Vac. Sci. Technol. A* **16**, 530 (1998).
- ¹⁵ R. N. Hall, *Phys. Rev.* **87**, 387 (1952).
- ¹⁶ W. Shockley and W. T. Read, *Phys. Rev.* **87**, 835 (1952).
- ¹⁷ R. S. Johnson, G. Lucovsky, and I. Baumvol, *J. Vac. Sci. Technol. A* **19**, 1353 (2001).
- ¹⁸ A. G. Aberle, S. Glunz, and W. Warta, *J. Appl. Phys.* **71**, 4422 (1992).
- ¹⁹ M. J. Cho, H. B. Park, J. Park, C. S. Hwang, J. C. Lee, S. J. Oh, J. Jeong, K. S. Hyun, H. S. Kang, Y. W. Kim, and J. H. Lee, *J. Appl. Phys.* **94**, 2563 (2003).

Chapter 5^{*}

Silicon Surface Passivation by Atomic Layer Deposited Al₂O₃

Thin Al₂O₃ films with a thickness of 7-30 nm synthesized by plasma-assisted atomic layer deposition (ALD) were used for surface passivation of crystalline silicon (c-Si) of different doping concentrations. The level of surface passivation in this study was determined by techniques based on photoconductance, photoluminescence and infrared emission. Effective surface recombination velocities of 2 cm/s and 6 cm/s were obtained on 1.9 Ω cm *n*-type and 2.0 Ω cm *p*-type c-Si, respectively. An effective surface recombination velocity below 1 cm/s was unambiguously obtained for high resistivity c-Si passivated by Al₂O₃. A high density of fixed negative charges was detected in the Al₂O₃ films and its impact on the level of surface passivation was demonstrated experimentally. The fixed negative charge density results in a flat injection level dependence of the effective lifetime on *p*-type c-Si and explains the excellent passivation of highly B-doped c-Si by Al₂O₃. For thermal ALD Al₂O₃, prepared in the same ALD reactor, the amount of fixed negative charge and the level of surface passivation was found to be significantly lower than for plasma-assisted ALD Al₂O₃.

* Submitted for publication: B. Hoex, J. Schmidt, P. Pohl, M.C.M. van de Sanden, W.M.M. Kessels.

I. Introduction

Surface passivation of crystalline silicon (c-Si) is becoming increasingly important in photovoltaics. Evidently, an excellent level of surface passivation is a requisite for high efficiency c-Si solar cells. However, also for more conventional solar cells, which experience an increasing surface-to-volume ratio due to the cost-driven reduction of the cell thickness, surface passivation is becoming of vital importance. Recombination losses at the c-Si surface can be reduced by two fundamentally different strategies. Because the recombination rate is proportional with the interface defect density the first strategy is based on the reduction of the number of defects states at the semiconductor surface. The surface defect density can for example be lowered by chemical passivation of unsaturated Si bonds (i.e., dangling bonds) by atomic hydrogen. The second strategy is based on the fact that surface recombination processes involve both electrons and holes. By the application of an internal electric field below the c-Si surface, either the electron or hole concentration can dramatically be reduced at the position of the c-Si surface. Consequently surface recombination is significantly reduced and the surface recombination velocity roughly scales with the minority carrier concentration at the c-Si surface obtained. Both surface passivation strategies are employed by the application of thin films on the c-Si surface.

Currently three thin film materials are industrially employed for surface passivation of c-Si solar cells. Passivation layers of thermally grown silicon dioxide (thermal SiO_2) form the state-of-the-art and effective surface recombination velocities of 2 cm/s and 12 cm/s have been reported on $1.5 \Omega \text{ cm}$ *n*-type and $1 \Omega \text{ cm}$ *p*-type c-Si, respectively.¹ The excellent level of surface passivation can mainly be attributed to the very high interface quality of thermal SiO_2 on c-Si. This high interface quality is warranted by the fact that the SiO_2 is thermally grown into the c-Si wafer at elevated temperatures (in the range of 900-1100 °C). Hence, the final interface quality remains rather unaffected by the initial c-Si surface condition. The interface quality is generally further improved by extensive post-deposition processing involving an anneal in a H_2 containing atmosphere (e.g., a forming gas anneal). The best interface quality is, however, obtained when first a sacrificial Al film is deposited on the SiO_2 film followed by an anneal at 450 °C (the so-called “alneal”).² Moreover also a small fixed positive charge density (up to 10^{11} cm^{-2}) is present in the thermal SiO_2 layer that provides field-effect passivation by shielding holes from the c-Si surface.³ Due to the high processing temperatures required to thermally grow a SiO_2 film, only c-Si with a low impurity content such as float zone (FZ) Si can be used without significant bulk lifetime degradation.⁴ As a consequence thermal SiO_2 is currently only applied in the manufacturing of high-efficiency solar cells in which low impurity c-Si wafers are employed.⁵

Silicon nitride ($a\text{-SiN}_x\text{:H}$) currently forms the industry standard for surface passivation of c-Si solar cells. Effective surface recombination velocities as low as 6 cm/s and 15 cm/s have been reported on $1.5 \Omega \text{ cm}$ *n*-type and $1.5 \Omega \text{ cm}$ *p*-type c-Si, respectively.^{6,7} The surface passivation mechanism of $a\text{-SiN}_x\text{:H}$ is mainly based on field effect passivation induced by the high positive fixed charge density in $a\text{-SiN}_x\text{:H}$ films ($\sim 10^{12} \text{ cm}^{-2}$).⁸ The positive fixed charge density is particularly beneficial for the passivation of *n*-type c-Si because the minority carriers (i.e., the holes) are effectively shielded from the c-Si surface. On the other hand, a high positive fixed charge density can be detrimental for surface passivation of highly doped *p*-type c-Si surfaces.⁹ A positive fixed charge density increases the minority electron concentration at a highly doped *p*-type c-Si surface and consequently increases the recombination rate. Moreover, the fixed positive charge density can induce a parasitic shunting when applied at the rear of a *p*-type solar cell.¹⁰ Recently it was however reported it is possible to effectively passivate highly doped *p*-type c-Si surfaces by Si-rich $a\text{-SiN}_x\text{:H}$ after a four hour post deposition anneal. The underlying mechanism in this case is still under investigation.¹¹

Amorphous silicon ($a\text{-Si:H}$) is the third material that is used in industry for surface passivation of c-Si. Films of $a\text{-Si:H}$ are employed in the HIT (hetero junction with intrinsic thin film) c-Si solar cell design of Sanyo.¹² In HIT cells the *p-n* junction is not formed by conventional dopant diffusion but by the deposition of a doped $a\text{-Si:H}$ film on a lightly doped c-Si wafer. An ultrathin intrinsic $a\text{-Si:H}$ film between the c-Si and the doped $a\text{-Si:H}$ film effectively passivates the c-Si surface and consequently exceptionally high open-circuit voltages in excess of 700 mV can be obtained by HIT solar cells.¹² The good surface passivation by $a\text{-Si:H}$ can mainly be attributed to the excellent electrical quality of the interface between c-Si and the $a\text{-Si:H}$ film.^{13,14} Additionally field-effect passivation plays a role which results from the amphoteric nature of the Si dangling bond defects.^{13,14} $a\text{-Si:H}$ has also successfully been applied for surface passivation on the rear side of diffused emitter c-Si solar cells.¹⁵ The main drawbacks associated with the use of $a\text{-Si:H}$ as surface passivation layer are the high absorption in the ultraviolet (UV) part of the solar spectrum and the low thermal stability of $a\text{-Si:H}$ films.

From the properties and performance of thermal SiO_2 , $a\text{-SiN}_x\text{:H}$, and $a\text{-Si:H}$, it is clear that there is still interest in alternative surface passivation layers for c-Si solar cells. A material that recently gained interest for c-Si surface passivation is amorphous aluminum oxide (Al_2O_3). In the late eighties Al_2O_3 was already applied for c-Si surface passivation in metal-insulator-semiconductor (MIS) solar cells by Hezel and Jaeger.⁸ They demonstrated that Al_2O_3 could provide a reasonable level of surface passivation with an effective surface recombination velocity of $\sim 200 \text{ cm/s}$ on $2 \Omega \text{ cm}$ *p*-type c-Si. The c-Si surface passivation was explained by a relative low mid-gap interface defect density of $\sim 1 \times 10^{11} \text{ eV}^{-1} \text{ cm}^{-2}$ and a fixed *negative* charge density of $\sim 3 \times 10^{12} \text{ cm}^{-2}$. The interface defect density of the c-Si/ Al_2O_3 system was also found to be unaffected by UV

radiation,⁸ in contrast to the strong increase in the interface defect density observed under UV exposure of both a-SiN_x:H and thermal SiO₂ on c-Si.^{8,16-18} As a matter of fact the fixed negative charge density in Al₂O₃ was even observed to increase during UV exposure due to photon-induced electron injection. Hence, UV exposure improved the field-effect passivation provided by the Al₂O₃ film.⁸ Recently Al₂O₃ was investigated as surface passivation layer again, now with the Al₂O₃ synthesized by atomic layer deposition (ALD). Agostinelli *et al.* and Hoex *et al.* demonstrated that ALD Al₂O₃ can provide an excellent level of surface passivation on *p*-type c-Si with effective surface recombination velocities close to 10 cm/s on 2 Ω cm *p*-type c-Si.^{19,20}

In this paper ALD grown Al₂O₃ has been used for surface passivation of c-Si with various doping concentrations. First of all, the method of ALD for the deposition of Al₂O₃ will be discussed as the technique is new in the field of c-Si solar cell fabrication. Subsequently the level of surface passivation provided by ALD Al₂O₃ on *n*- and *p*-type c-Si of different doping concentrations will be presented. The field-effect passivation by Al₂O₃ will be demonstrated experimentally and its consequences for the passivation of *n*- and *p*-type c-Si will be addressed. The level of surface passivation in the experiments reported has been determined from techniques based on photoconductance, photoluminescence and infrared emission. Moreover the level of surface passivation by Al₂O₃ grown by thermal and plasma-assisted ALD methods will be compared experimentally.

II. Atomic Layer Deposition of Al₂O₃

ALD is a chemical vapor deposition-like method in which the deposition is controlled at the atomic level by self-limiting surface reactions. The substrate surface is alternately exposed to gas phase precursors which react with the surface species until the surface is saturated. After such a self-limiting half-reaction the reactor is purged and/or pumped down to remove the reactants and the reaction products from the reactor before the start of the next half-reaction. By carrying out these half reactions in a cyclic manner, ultrathin films can be deposited with precise thickness control, high uniformity over large substrates, and with an excellent conformality on three-dimensional surface topologies. The most common ALD process is the deposition of Al₂O₃ by alternating exposures of Al(CH₃)₃ and H₂O.²¹ In addition to H₂O also other oxidation sources can be employed, such as O₃ and an O₂ plasma. When an O₂ plasma is used, the method is referred to as plasma-enhanced or plasma-assisted ALD, compared to thermal ALD when H₂O or O₃ are employed.

The fact that the ALD process allows the deposition of thin Al₂O₃ films with precise thickness control is illustrated in Fig. 1. In this figure it is shown that the Al₂O₃ film thickness scales linear with the number of ALD cycles for both the thermal and

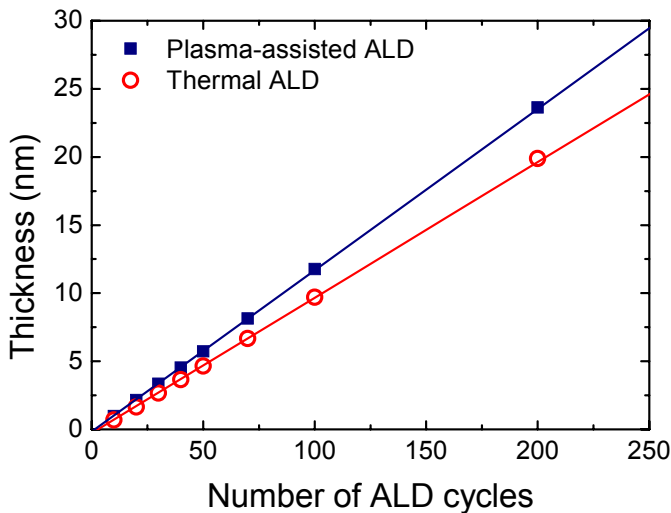


Figure 1: Al_2O_3 thickness as a function of the number of cycles for plasma-assisted ALD and thermal ALD. The thickness of the Al_2O_3 films was determined by *in situ* spectroscopic ellipsometry. Both films were grown at a substrate temperature of 200 °C.

plasma-assisted ALD process. Both films were deposited in the same ALD reactor and at the same substrate temperature of 200 °C. The slope of the film thickness as a function of the number of ALD cycles defines the so-called growth-per-cycle (GPC) of the ALD process. The GPC of 0.13 nm/cycle for the Al_2O_3 deposited by plasma-assisted ALD is significantly higher than the GPC of 0.10 nm/cycle for the Al_2O_3 deposited by thermal ALD. The material properties of Al_2O_3 films deposited by plasma-assisted and thermal ALD were studied in detail and reported in the literature.²² Briefly, the structural material properties of the Al_2O_3 films deposited by thermal and plasma-assisted ALD are very similar for substrate temperatures ranging from 200 to 300 °C. The films are stoichiometric of composition ($[\text{O}]/[\text{Al}] = 1.5$) and a hydrogen content [H] of ~2 at.% and ~1 at.% was observed for films deposited at 200 °C and 300 °C, respectively. Figure 2 shows the thickness distribution of an Al_2O_3 film deposited by plasma-assisted ALD on a 200 mm wafer. With spectroscopic ellipsometry the thickness was sampled at 300 points. The thickness decreases from 79.8 nm in the middle of the wafer to 78.6 nm at 1 cm of the edge of the wafer indicating a good thickness uniformity. In another study it was demonstrated that the plasma-assisted ALD process of Al_2O_3 yields an excellent conformality on high aspect ratio structures with an aspect-ratio of ~8.²²

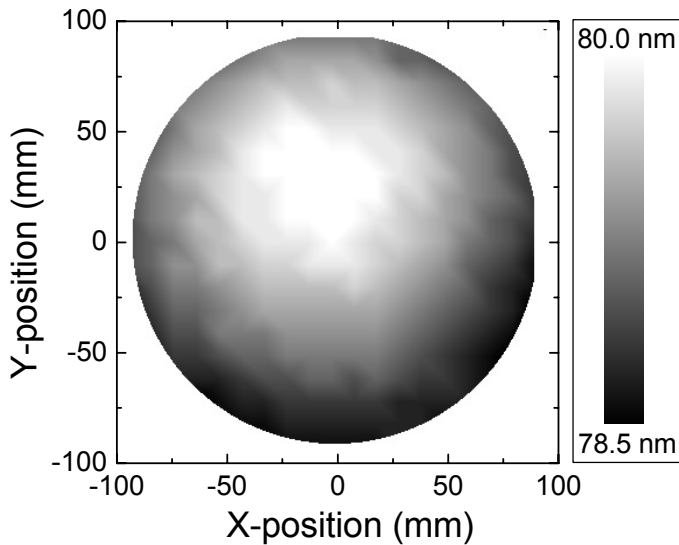


Figure 2: Al_2O_3 thickness uniformity on a 200 mm diameter wafer as determined by spectroscopic ellipsometry. 300 data points were measured over the wafer up to a distance of 1 cm from the wafer edge.

III. Experimental Details

A. ALD reactors

The experiments were conducted in a lab-scale reactor (ALD-I, home-built)²³ and in a commercially available reactor (FlexAL™, Oxford Instruments Plasma Technology) with a loadlock system.²⁴ Both systems are equipped with a remote inductively coupled plasma (ICP) source located above the wafer for plasma-assisted ALD. The ALD-I and FlexAL reactor are capable of handling wafers up to 100 mm and 200 mm, respectively. The FlexAL reactor is equipped with multiple precursor pods and it can be used both for plasma-assisted and thermal ALD processes. Both reactors have optical viewports that enable *in situ* monitoring of the film growth by, e.g., spectroscopic ellipsometry.²² Other *in situ* diagnostic techniques have been fitted as well.²⁵

In the current study, the Al_2O_3 films were deposited at 200 °C unless indicated otherwise. The precursor doses and exposure times were chosen such that all films were deposited under saturated, self-limiting conditions.²² A typical plasma-assisted ALD cycle at the FlexAL reactor consisted of a 20 ms injection of $\text{Al}(\text{CH}_3)_3$ vapor followed by a 1.5 s purging with O_2 . Subsequently a 400 W O_2 plasma was ignited for 2 s followed by a 0.5 s purging with O_2 . Consequently the ALD cycle time for plasma-assisted ALD on the FlexAL reactor was typically 4 s. A thermal ALD cycle at the FlexAL reactor

consisted of a 20 ms injection of $\text{Al}(\text{CH}_3)_3$ vapor followed by a 3 s Ar purge. The oxidation step consisted of a 240 ms injection of H_2O vapor followed by a 12 s purge with Ar resulting in an ALD cycle time of 16 s. The ALD process in the ALD-I reactor was not optimized with respect to cycle time and it consisted of 5 consecutive $\text{Al}(\text{CH}_3)_3$ dosings, 2 s Ar purging, and 2 s 100 W O_2 plasma exposure. This resulted in a total ALD cycle time of 22 s.

H-terminated c-Si wafers were loaded in the reactor and pre-heated at the deposition temperature for 5 min before the start of the ALD process. Typically 50-255 ALD cycles were carried out resulting in Al_2O_3 films with a thickness of 7-30 nm as was monitored by *in situ* spectroscopic ellipsometry. For the lifetime measurements the c-Si wafers were coated at both sides. To do so, the wafer was turned over after the Al_2O_3 ALD on the front side. Subsequently the sample was reloaded in the reactor without additional cleaning steps and an identical Al_2O_3 film was deposited at the rear side of the wafer. This resulted in symmetrically coated c-Si wafers. For the depositions in the FlexAL reactor, a c-Si carrier wafer was used to protect the uncoated rear side of the c-Si wafer during the deposition of the Al_2O_3 film on the front side.

B. *In situ* spectroscopic ellipsometry

The Al_2O_3 ALD processes were monitored by *in situ* spectroscopic ellipsometry measurements in the 1.24-6.50 eV photon energy range (J.A. Woollam M2000-D ellipsometer). Measurements were taken both prior to and during the Al_2O_3 deposition process. Spectroscopic ellipsometry measures the change in polarization of the reflected light expressed in the two ellipsometric angles Ψ and Δ .²⁶ From the ellipsometric angles a pseudodielectric function $\langle \epsilon \rangle = \langle \epsilon_1 \rangle + i \langle \epsilon_2 \rangle$ can be calculated by assuming that Ψ and Δ arise from the reflection on a planar interface between air and a semi-infinite material with a pseudo dielectric function $\langle \epsilon \rangle$.²⁶ The imaginary part $\langle \epsilon_2 \rangle$ of a c-Si substrate is extremely sensitive to the presence of native oxide or surface roughness at the c-Si surface, especially at the c-Si bulk critical point energy of 4.2 eV.²⁷ Therefore the $\langle \epsilon \rangle$ of c-Si was used to evaluate the condition of the c-Si surfaces (both for front and rear sides of the wafer) prior to the deposition of the Al_2O_3 film.

Figure 3 shows $\langle \epsilon_2 \rangle$ for a c-Si wafer as measured at both surfaces prior to the deposition of Al_2O_3 film. For the front side the value of $\langle \epsilon_2 \rangle$ of 47 at the E_2 bulk critical point energy indicates a clean H-terminated c-Si surface.²⁷ For the rear side the value of $\langle \epsilon_2 \rangle$ at the E_2 bulk critical point energy is only 33. This significantly lower $\langle \epsilon_2 \rangle$ value can be attributed to the presence of a native oxide on the rear side of the wafer; from model calculations the presence of a 2.2 nm native oxide film on the c-Si could be derived. From a large set of (initial) measurements, it appeared that the oxidation of the c-Si wafer strongly correlated with the obtained level of surface passivation of the Al_2O_3

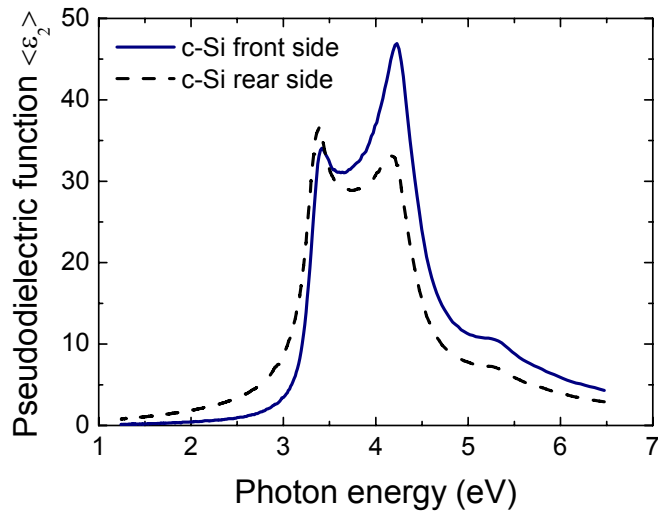


Figure 3: Imaginary part of the pseudodielectric function $\langle \epsilon_2 \rangle$ of the front and rear side of a c-Si wafer as measured *before* the deposition of the Al_2O_3 film on both wafer sides. The difference between the two dielectric functions can be explained by the formation of native oxide on the rear side of the c-Si wafer while an Al_2O_3 film is deposited on the front side. The formation of this native oxide on the rear side could be avoided through the usage of a Si carrier wafer instead of placing the wafers directly on the reactor's substrate stage.

film. In the experiments discussed in Sec. IV, oxidation of the rear surface during ALD of Al_2O_3 film on the front side was prevented by the usage of a c-Si carrier wafer.

The ellipsometry spectra of the wafers as obtained during the Al_2O_3 deposition process were analyzed by a two layer optical model. This model consisted of a substrate, with the optical properties defined by the measurement prior to deposition, and an Al_2O_3 film with the optical properties described by a Cauchy model.²⁶ The typical refractive index for the Al_2O_3 films was in the range of 1.60-1.65 at a photon energy of 2 eV and the Al_2O_3 films did not show any absorption in the photon energy range investigated.

C. C-Si surface passivation

The surface passivation induced by the Al_2O_3 films was tested on double-side polished FZ *p*-type and *n*-type c-Si substrates of different doping concentrations. The c-Si substrates were cleaned using a conventional RCA1 and RCA2 clean and received a final treatment in diluted HF (1%) prior to deposition.²⁸ After being symmetrically coated with Al_2O_3 , the c-Si wafers were annealed at 425 °C for 30 minutes in a N_2 atmosphere.

The injection level dependent effective lifetime of the charge carriers in the symmetrically passivated c-Si wafer was determined by two different techniques. In the

first technique, the injection level dependence of the effective lifetime was determined by the photoconductance technique (Sinton Consulting WCT-100 lifetime tester).²⁹ The effective lifetime of a passivated c-Si wafer was determined over a broad injection level range by measuring the excess conductance (photoconductance) by a contactless inductively coupled coil during a short [$\sim 10\mu\text{s}$, photoconductance decay (PCD)] or long [~ 2 ms, quasi-steady-state photoconductance (QSSPC)] light flash.²⁹ As all charge carriers contribute equally to the excess conductance the photoconductance technique is sensitive to carrier trapping or depletion region modulation.^{30,31} Both carrier trapping and depletion region modulation can lead to an overestimation of the effective lifetime at lower injection level if they are not properly taken into account.

The second technique which was used for determining the injection level dependent effective lifetime was the quasi-steady-state photoluminescence technique as recently developed at the University of New South Wales.³² The injection level dependent effective lifetime is determined from the steady-state radiative recombination of charge carriers under steady-state illumination using the self-consistent calibration method proposed by Trupke *et al.*³³ As the photoluminescence signal is proportional to the electron-hole product the measurements are basically unaffected by carrier trapping and depletion region modulation. Consequently the effective lifetime can be determined at lower injection levels when compared with the photoconductance technique.

The uniformity of the surface passivation was determined by the infrared lifetime mapping method.³⁴ The effective lifetime of the charge carriers was determined from the steady-state infrared emission by the free carriers during steady-state illumination. The infrared emission is proportional to the total carrier concentration and, hence, is sensitive to carrier trapping and depletion region modulation. As a matter of fact the sensitivity for carrier trapping is exploited when infrared lifetime mapping is used for the mapping of the trap density of (multi)crystalline Si wafers.³⁵

The level of surface passivation is expressed in terms of the effective lifetime τ_{eff} of the symmetrically passivated c-Si wafers as determined by the three techniques. The effective surface recombination velocity S_{eff} can be calculated from τ_{eff} by the expression:

$$\frac{1}{\tau_{\text{eff}}} = \frac{1}{\tau_{\text{Bulk}}} + \frac{2S_{\text{eff}}}{d}, \quad (1)$$

with τ_{bulk} being the c-Si bulk lifetime and d the wafer thickness. As high purity FZ c-Si with a moderate doping level was used in this study, no empirically determined upper level for the intrinsic c-Si bulk lifetime (e.g., due to Auger recombination) was assumed throughout this paper. Hence the bulk lifetime was set to be infinite and the values of the effective surface recombination velocity $S_{\text{eff},\text{max}}$ reported in this work are upper limits.

D. Capacitance voltage and corona charging experiments

Capacitance-voltage (CV) measurements on metal-oxide-semiconductor (MOS) structures were carried out on selected samples. The Al_2O_3 films, deposited HF-dipped 20-30 Ω cm p-type c-Si wafers, were annealed for 30 min at 425 °C in N_2 . Subsequently Al dots with an area of $\sim 1 \text{ mm}^2$ were sputtered on the Al_2O_3 film. The C-V curves were measured at 10 kHz with an HP4275A multi-frequency LCR meter.²²

Corona charging experiments were conducted to study the impact of the fixed negative charge density in the Al_2O_3 films on the level of c-Si surface passivation. By applying a high electric field at a tungsten needle air particles and molecules were ionized in a corona chamber and positive ions were created.^{36,37} The positive charges, mainly consisting of $(\text{H}_2\text{O})_n\text{H}^+$ ions, were deposited in small amounts on a single side of a symmetrically passivated c-Si wafer.³⁸ Subsequently the surface potential was determined by a vibrating Kelvin probe and the positive surface charge density was calculated using the information on the dielectric constant from the C-V measurements and the film thickness from spectroscopic ellipsometry. Simultaneously the effective lifetime of the passivated c-Si wafer was determined by infrared lifetime mapping. This procedure was repeated multiple times for different positive surface charge densities up to a maximum positive surface charge density of $2 \times 10^{13} \text{ cm}^{-2}$.

IV. Results and Discussion

A. N-type c-Si passivated by plasma-assisted ALD Al_2O_3

The level of surface passivation was tested on *n*-type c-Si wafers (1.9 Ω cm <100>) with a thickness of 275 μm . In Fig. 4 the effective lifetimes are shown for the c-Si wafers passivated by Al_2O_3 deposited in the ALD-I and FlexAL reactor. The results obtained on the ALD-I reactor were reported previously.²⁰ From Fig. 4 it is clear that lifetimes in excess of 3 ms were obtained on both reactors. The 7 nm and 13 nm thick Al_2O_3 films deposited on the ALD-I reactor had a better level of surface passivation than the 10 and 20 nm thick Al_2O_3 film deposited on the FlexAL reactor. This difference is not yet understood. The highest lifetimes obtained on the ALD-I and FlexAL reactor correspond to $S_{\text{eff},\text{max}}$ values of 2 cm/s and 4 cm/s, respectively. At the FlexAL reactor also the deposition temperature and O_2 plasma exposure time during Al_2O_3 deposition were varied to study its impact on the effective lifetime. Within the range studied, no significant influence of these parameters on the effective lifetime was detected. This is for example illustrated in Fig. 4(b) by the effective lifetime obtained for an Al_2O_3 film deposited at 300 °C and with a 4 s O_2 plasma exposure time. Consequently all experiments at the FlexAL reported in the remainder of this paper were carried out at 200 °C and with a 2 s O_2 plasma exposure time.

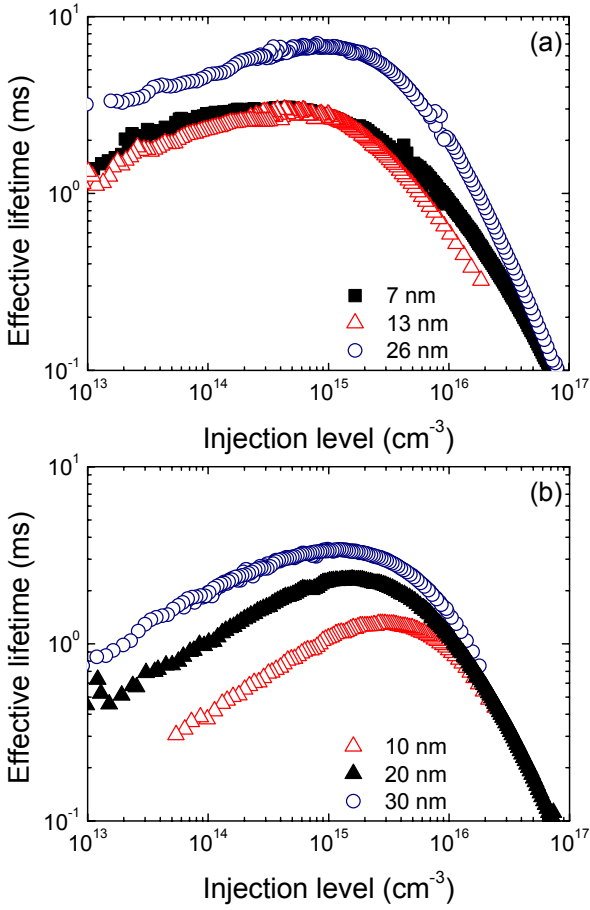


Figure 4: Injection level dependent effective lifetimes of n -type c-Si ($1.9 \Omega \text{ cm}$, $<100>$, $275 \mu\text{m}$) wafers symmetrically passivated by Al_2O_3 as measured by photoconductance. The Al_2O_3 films were deposited by plasma-assisted ALD at (a) the lab-scale ALD-I reactor and (b) the commercial FlexAL reactor. The films in the ALD-I and FlexAL reactor were deposited at a substrate temperature of 200°C and a O_2 plasma exposure of 2 s. Only for the 20 nm film deposited at the FlexAL reactor the substrate temperature was 300°C and the plasma exposure time was 4 s. The thickness of the Al_2O_3 films ranged from 7 to 30 nm as measured by *in situ* spectroscopic ellipsometry.

As mentioned above the high negative fixed charge density in the Al_2O_3 films provides field-effect passivation by electrostatically shielding electrons from the c-Si surface. This was experimentally demonstrated by depositing *positive* corona charges on the Al_2O_3 surface to compensate the fixed negative charge density in the Al_2O_3 film. A similar approach was used by Glunz *et al.* and Dauwe *et al.* to study the fixed positive

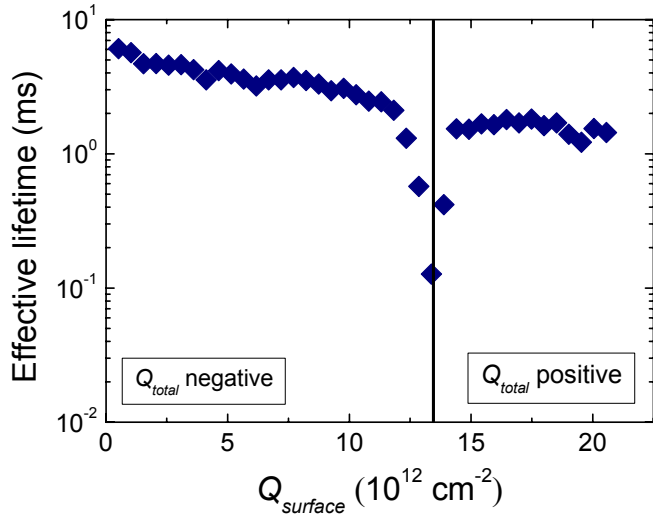


Figure 5: Effective lifetime of a *n*-type c-Si ($1.9 \Omega \text{ cm}$, $<100>$, $275 \mu\text{m}$) wafer symmetrically passivated by a 26 nm Al_2O_3 film as a function of the positive charge density $Q_{surface}$ at the surface. For a $Q_{surface} < 1.3 \times 10^{13} \text{ cm}^{-2}$ the total amount of charge (the sum of the fixed charge density in the Al_2O_3 film and the surface charge density) is negative and for $Q_{surface} > 1.3 \times 10^{13} \text{ cm}^{-2}$ the total charge is positive. The effective lifetime was measured by infrared lifetime mapping at an injection level of $10^{14}\text{-}10^{15} \text{ cm}^{-3}$.

charge density in thermal SiO_2 and a- $\text{SiN}_x\text{:H}$ films.^{36,37} The effective lifetime as a function of the positive charge density $Q_{surface}$ deposited at the Al_2O_3 surface in a corona chamber is shown in Fig. 5. Apart from a steady decline, which can most likely be attributed to extensive handling of the c-Si wafer, the effective lifetime of the c-Si wafer is initially hardly affected by the positive charge density at the surface. The effective lifetime remains $> 3 \text{ ms}$ up to a positive $Q_{surface}$ of $1.0 \times 10^{13} \text{ cm}^{-2}$. However, for a $Q_{surface}$ between $(1.2\text{-}1.4)} \times 10^{13} \text{ cm}^{-2}$ a strong decrease in the effective lifetime is observed. A minimal effective lifetime of $\sim 100 \mu\text{s}$ is obtained for a positive $Q_{surface}$ of $1.3 \times 10^{13} \text{ cm}^{-2}$. Consequently, the recombination rate at the c-Si surface is maximized for a positive $Q_{surface}$ of $1.3 \times 10^{13} \text{ cm}^{-2}$. When the $Q_{surface}$ at the surface is further increased to $2 \times 10^{13} \text{ cm}^{-2}$ the effective lifetime increases again to values close to 2 ms.

The surface recombination rate is maximized when the electron and hole concentration at the surface are approximately equal. The charge density required to obtain an equal electron and hole concentration at the surface of a $1.9 \Omega \text{ cm}$ *n*-type c-Si was estimated from model calculations with the software package PC1D.³⁹ In PC1D the coupled non-linear electron and hole transport equations in crystalline semiconductors are solved numerically by the finite-element method.³⁹ From the calculations it was derived

that a negative charge density of only $1 \times 10^{11} \text{ cm}^{-2}$ is required to obtain an equal electron and hole concentration at the c-Si surface of a 1.9 cm *n*-type c-Si surface. This is well within the experimental error of the measured surface charge density in Fig. 5. It can therefore be stated that an equal electron and hole density is obtained for a positive Q_{surface} of $1.3 \times 10^{13} \text{ cm}^{-2}$ and consequently the *negative* charge density in the 26 nm Al₂O₃ can be estimated at $1.3 \times 10^{13} \text{ cm}^{-2}$. Figure 5 therefore clearly illustrates that a high negative fixed charge density is present in the Al₂O₃ film and through electrostatically shielding these negative fixed charges fulfill an important role in the surface passivation mechanism of Al₂O₃ on c-Si. For a $Q_{\text{surface}} > 1.3 \times 10^{13} \text{ cm}^{-2}$ the sum of Q_{surface} and fixed charge density in the Al₂O₃ film is positive. Hence, field-effect passivation is provided by a net *positive* charge density for a positive Q_{surface} in the $1.3\text{-}2.0 \times 10^{13} \text{ cm}^{-2}$ range.

The polarity of the fixed charge density in Al₂O₃ could also explain the injection level dependence of the effective lifetime as shown in Fig. 4. The effective lifetime has a maximum at an injection level in the range of $(1\text{-}3) \times 10^{15} \text{ cm}^{-3}$. At higher injection levels ($> 5 \times 10^{15} \text{ cm}^{-3}$) the effective lifetime is dominated by Auger recombination in the bulk of the c-Si wafer.⁴⁰ At lower injection levels the effective lifetime decreases. This decrease at lower injection levels is even more pronounced for the samples deposited on the FlexAL reactor than for the samples deposited at the ALD-I reactor. A similar injection level dependence of the effective lifetime was reported for *p*-type c-Si passivated by dielectrics with a fixed *positive* charge density such as thermal SiO₂ and a-SiN_x:H.^{6,37} In the latter case, this injection level dependence was primarily attributed to recombination in the depletion region that is formed by the shielding of holes from the c-Si surface.^{36,37} Consequently, the injection level dependence of the effective lifetime of *n*-type c-Si passivated by Al₂O₃ could have a similar physical origin and be the result of recombination losses in the depletion region in the c-Si wafer induced by the *negative* fixed charge in the Al₂O₃ film.

Also nearly intrinsic *n*-type c-Si (2 kΩ cm, <111> and 20 kΩ cm, <100>) wafers were passivated by 30 nm thick Al₂O₃ films deposited by plasma-assisted ALD in the FlexAL reactor. The injection level dependent lifetime is shown in Fig. 6 and was determined from the quasi-steady-state photoluminescence technique. This figure reveals that lifetimes in excess of 18 ms can be obtained for c-Si wafers passivated by Al₂O₃. These are among the highest measured effective lifetimes for a passivated c-Si wafer reported in the literature. The injection level dependence of the effective lifetime for these high resistivity c-Si wafers is flat at low injection level which could possibly be related to the fact that these c-Si are only lightly doped with a [P] in the range of $10^{11}\text{-}10^{12} \text{ cm}^{-3}$. The effective lifetimes obtained for these nearly intrinsic c-Si wafers unambiguously demonstrate that $S_{\text{eff}, \text{max}}$ values below 1 cm/s can be obtained on c-Si passivated by ALD-grown Al₂O₃ films.

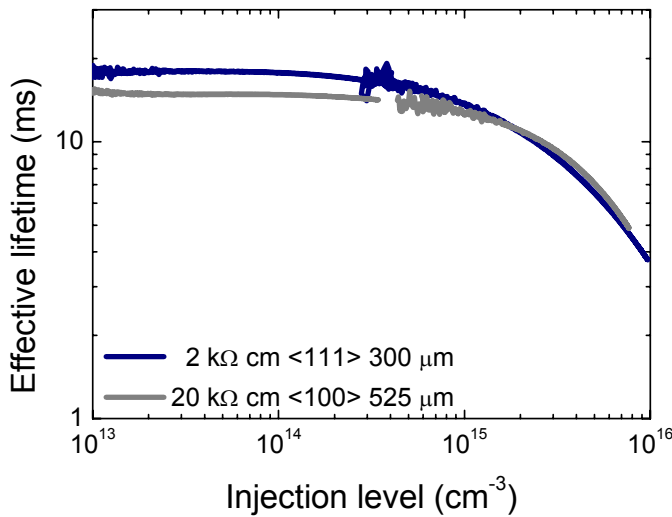


Figure 6: Injection level dependent effective lifetime of high-resistivity *n*-type c-Si wafers symmetrically passivated by a 30 nm Al_2O_3 film deposited by plasma-assisted ALD. The effective lifetime was measured by quasi-steady-state photoluminescence.

The high resistivity samples were also measured by the photoconductance technique but these results, yielding even higher lifetimes, were significantly different from the effective lifetimes extracted from the photoluminescence technique. The effective lifetimes extracted from the photoconductance technique also appear less physical making the interpretation of the data for high resistivity wafers questionable as reported in the Appendix.

B. *P*-type c-Si passivated by plasma-assisted ALD grown Al_2O_3

In Fig. 7 the results obtained on *p*-type c-Si ($2.0 \Omega \text{ cm } <111>$) wafers with a thickness of 300 μm are shown. Effective lifetimes in excess of 1 ms were obtained for films deposited on both the ALD-I and FlexAL system. The results obtained on the ALD-I reactor, which were already reported previously,²⁰ reveal that the maximum effective lifetime of the c-Si wafers passivated by a 15 and 30 nm Al_2O_3 film is almost equal, i.e., 1.2 ms. However, the injection level dependence of the effective lifetime is completely different for these c-Si wafers and this difference will be addressed in more detail later. For Al_2O_3 films deposited at the FlexAL effective lifetimes of 1.2 ms and 2.5 ms were obtained for c-Si wafers passivated by a 10 and 30 nm thick Al_2O_3 film, respectively. The latter value exceeds the results obtained on the ALD-I reactor and corresponds to a $S_{\text{eff}, \text{max}}$ of 6 cm/s.

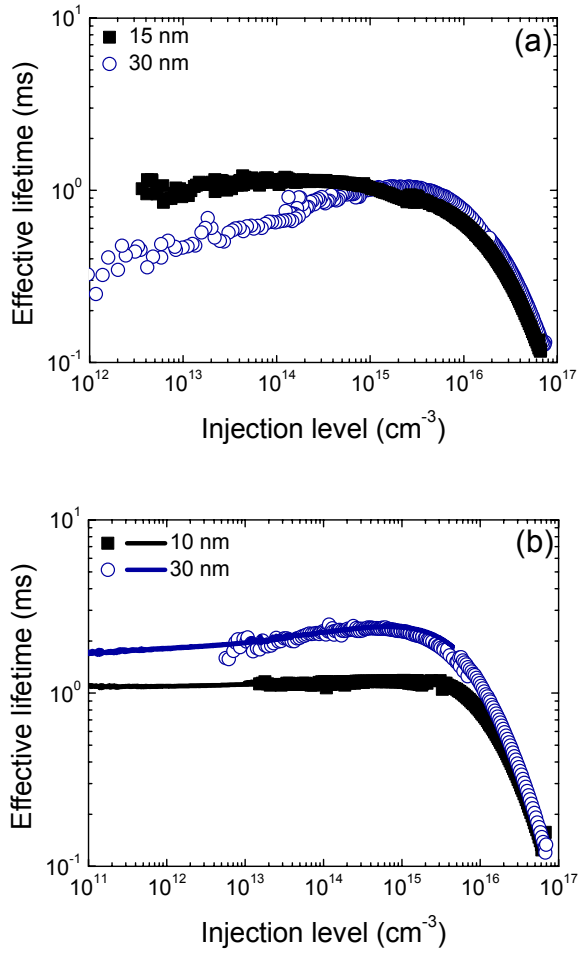


Figure 7: Injection level dependent effective lifetime of a *p*-type c-Si ($2 \Omega \text{ cm}$, $<111>$, $300 \mu\text{m}$) wafer symmetrically passivated by Al_2O_3 deposited on (a) the lab-scale ALD-I reactor and (b) the commercial FlexAL reactor. The effective lifetime was measured by the photoconductance technique for all samples (symbols). For the samples deposited at the FlexAL reactor the effective lifetime was also measured by quasi-steady-state photoluminescence (solid lines). The thickness of the Al_2O_3 films ranged from 10 to 30 nm and was determined by *in situ* spectroscopic ellipsometry.

The uniformity of the surface passivation was determined by means of infrared lifetime mapping on 100 mm c-Si wafers. The results are shown in Fig. 8 for samples deposited at both the ALD-I and FlexAL reactor. The measured effective lifetimes are in good agreement with the values obtained from photoconductance. The uniformity of the sample deposited on the ALD-I reactor was rather poor whereas the uniformity was

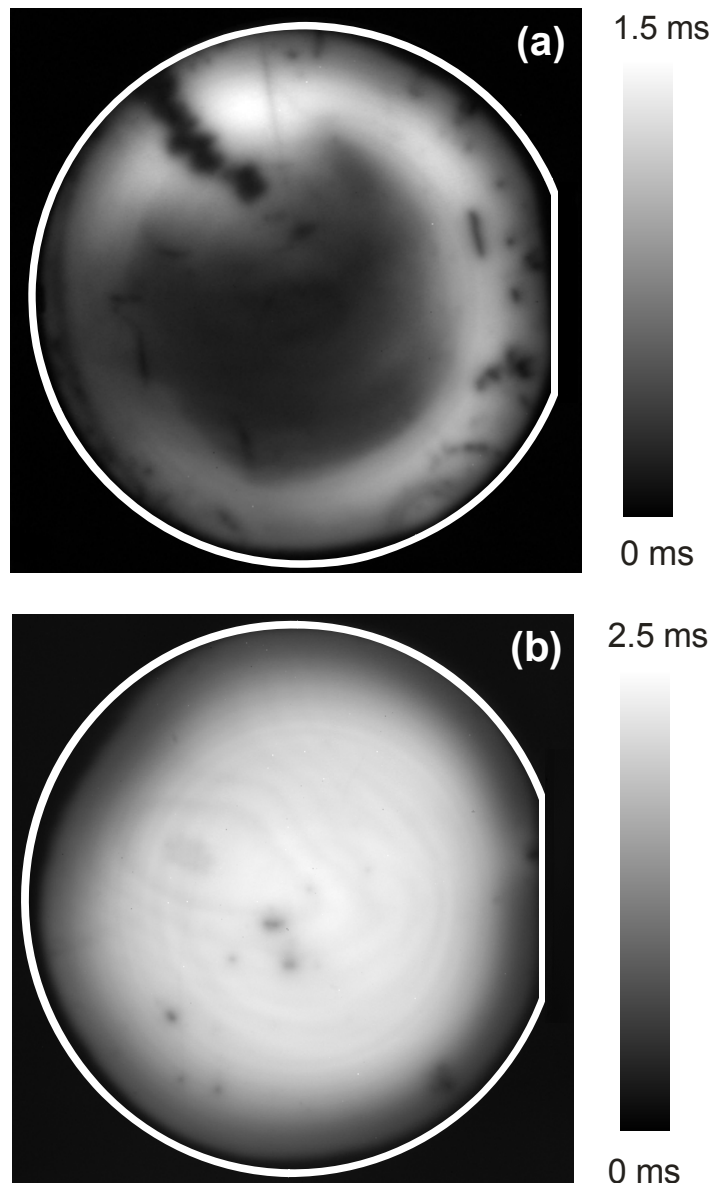


Figure 8: Infrared lifetime mapping of a 100 mm diameter p -type c-Si wafer ($2 \Omega \text{ cm}$, $<111>$, $300 \mu\text{m}$) symmetrically passivated by a 30 nm Al_2O_3 film deposited on (a) the lab-scale ALD-I reactor and (b) the commercial FlexAL reactor. The effective lifetime was measured for an injection level of $5\text{-}10 \times 10^{14} \text{ cm}^{-3}$. The edge of the wafer has been indicated for clarity.

rather good for the sample deposited on the FlexAL reactor. As shown in Fig. 8(b) the effective lifetime of the 100 mm c-Si wafer deposited in the FlexAL reactor is $> 2 \text{ ms}$ for the largest part of the wafer and it only decreases slightly at the edges. The better uniformity obtained for the c-Si wafer deposited with Al_2O_3 at the FlexAL reactor can most probably be attributed to the usage of a carrier wafer.

In addition to the photoconductance measurements, the injection level dependence of the effective lifetime was also determined from quasi-steady-state photoluminescence measurements for the c-Si wafers passivated by Al_2O_3 deposited on the FlexAL reactor. From Fig. 7(b) it can be observed that there is excellent agreement between the effective lifetime determined by both techniques down to an injection level of $1 \times 10^{13} \text{ cm}^{-3}$. This indicates that the lifetime measurements on these *p*-type wafers are not affected by carrier trapping or depletion region modulation and consequently the injection level dependence can be related to the surface passivation mechanism.^{31,41} The effective lifetime of the passivated *p*-type wafers in Fig. 7 is dominated by Auger recombination in the bulk of the c-Si wafer for injection levels $> 5 \times 10^{15} \text{ cm}^{-3}$.⁴⁰ For lower injection levels the effective lifetime is roughly flat for the *p*-type c-Si wafers passivated by 10 and 30 nm thick Al_2O_3 deposited on the FlexAL reactor and 10 nm thick Al_2O_3 deposited on the ALD-I reactor. The *p*-type c-Si wafer passivated by the 30 nm thick film deposited on the ALD-I reactor, however, shows a decrease of the effective lifetime for lower injection levels. A similar injection level dependence of the effective lifetime (i.e., a decrease at lower injection levels) was reported by Agostinelli *et al.* for $2 \Omega \text{ cm}$ *p*-type c-Si passivated by Al_2O_3 deposited by thermal ALD (see also Sec. IV. C).¹⁹ As shown in Fig. 8 (a) the uniformity of the effective lifetime of the c-Si wafer passivated by a 30 nm thick Al_2O_3 film deposited on the ALD-I reactor was rather poor. We argue therefore that this non-uniformity of the effective lifetime over the c-Si wafer could well result in an *apparent* injection level dependence of the effective lifetime determined by the photoconductance technique due to its rather large detection area of $\sim 6 \text{ cm}^2$.²⁹ It should be noted that all of the *p*-type c-Si wafers passivated by Al_2O_3 films deposited by plasma-assisted ALD on the FlexAL reactor demonstrated a good uniformity in the level of surface passivation and a fairly constant effective lifetime at low injection levels.

The flat injection level dependence of the effective lifetime at low injection levels is consistent with the extended Shockley-Read-Hall model proposed by Girish *et al.*,⁴² because for *p*-type silicon the *minority* electrons are effectively shielded by the fixed negative charge present in the Al_2O_3 film. On the other hand, *p*-type c-Si wafers passivated by dielectrics with a fixed positive charge density such as thermal SiO_2 and a- $\text{SiN}_x:\text{H}$ demonstrate a significant injection level dependence of the effective lifetime.^{1,6} This pronounced injection level dependence can primarily be attributed to the fact that in this case the *majority* holes are shielded from the c-Si surface which results in an inversion layer at the c-Si surface. For dielectrics containing a fixed positive charge density the injection level dependence of the effective lifetime is flat for low injection levels on *n*-type c-Si when the *minority* holes are shielded from the surface.^{1,6} Consequently, the injection level dependence of the effective lifetime of c-Si passivated by the negative-charge dielectric Al_2O_3 is basically “mirroring” the injection level dependence for c-Si wafers passivated by positive-charge dielectrics such as thermal SiO_2 .

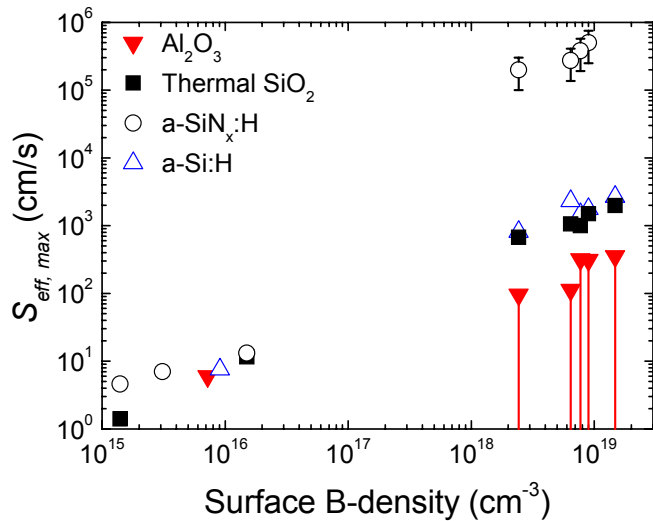


Figure 9: Upper level of the effective surface recombination velocity as a function of the B-density at the surface of c-Si wafers passivated by thermal SiO₂, a-SiN_x:H, a-Si:H and Al₂O₃. The values for highly B-doped surfaces for thermal SiO₂, a-Si:H and Al₂O₃ were taken from a previously published study.⁴³ The effective surface recombination values for low B-densities were calculated from the lifetime values reported by Kerr *et al.* and Dauwe *et al.* and assuming an infinite bulk lifetime.^{1,6,44} The error bars are smaller than the symbol size unless indicated otherwise.

and a-SiN_x:H.^{1,6} The effective lifetime can thus be made fairly constant at low injection levels for both *n*-type and *p*-type c-Si wafers by employing a surface passivation dielectric with fixed charges whose polarity lead to shielding of *minority* carriers from the c-Si surface. We note that the injection level dependence of the effective lifetime is not only of academic interest. A low level of surface passivation at low injection levels is detrimental for low-light performance of c-Si solar cells and will therefore have a negative effect on their yearly kWh output per Watt-peak. Moreover, when the positive-charge dielectric a-SiN_x:H is applied at the rear of a *p*-type c-Si solar cell the positive fixed charge density causes a parasitic shunting effect which significantly lowers the c-Si solar cell efficiency.¹⁰ This parasitic shunting effect is not observed when the negative-charge dielectric Al₂O₃ is applied at the rear of *p*-type c-Si solar cells.⁴⁵ The excellent level of surface passivation of lightly doped *p*-type c-Si by Al₂O₃ was recently confirmed by solar cells in which Al₂O₃ yielded an equal performance as *alnealed* thermal SiO₂. An independently confirmed solar cell efficiency of 20.6 % was obtained for these solar cells.⁴⁵

In Fig. 9 the level of surface passivation obtained by Al₂O₃ films synthesized by plasma-assisted ALD on *p*-type c-Si is compared with the best results published to date

for thermal SiO_2 , *as-deposited* $\text{a-SiN}_{\text{x}}:\text{H}$, and a-Si:H . The surface recombination velocity for the lightly B-doped c-Si surfaces was calculated from the highest effective lifetimes reported in the literature^{1,6,44} by assuming an infinite bulk lifetime (see Sec. III. A). The surface recombination velocities at the heavily B-doped c-Si surfaces were extracted by the device simulation package SENTUAURUS as described by Altermatt *et al.* and Hoex *et al.*^{9,43} As mentioned earlier the level of surface passivation of *as-deposited* $\text{a-SiN}_{\text{x}}:\text{H}$ on heavily B-doped surfaces could significantly be improved by extensive annealing.¹¹ From Fig. 9 it is clear that Al_2O_3 provides a state-of-the-art level of surface passivation on *p*-type c-Si with an arbitrary doping level. The high fixed negative charge density effectively shields the *minority* electrons from the *p*-type c-Si surfaces. The level of surface passivation obtained by Al_2O_3 on low resistivity *p*-type c-Si is comparable to the best results reported for thermal SiO_2 , $\text{a-SiN}_{\text{x}}:\text{H}$ and a-Si:H whereas heavily B-doped c-Si surfaces are even more effectively passivated by Al_2O_3 .⁴³

C. Low-resistivity *p*-type c-Si passivated by thermal ALD Al_2O_3

The results presented in this work so far were obtained for Al_2O_3 deposited by plasma-assisted ALD. The study of Agostinelli *et al.* demonstrated that also Al_2O_3 films deposited by thermal ALD with H_2O as oxidizing agent can provide an excellent level of surface passivation on *p*-type c-Si.¹⁹ To directly investigate a possible influence of the oxidizing agent selected, the level of surface passivation obtained by thermal and plasma-assisted ALD was compared by synthesizing the Al_2O_3 films by both processes in the same reactor.

The injection level dependent effective lifetime of a *p*-type c-Si wafer ($2 \Omega \text{ cm}$, $<111>$) wafer passivated by a 30 nm Al_2O_3 deposited by thermal and plasma-assisted ALD in the FlexAL reactor is shown in Fig. 10. For comparison the effective lifetime determined in the study of Agostinelli *et al.* is also included in the figure.¹⁹ As can be observed in Fig. 10 the effective lifetime of the c-Si wafer passivated by thermal ALD Al_2O_3 is significantly lower than the effective lifetime of the c-Si wafer passivated by plasma-assisted ALD Al_2O_3 . For the thermal ALD process, the effective lifetime is $\sim 400 \mu\text{s}$ for an injection level of $1 \times 10^{16} \text{ cm}^{-3}$ and shows the expected decrease due to Auger recombination at higher injection levels. The effective lifetime for the thermal ALD Al_2O_3 sample prepared in the FlexAL reactor is also significantly lower than the maximum effective lifetime of $950 \mu\text{s}$ (at an injection level of $1 \times 10^{15} \text{ cm}^{-3}$) as reported by Agostinelli *et al.*¹⁹ Remarkably, the effective lifetime for the thermal ALD Al_2O_3 films decrease at low injection levels for the *p*-type c-Si wafers which is in contrast to the

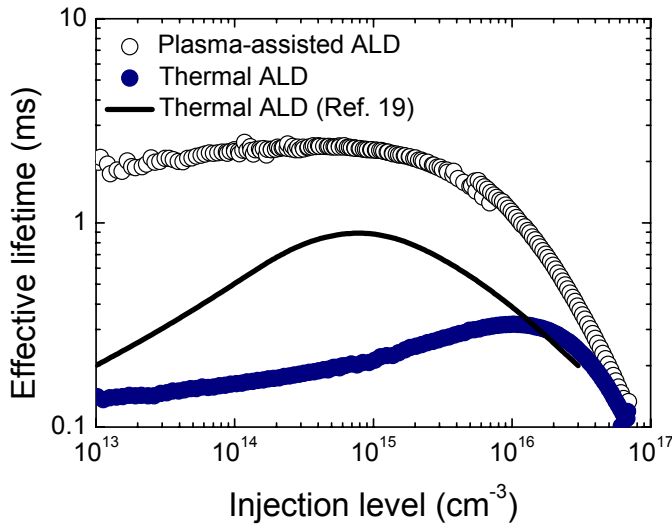


FIG. 10. Injection level dependent effective lifetime of a *p*-type c-Si (FZ, 2 Ω cm, <111>, 300 μm) wafer symmetrically passivated by a 30 nm Al_2O_3 film deposited by plasma-assisted ALD and thermal ALD on the FlexAL reactor. For comparison also the effective lifetime of a *p*-type c-Si (Czochralski (CZ) Si, 2 Ω cm) wafer passivated by thermal ALD Al_2O_3 in the study of Agostinelli *et al.* is included.¹⁹

constant effective lifetime observed at low injection levels for the c-Si wafer passivated by plasma-assisted ALD Al_2O_3 . This discrepancy between the results obtained by thermal and plasma-assisted ALD is not yet understood.

As mentioned in Sec. II the structural film properties of the Al_2O_3 films synthesized by thermal and plasma-assisted ALD were basically indistinguishable.²² However, electrical measurements on both types of Al_2O_3 films revealed significant differences in the fixed charge density in the films. In Fig. 11 two typical CV curves are shown obtained for MOS structures with a ~20 nm Al_2O_3 film deposited by thermal and plasma-assisted ALD in the FlexAL reactor. Similar to the lifetime samples, these MOS structures were annealed for 30 min at 425 °C in N_2 . It can clearly be seen that the flatband voltage, which is related to the fixed charge density,⁴⁶ is significantly different for the two Al_2O_3 films. The flat-band voltage of MOS structures with the 20 nm thick thermal and plasma-assisted ALD Al_2O_3 films correspond to fixed negative charge densities of $1 \times 10^{12} \text{ cm}^{-2}$ and $7 \times 10^{12} \text{ cm}^{-2}$, respectively. A higher fixed negative charge density provides a higher level of field-effect passivation and this can explain the discrepancy observed in the level of surface passivation obtained by the thermal and plasma-assisted ALD processes. Cho *et al.* and Kim *et al.* also reported significant differences in the electrical properties of thermal and plasma-assisted ALD Al_2O_3 .^{47,48}

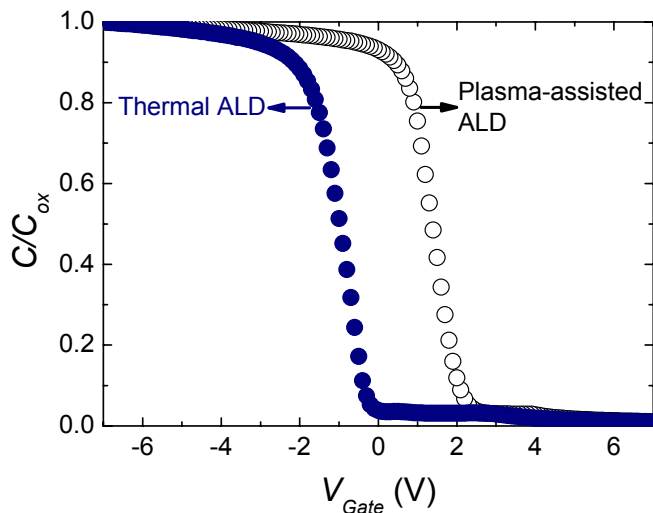


Figure 11: Capacitance voltage measurements of a metal-oxide-semiconductor structure containing a 20 nm Al_2O_3 film. The Al_2O_3 films were deposited by thermal and plasma-assisted ALD on a H-terminated 20-30 $\Omega \text{ cm}$ p-type c-Si wafer and annealed for 30 min at 425 °C in N_2 .

The thermal post-treatment employed in the study of Agostinelli *et al.* for thermal ALD Al_2O_3 was not reported but they were able to reach fixed negative charge densities up to $1 \times 10^{13} \text{ cm}^{-2}$.¹⁹ However, the fixed negative charge density in the Al_2O_3 film used for c-Si surface passivation was only $1.3 \times 10^{12} \text{ cm}^{-2}$.¹⁹ Consequently, the thermal ALD Al_2O_3 films used for c-Si surface passivation experiments in the study of Agostinelli *et al.*¹⁹ and in this work have a comparable fixed negative charge density, which is in turn significantly lower than the fixed negative charge density in the plasma-assisted ALD Al_2O_3 . It is therefore plausible that the optimal post-deposition thermal treatment required to obtain an optimal level of surface passivation is different for thermal and plasma-assisted ALD synthesized Al_2O_3 .⁴⁹ In a future publication we will address the c-Si surface passivation mechanism of Al_2O_3 in more detail and also the bulk and interface electronic properties of Al_2O_3 deposited on c-Si by various deposition techniques will be discussed.⁵⁰

V. Conclusions

From the results reported it is evident that Al_2O_3 films deposited by plasma-assisted ALD are an interesting candidate for passivation of c-Si surfaces as required for (high efficiency) c-Si solar cells. The self-limiting nature of the ALD process results intrinsically in precise thickness control and good thickness uniformity of the thin films. Moreover, the level of surface passivation provided by the Al_2O_3 is at least equal to the state-of-the-art level of surface passivation obtained by thermal SiO_2 films on lightly doped *n*-type c-Si wafers and *p*-type c-Si wafers with an arbitrary doping level. The excellent surface passivation by Al_2O_3 can mainly be attributed to a high fixed *negative* charge density in the Al_2O_3 as directly demonstrated in this work and whose underlying mechanism will be discussed in more detail in a future publication.⁵⁰ Due to the fixed negative charge density the injection level dependence of c-Si passivated by Al_2O_3 is “mirroring” that of c-Si passivated by positive-charge-dielectrics such as thermal SiO_2 and a- $\text{SiN}_x:\text{H}$. As such, it is demonstrated that a constant level of surface passivation for low injection levels can be obtained even for *p*-type c-Si when applying a negative-charge dielectric which shields the *minority* carriers from the c-Si surface. A constant level of surface passivation at low injection levels is especially beneficial for the low-light performance of c-Si solar cells. Moreover, the parasitic-shunting effect that is observed when the positive-charge dielectric a- $\text{SiN}_x:\text{H}$ is applied at the rear of a *p*-type c-Si solar cell is avoided when Al_2O_3 is applied at the rear of a *p*-type c-Si solar cell.⁴⁵ Thermal ALD Al_2O_3 demonstrated a significantly poorer level of surface passivation when compared to plasma-assisted ALD Al_2O_3 deposited with the same ALD reactor. This can most probably be related to a significantly higher fixed negative charge density in the plasma-assisted ALD Al_2O_3 films compared to the thermal ALD Al_2O_3 films.

ACKNOWLEDGMENTS

The authors thank W. Keuning, J.L. van Hemmen, M.J.F. van de Sande, J.F.C. Jansen and J.J.A. Zeebregts for their technical assistance and help during the experiments. E.J. Geluk, E. Smalbrugge, and T. de Vries are thanked for their assistance in the clean room operation. Dr. T. Trupke (University of New South Wales) and Dr. K.R. McIntosh (Australian National University) are acknowledged for the quasi-steady-state photoluminescence measurements and the fruitful discussions on the photoconductance data for high resistivity c-Si wafers, respectively. This work is supported by the Netherlands Technology Foundation STW and the German State of Lower Saxony. The work of B. Hoex is financially supported by OTB Solar.

APPENDIX: Effective lifetime for nearly intrinsic c-Si as determined by the photoconductance and photoluminescence techniques

Figure 12 shows the injection level dependence of the effective lifetime as determined from the photoconductance and photoluminescence technique for a low resistivity *n*-type c-Si ($2 \text{ k}\Omega \text{ cm}$, $<111>$) wafer symmetrically passivated by Al_2O_3 . The Al_2O_3 has a thickness of 30 nm and was deposited by plasma-assisted ALD. It can be observed that a strong discrepancy exists between the two results. The photoluminescence measurement shows a constant effective lifetime of 18 ms at low injection levels and a decrease at higher injection levels due to Auger recombination. The photoconductance data shows a pronounced behavior with an extremely high effective lifetime of 72 ms at an injection level of $2\text{-}4 \times 10^{14} \text{ cm}^{-3}$. A similar, but less pronounced, anomalous behavior of the effective lifetime was deduced from photoconductance measurements by Kerr *et al.* for $90 \Omega \text{ cm}$ *n*-type c-Si passivated with forming gas annealed thermal SiO_2 .¹ If the photoconductance measurement in Fig. 12 would be affected by depletion region modulation or trapping the effective lifetime would demonstrate a steady increase for low injection levels.^{30,31} However, to date no physical mechanism has been reported that can explain the subsequent decrease in the effective lifetime for injection levels lower than $2 \times 10^{14} \text{ cm}^{-3}$. On the other hand, it was shown by McIntosh *et al.* that the photoconductance voltage inductively measured by the Sinton WCT-100²⁹ lifetime tester, which is routinely used within the photovoltaics community, shows a strong non-linearity for a conductance lower than 1 mS (i.e. a 300 μm c-Si wafer of $> 30 \Omega \text{ cm}$).⁵¹ Although the physical origin of this non-linearity is still under investigation this non-linear response can possibly explain the particular values of the effective lifetime deduced from the photoconductance measurements for these high resistivity *n*-type c-Si wafers. Accordingly, for the high resistivity c-Si wafers discussed in this work it was decided to use the effective lifetimes extracted from the photoluminescence measurements with the self-consistent calibration proposed by Trupke *et al.*³³

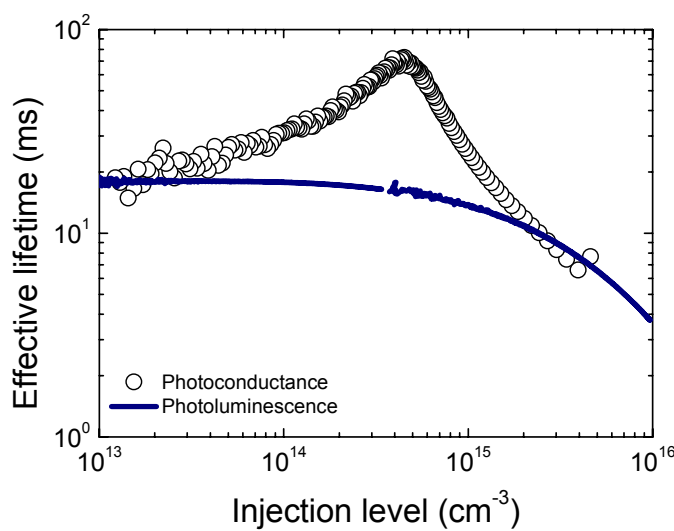


Figure 12: Injection level dependent effective lifetime of a *n*-type, high-resistivity c-Si wafer (2 k Ω cm, <111>, 300 μm) symmetrically passivated by a 30 nm Al_2O_3 film deposited by plasma-assisted ALD. The effective lifetime was measured by photoconductance (both in PCD and QSSPC mode) and quasi-steady-state photoluminescence.

REFERENCES:

- ¹ M. J. Kerr and A. Cuevas, *Semicond. Sci. Tech.* **17**, 35 (2002).
- ² W. Fussel, M. Schmidt, H. Angermann, G. Mende, and H. Flietner, *Nucl. Instrum. Methods Phys. Res. A* **377**, 177 (1996).
- ³ A. G. Aberle, S. Glunz, and W. Warta, *J. Appl. Phys.* **71**, 4422 (1992).
- ⁴ J. Zhao, A. H. Wang, and M. A. Green, *Sol. Energy Mat. Sol. Cells* **66**, 27 (2001).
- ⁵ P. M. Mulligan, D. H. Rose, M. J. Cudzinovic, and D. M. de Ceuster, *Proc. of the 19th EU-PVSEC*, Paris, (WIP Renewable Energies, Munich, 2004), p. 387.
- ⁶ M. J. Kerr and A. Cuevas, *Semicond. Sci. Tech.* **17**, 166 (2002).
- ⁷ T. Lauinger, J. Schmidt, A. G. Aberle, and R. Hezel, *Appl. Phys. Lett.* **68**, 1232 (1996).
- ⁸ R. Hezel and K. Jaeger, *J. Electrochem. Soc.* **136**, 518 (1989).
- ⁹ P. P. Altermatt, H. Plagwitz, R. Bock, J. Schmidt, R. Brendel, M. J. Kerr, and A. Cuevas, *Proc. of the 21st EU-PVSEC*, Dresden, (WIP Renewable Energies, Munich, 2006), p. 647.
- ¹⁰ S. Dauwe, L. Mittelstadt, A. Metz, and R. Hezel, *Prog. Photovoltaics* **10**, 271 (2002).
- ¹¹ F. W. Chen, T. T. A. Li, and J. E. Cotter, *Appl. Phys. Lett.* **88**, 263514 (2006).
- ¹² M. Taguchi, K. Kawamoto, S. Tsuge, T. Baba, H. Sakata, M. Morizane, K. Uchihashi, N. Nakamura, S. Kiyama, and O. Oota, *Prog. Photovoltaics* **8**, 503 (2000).
- ¹³ M. Garin, U. Rau, W. Brendle, I. Martin, and R. Alcubilla, *J. Appl. Phys.* **98**, 093711 (2005).
- ¹⁴ S. Olibet, E. Vallat-Sauvain, and C. Ballif, *Phys. Rev. B* **76**, 035326 (2007).
- ¹⁵ M. Schaper, J. Schmidt, H. Plagwitz, and R. Brendel, *Prog. Photovoltaics* **13**, 381 (2005).
- ¹⁶ T. Lauinger, J. Moschner, A. G. Aberle, and R. Hezel, *J. Vac. Sci. Technol. A* **16**, 530 (1998).
- ¹⁷ P. E. Gruenbaum, R. A. Sinton, and R. M. Swanson, *Appl. Phys. Lett.* **52**, 1407 (1988).
- ¹⁸ A. G. Aberle and R. Hezel, *Prog. Photovoltaics* **5**, 29 (1997).
- ¹⁹ G. Agostinelli, A. Delabie, P. Vitanov, Z. Alexieva, H. F. W. Dekkers, S. De Wolf, and G. Beaucarne, *Sol. Energy Mat. Solar Cells* **90**, 3438 (2006).
- ²⁰ B. Hoex, S. B. S. Heil, E. Langereis, M. C. M. van de Sanden, and W. M. M. Kessels, *Appl. Phys. Lett.* **89**, 042112 (2006).
- ²¹ R. L. Puurunen, *J. Appl. Phys.* **97**, 121301 (2005).
- ²² J.L. van Hemmen, S. B. S. Heil, J. Klootwijk, F. Roozeboom, C.J. Hodson, M. C. M. van de Sanden, and W. M. M. Kessels, *J. Electrochem. Soc.* **154**, G165 (2007).

- 23 S. B. S. Heil, E. Langereis, F. Roozeboom, M. C. M. van de Sanden, and W. M. M. Kessels, J. Electrochem. Soc. **153**, G956 (2006).
- 24 S. B. S. Heil, J.L. Hemmen, C.J. Hodson, N. Singh, J.H. Klootwijk, F. Roozeboom, M. C. M. van de Sanden, and W. M. M. Kessels, J. Vac. Sci. Technol. A **25** 1357 (2007).
- 25 S. B. S. Heil, P. Kudlacek, E. Langereis, R. Engeln, M. C. M. van de Sanden, and W. M. M. Kessels, Appl. Phys. Lett. **89**, 131505 (2006).
- 26 J. Humlicek, *Handbook of Ellipsometry*. (William Andrew, Inc., New York, 2005).
- 27 T. Yasuda and D. E. Aspnes, Appl. Optics **33**, 7435 (1994).
- 28 W. Kern, J. Electrochem. Soc. **137**, 1887 (1990).
- 29 R. A. Sinton and A. Cuevas, Appl. Phys. Lett. **69**, 2510 (1996).
- 30 P. J. Cousins, D. H. Neuhaus, and J. E. Cotter, J. Appl. Phys. **95**, 1854 (2004).
- 31 D. Macdonald and A. Cuevas, Appl. Phys. Lett. **74**, 1710 (1999).
- 32 T. Trupke and R. A. Bardos, Proc. of the IEEE PVSEC, Lake Buena Vista, FL, (IEEE, Piscataway, NJ, 2005), p. 903.
- 33 T. Trupke, R. A. Bardos, and M. D. Abbott, Appl. Phys. Lett. **87**, 184102 (2005).
- 34 P. Pohl and R. Brendel, Proc. of the 19th European PVSEC, Paris, (WIP Renewable Energies, Munich, 2004), p. 46.
- 35 P. Pohl, J. Schmidt, K. Bothe, and R. Brendel, Appl. Phys. Lett. **87**, 142104 (2005).
- 36 S. Dauwe, J. Schmidt, A. Metz, and R. Hezel, Proc. of the 29th IEEE Photovoltaic Specialist Conference, New Orleans, (IEEE, Piscataway, NJ, 2002), p. 162.
- 37 S. W. Glunz, D. Biro, S. Rein, and W. Warta, J. Appl. Phys. **86**, 683 (1999).
- 38 M. M. Shahin, J. Chem. Phys. **45**, 2600 (1966).
- 39 P. A. Basore, IEEE Trans. Electron. Dev. **37**, 337 (1990).
- 40 M. J. Kerr and A. Cuevas, J. Appl. Phys. **91**, 2473 (2002).
- 41 M. Bail, M. Schulz, and R. Brendel, Appl. Phys. Lett. **82**, 757 (2003).
- 42 R. B. M. Girisch, R. P. Mertens, and R. F. Dekeersmaecker, IEEE Trans. Electron Devices **35**, 203 (1988).
- 43 B. Hoex, J. Schmidt, R. Bock, P. P. Altermatt, M. C. M. van de Sanden, and W. M. M. Kessels, Appl. Phys. Lett. **91**, 112107 (2007).
- 44 S. Dauwe, J. Schmidt, and R. Hezel, Proc. of the 29th IEEE Photovoltaic Specialist Conference, New Orleans, (IEEE, Piscataway, NJ, 2002), p. 1246.
- 45 J. Schmidt, A. Merkle, R. Brendel, B. Hoex, M. C. M. van de Sanden, and W. M. M. Kessels, accepted for publication in Progress in Photovoltaics (2007).
- 46 D.K. Schroder, *Semiconductor Material and Device Characterization*, 3rd ed. (Wiley-Interscience Hoboken, NJ, 2006).
- 47 M. Cho, H. B. Park, J. Park, S. W. Lee, C. S. Hwang, J. Jeong, H. S. Kang, and Y. W. Kim, J. Electrochem. Soc. **152**, F49 (2005).

-
- ⁴⁸ J. W. Lim and S. J. Yun, *Electrochem. Sol. State Lett.* **7**, F45 (2004).
- ⁴⁹ In a future publication we will show that field-effect passivation scales with Q_f^2 and, hence, the small difference in the fixed charge density of the thermal ALD Al₂O₃ films could explain the difference in the level of surface passivation.
- ⁵⁰ B. Hoex, J. J. H. Gielis, M. C. M. van de Sanden, and W. M. M. Kessels, to be published.
- ⁵¹ K.R. McIntosh, J.H. Guo, M. D. Abbott, and R. A. Bardos, *Progr. Photovoltaics*, 10.1002/pip.810 (2008).

Chapter 6^{*}

Excellent Passivation of Highly Doped *p*-type Si Surfaces by the Negative-Charge-Dielectric Al₂O₃

From lifetime measurements, including a direct experimental comparison with thermal SiO₂, a-Si:H, and as-deposited a-SiN_x:H, it is demonstrated that Al₂O₃ provides an excellent level of surface passivation on highly B-doped c-Si with doping concentrations around 10¹⁹ cm⁻³. The Al₂O₃ films, synthesized by plasma-assisted atomic layer deposition and with a high fixed negative charge density, limit the emitter saturation current density of B-diffused *p*⁺-emitters to ~10 and ~30 fA/cm² on >100 Ω/sq and 54 Ω/sq sheet resistance *p*⁺-emitters, respectively. These results demonstrate that highly doped *p*-type Si surfaces can be passivated as effectively as highly doped *n*-type surfaces.

^{*} Published as: B. Hoex, J. Schmidt, R. Bock, P.P. Altermatt, M.C.M. van de Sanden, W.M.M. Kessels, Appl. Phys. Lett. **91**, 112107 (2007).

Research within the crystalline silicon (c-Si) photovoltaic community is driven by the necessity to decrease the costs per watt peak. As a consequence, the thickness of c-Si solar cells is reduced and alternative c-Si material and production processes are investigated. Presently, most Si solar cells are fabricated from *p*-type c-Si base material. However, the relative insensitivity of *n*-type c-Si to various impurities and defects could well result in a switch in the future to predominantly *n*-type base material.¹ The success of these developments will depend, among others, on the level of surface passivation that can be obtained on the surfaces of interest. Especially the passivation of highly doped *p*-type surfaces is of key interest for diffused emitter cells based on *n*-type silicon.

The passivation of highly B-doped *p*-type c-Si (for example a *p*⁺-emitter on a *n*-type Si wafer) is still trailing behind the results obtained on highly doped *n*-type c-Si.^{2,3} This gap in performance can, at least partly, be explained by the presence of positive built-in charges in the commonly used passivation films such as thermal SiO₂ and as-deposited a-SiN_x:H.² Recently, Chen *et al.*, however, demonstrated that highly B-doped *p*-type c-Si can be effectively passivated by silicon rich a-SiN_x:H after prolonged annealing (up to 4 h) yielding an at least equal performance to as-grown thermal SiO₂ for sheet resistances > 130 Ω/sq.⁴ Furthermore, it was shown that a-Si:H can yield a surface passivation of *p*⁺-emitters comparable to forming gas annealed thermal oxide² whereas the performance of a-SiC_x:H remained significantly poorer.⁵

An appealing approach is to passivate highly doped *p*-type c-Si by a dielectric containing a fixed *negative* charge density. In this way, the minority carrier (electron) concentration is effectively reduced at the highly defective surface and consequently the recombination rate is reduced. It is well known that Al₂O₃ can contain a high density of built-in negative charges (up to ~10¹³ elementary charges/cm²) and Al₂O₃ has recently been shown to provide a state-of-the-art level of surface passivation on moderately doped *p*- and *n*-type c-Si.^{6,7} In this Letter, we show that Al₂O₃ synthesized by plasma-assisted atomic layer deposition (ALD) provides an excellent level of surface passivation on B doped *p*⁺-type emitters with surface concentrations ranging from 5×10¹⁸ to 3×10¹⁹ cm⁻³. From a direct experimental comparison, it is established that Al₂O₃ yields a higher level of surface passivation than forming gas annealed thermal SiO₂, a-Si:H and as-deposited a-SiN_x:H applied on the same samples. Moreover, it is demonstrated that highly B-doped *p*-type c-Si surfaces can as effectively be passivated as highly doped *n*-type c-Si surfaces.

The *p*⁺/*n/p*⁺ structures used in this study were prepared at the Australian National University by exposing <100> shiny- etched *n*-type c-Si (90 and 20 Ω cm) with a thickness of ~260 μm to BBr₃ at T=895–1010 °C.⁸ After stripping the B containing glass, B-diffusion was driven by thermal oxidation at 1050 °C.⁸ The sheet resistance of the samples was determined by four-point probe measurements and the doping profile, shown in Fig. 1, was determined by both electrochemical capacitance-voltage (ECV)

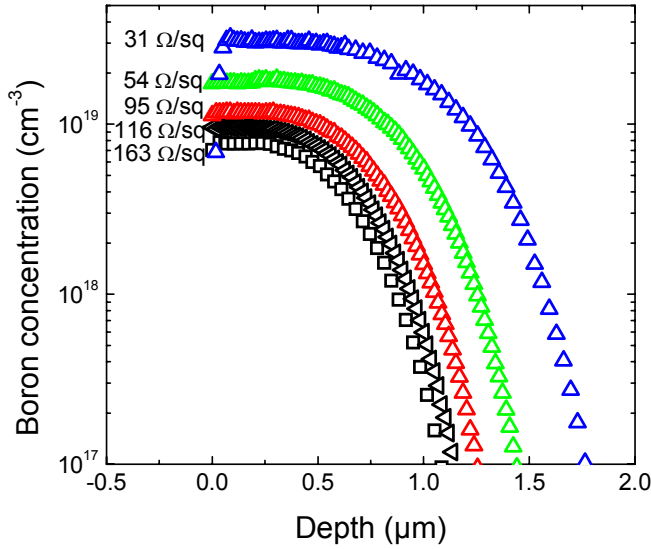


Figure 1: B-doping profiles of the $p^+/n/p^+$ samples with various sheet resistances as determined by ECV profiling and experimentally verified by SIMS measurements ($54 \Omega/\text{sq}$ and $95 \Omega/\text{sq}$).

profiling and secondary ion mass spectrometry (SIMS). The level of surface passivation of thermal SiO_2 , a- $\text{SiN}_x\text{:H}$ and a-Si:H on these p^+ -emitter samples was already reported in a previous study.^{2,8} Before deposition a possibly remaining film from previous experiments was stripped off and the samples received a conventional RCA cleaning with a final dip in diluted HF (1%). Al_2O_3 films were deposited on both sides of the samples by alternating $\text{Al}(\text{CH}_3)_3$ dosing and O_2 plasma exposure in a remote plasma ALD reactor (Oxford Instruments FlexAL™) at a substrate temperature of 200°C .⁹ 255 ALD cycles of 4 s resulted in 30 nm thick Al_2O_3 as determined by *in situ* spectroscopic ellipsometry. Subsequently, the samples received a 30 min anneal at 425°C in N_2 .⁷ The passivation quality of the films was quantified by the emitter saturation current density J_{0e} of the p^+ -emitters. The emitter saturation current density J_{0e} was determined from contactless photo-conductance decay measurements in both the quasi-steady-state and transient mode (Sinton WCT-100)¹⁰ from the relation proposed by Kane and Swanson¹¹

$$\frac{1}{\tau_{\text{eff}}} - \frac{1}{\tau_{\text{Auger}}} = \frac{1}{\tau_{\text{SRH}}} + 2 \frac{J_{0e}(N_d + \Delta n)}{qn_i^2 W}, \quad (1)$$

where τ_{eff} is the measured effective excess carrier lifetime, τ_{Auger} the intrinsic Auger

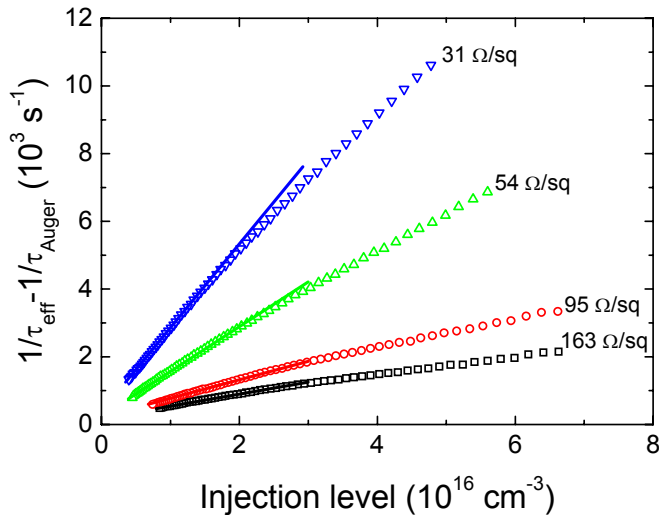


Figure 2: Measured Auger corrected inverse effective lifetime as a function of the injection level for c-Si samples with double sided B-doped p^+ -emitter and various sheet resistances passivated on both sides by a 30 nm Al_2O_3 film. The emitter saturation current density is extracted from the linear fit up to $2 \times 10^{16} \text{ cm}^{-3}$ by means of Eq. 1.

lifetime,¹² τ_{SRH} the defect-related bulk lifetime, N_d the base doping level, n_i the intrinsic carrier concentration of c-Si,¹³ q the elementary charge, Δn the excess carrier density, and W the sample thickness.

In Fig. 2, the Auger-corrected inverse lifetimes are shown for samples with various sheet resistances passivated by 30 nm Al_2O_3 films. The curves do not show a strong non-linear behavior such as in the case of a-SiN_x:H.⁸ Consequently Eq. (1) can be used to extract J_{oe} and no alternative quantification such as implied open-circuit voltage has to be used in this case.¹⁴ Nevertheless a small non-linearity is still observed, possibly explained by minor experimental uncertainties or uncertainty in the empirically determined Auger lifetime at high injection level.¹² Therefore, J_{oe} is determined for a moderate injection level up to $2 \times 10^{16} \text{ cm}^{-3}$ where Auger recombination does not dominate. Similar to the results obtained on lightly doped n - and p -type c-Si,⁷ the level of surface passivation by Al_2O_3 is dramatically affected by the postdeposition annealing. The emitter saturation current for the 163 Ω/sq sample coated with an as-deposited Al_2O_3 film (not shown) is in the order of $\sim 1.2 \times 10^3 \text{ fA/cm}^2$, which is comparable to a nonpassivated sample, and is reduced to below 10 fA/cm^2 after a 30 min anneal at 425 °C in N_2 . This dramatic improvement in surface passivation is related to changes at the c-Si/ Al_2O_3 interface affecting both the amount of built-in negative charge and the

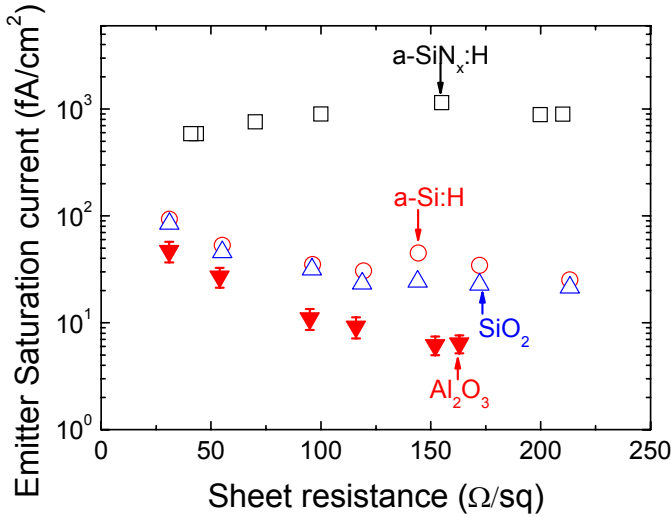


Figure 3: Measured emitter saturation current density (J_{0e}) as a function of the sheet resistance for B-doped p^+ -emitter samples passivated by Al_2O_3 , as-deposited a- $\text{SiN}_x\text{:H}$, a- Si:H , and forming gas annealed thermal SiO_2 .

interface defect density as will be reported in a separate study.

In Fig. 3, the extracted J_{0e} values are shown as a function of the emitter sheet resistance of p^+ -emitters passivated by Al_2O_3 , and are compared to earlier published results for thermal SiO_2 , a- Si:H and a- $\text{SiN}_x\text{:H}$.^{2,8} The p^+ -emitter samples with SiO_2 were forming gas annealed and those with a- $\text{SiN}_x\text{:H}$ were as-deposited. Clearly, the J_{0e} values obtained for Al_2O_3 are significantly lower for the complete sheet resistance range tested; J_{0e} values below 10 fA/cm² are obtained for a sheet resistance $>100 \Omega/\text{sq}$ and J_{0e} is only ~ 50 fA/cm² for a 31 Ω/sq emitter. The emitter saturation currents on p^+ -emitters are even lower than obtained on highest-quality n^+ -emitters with a comparable sheet resistance passivated with aluminum annealed thermal SiO_2 or as-deposited a- $\text{SiN}_x\text{:H}$.¹⁵ The emitter saturation current density obtained in this study for a 95 Ω/sq emitter would limit the room temperature open circuit voltage of a solar cell to 747 mV by applying the ideal diode law and assuming a short-circuit current of 40 mA/cm².¹⁶

The most fundamental property to compare, however, is the surface recombination velocity at the highly doped B surface which strongly depends on the surface doping concentration. The S_{n0} values were extracted from the experimental J_{0e} values and dopant profiles by numerical modeling using the device simulation package SENTAURUS¹⁷ and the physical models established in Ref. 2 and 3 and the results are shown in Fig. 4. The experimental errors in both J_{0e} and the dopant profile and the relative strong Auger recombination in these emitters only allowed extraction of the maximum error bounds for the Al_2O_3 . For comparison also the S_{n0} values obtained for

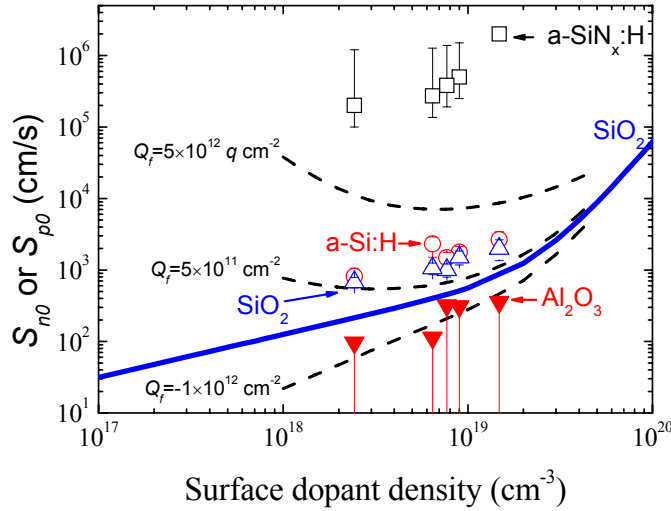


Figure 4: Surface recombination velocity S_{n0} at the B-doped p^+ -type c-Si surface as a function of the surface dopant density as determined by ECV measurements. The S_{n0} values were deduced by device simulation using the values in Figs. 1 and 3. The solid blue line indicates the empirical relation obtained for S_{p0} obtained on heavily doped n -type surfaces passivated by aluminum annealed thermal SiO_2 (see Ref. 3). By assuming $S_{p0}=S_{n0}$ this empirical relation is used to simulate the impact of positive and negative built-in charges Q_f on S_{n0} as indicated by the dashed lines.

thermal SiO_2 , a-Si:H and a- SiN_x :H are given as determined on the same sample set.² The solid blue line in Fig. 4 shows the empirically determined limit of the surface recombination velocity S_{p0} obtained by aluminum annealed thermal SiO_2 on highly doped n^+ -emitters.³ From Fig. 4 it is evident that the level of surface passivation on highly doped p -type c-Si provided by thermal SiO_2 , a-Si:H and a- SiN_x :H was significantly poorer than what is obtained on highly doped n -type c-Si. Moreover, the S_{n0} values obtained by Al_2O_3 on the highly doped p -type c-Si are well below the best values obtained on highly doped n -type surfaces which indicates that highly doped p -type surfaces can as effectively be passivated as highly doped n -type c-Si. Figure 4 also illustrates that a *negative* built-in charge is indeed very beneficial for passivating highly doped p -type surfaces compared to the *positive* built-in charge commonly present in thermal SiO_2 and as-deposited a- SiN_x :H. At the same time the excellent results for B concentrations of $\sim 10^{19} \text{ cm}^{-3}$ indicate that also the c-Si/ Al_2O_3 interface defect density is sufficiently low and/or that the dominant interface defect has a relatively low electron capture cross section.

In summary, we have demonstrated that Al_2O_3 synthesized by plasma-assisted atomic layer deposition shows an excellent level of surface passivation on highly doped

p-type c-Si. Consequently, highly doped *p*-type c-Si can as effectively be passivated as highly doped *n*-type c-Si allowing maximum freedom in the solar cell design either using *p*-type or *n*-type c-Si base material.

ACKNOWLEDGMENTS

The authors acknowledge the experimental work of M. Kerr and A. Cuevas, and thank W. Keuning, M.J.F. van de Sande, J.F.C. Jansen and J.J.A. Zeebregts for their skillful technical assistance. The Netherlands Technology Foundation STW is acknowledged for their financial support. The work of one of the authors (BH) is financially supported by OTB Solar. The research of another author (WK) has been made possible by a fellowship of the Royal Netherlands Academy of Arts and Sciences (KNAW).

REFERENCES:

- ¹ D. Macdonald and L. J. Geerligs, *Appl. Phys. Lett.* **85**, 4061 (2004).
- ² P. P. Altermatt, H. Plagwitz, R. Bock, J. Schmidt, R. Brendel, M. J. Kerr, and A. Cuevas, Proc. of the 21st EU-PVSEC, Dresden, (WIP Renewable Energies, Munich, 2006), p. 647.
- ³ P. P. Altermatt, J. O. Schumacher, A. Cuevas, M. J. Kerr, S. W. Glunz, R. R. King, G. Heiser, and A. Schenk, *J. Appl. Phys.* **92**, 3187 (2002).
- ⁴ F. W. Chen, T. T. A. Li, and J. E. Cotter, *Appl. Phys. Lett.* **88**, 263514 (2006).
- ⁵ M. Vetter, R. Ferre, I. Martin, P. Ortega, R. Alcubilla, R. Petres, J. Libal, and R. Kopecek, Proc. of the 4th WCPEC, Hawaii, (IEEE, Piscataway, NJ, 2006), p. 1271.
- ⁶ G. Agostinelli, A. Delabie, P. Vitanov, Z. Alexieva, H. F. W. Dekkers, S. De Wolf, and G. Beaucarne, *Sol. Energy Mat. Solar Cells* **90**, 3438 (2006).
- ⁷ B. Hoex, S. B. S. Heil, E. Langereis, M. C. M. van de Sanden, and W. M. M. Kessels, *Appl. Phys. Lett.* **89**, 042112 (2006).
- ⁸ M.J. Kerr, Ph.D. thesis, Australian National University, 2002.
- ⁹ J.L. van Hemmen, S. B. S. Heil, J. Klootwijk, F. Roozeboom, C.J. Hodson, M. C. M. van de Sanden, and W. M. M. Kessels, *J. Electrochem. Soc.* **154**, G165 (2007).
- ¹⁰ R. A. Sinton and A. Cuevas, *Appl. Phys. Lett.* **69**, 2510 (1996).
- ¹¹ D.E. Kane, Swanson, R.M., Proc. of the 18th IEEE Photovoltaic Specialists Conference, Las Vegas, (IEEE, Piscataway, NJ, 1985), p. 578.
- ¹² M. J. Kerr and A. Cuevas, *J. Appl. Phys.* **91**, 2473 (2002).
- ¹³ P. P. Altermatt, A. Schenk, F. Geelhaar, and G. Heiser, *J. Appl. Phys.* **93**, 1598 (2003).
- ¹⁴ A. Cuevas and R. A. Sinton, *Prog. Photovoltaics* **5**, 79 (1997).
- ¹⁵ M. J. Kerr, J. Schmidt, A. Cuevas, and J. H. Bultman, *J. Appl. Phys.* **89**, 3821 (2001).
- ¹⁶ J. H. Zhao, A. H. Wang, M. A. Green, and F. Ferrazza, *Appl. Phys. Lett.* **73**, 1991 (1998).
- ¹⁷ SENTAURUS, Mountain View, CA, www.synopsys.com/products/tcad/tcad.html

Chapter 7^{*}

On the c-Si Surface Passivation Mechanism by the Negative Charge Dielectric Al₂O₃

Al₂O₃ is a versatile high- κ dielectric that has excellent surface passivation properties on crystalline Si (c-Si), which are of vital importance for devices such as light emitting diodes and high-efficiency solar cells. We demonstrate both experimentally and by simulations that the surface passivation can mainly be attributed to field-effect passivation induced by a high negative fixed charge density Q_f up to 10^{13} cm⁻² that is present in the Al₂O₃ film at the interface with the underlying Si substrate. The unique polarity of Q_f in Al₂O₃ is especially beneficial for the passivation of *p*-type c-Si as the bulk minority carriers are shielded from the c-Si surface. As the level of field-effect passivation is shown to scale with Q_f^2 the high Q_f in Al₂O₃ tolerates a higher interface defect density on c-Si compared to alternative surface passivation schemes.

^{*} In preparation for publication.

An excellent electrical interface quality is essential for many devices relying on the bulk electronic properties of semiconductors.¹ Electrical losses at a semiconductor interface or surface should be minimized in photonic devices based on group III-V or group IV semiconductors where radiative recombination should be the dominant process.^{2,3} In complementary metal-oxide-semiconductor (CMOS) devices the channel is in direct contact with the interface between the gate dielectric and the semiconductor.⁴ Moreover, electronic losses at the c-Si surface have become increasingly important in the field of c-Si solar cells due to the trend towards thinner c-Si wafers used as base material.⁵ Consequently, the reduction of recombination losses at semiconductor interfaces is a prime concern for numerous semiconductor applications.

Recombination losses at a semiconductor interface or surface can be reduced by two different passivation strategies. As the recombination rate is directly proportional to the interface defect density the first strategy is based on the reduction of the number of defect states at the interface. The interface defect density can be reduced significantly by the passivation of undercoordinated atoms by, e.g., atomic H or by a thin dielectric or semiconductor film. This strategy is commonly referred to as chemical passivation. For example the mid-gap interface defect density of c-Si can be as low as $1 \times 10^9 \text{ eV}^{-1} \text{ cm}^{-2}$ after the growth of a high quality thermal SiO₂ film and a subsequent anneal in a H₂ atmosphere, e.g., a forming gas anneal.⁶

The second strategy to reach surface passivation is based on a significant reduction of the electron or hole concentration at the semiconductor interface by means of a built-in electric field. As recombination processes require both electrons and holes, the highest recombination rate is obtained when the electron and hole concentration at the interface are approximately equal in magnitude (assuming identical capture cross-sections for electrons and holes). In other cases the recombination rate scales with the minority carrier concentration at the surface. In the so-called field-effect passivation, the electron or hole concentration at the semiconductor interface is altered by electrostatic shielding of the charge carriers through an internal electric field present at the interface. This internal electric field can either be obtained by a doping profile below the interface or by the presence of fixed electrical charges at the semiconductor interface. Obviously, the principle of field-effect passivation does not apply for CMOS devices such as field effect transistors (FET). A high fixed charge density is even deleterious for the transistor performance as it influences the threshold voltage and the transport of electron and holes in the semiconductor channel.^{4,7} Consequently, the application areas of field-effect passivation are limited but the effect can be employed successfully in devices such as light emitting diodes and solar cells.

Recently it was demonstrated that amorphous Al₂O₃ films synthesized by atomic layer deposition (ALD) yield an excellent level of surface passivation on c-Si.⁸⁻¹¹ In our previous work a similar level of surface passivation as state-of-the-art thermal SiO₂ was demonstrated on low resistivity *n*- and *p*-type c-Si,⁹ whereas highly doped *p*-type Si

surfaces were found to be even more effectively passivated by Al₂O₃ than by thermal SiO₂.¹⁰ Remarkably, the Al₂O₃ films, synthesized by plasma-assisted ALD at a substrate temperature of 200 °C, demonstrated no significant level of surface passivation in the *as-deposited* state.^{9,10} A 30 min post-deposition anneal at 425 °C in N₂ was required to obtain the level of surface passivation reported. A non-specified thermal treatment was also required for an optimal level of surface passivation in the study of Agostinelli *et al.* for Al₂O₃ films synthesized by thermal ALD.⁸

In this paper we will address the underlying mechanism of c-Si surface passivation by an amorphous Al₂O₃ film. From results obtained on Al₂O₃ films synthesized by plasma-assisted ALD it will be demonstrated that the surface passivation can, for the largest part, be explained by a strong field-effect passivation induced by a relatively high fixed negative charge density Q_f in the Al₂O₃ film. On the basis of simulations it will be discussed that the field-effect passivation scales with Q_f^2 and, consequently, the high Q_f in Al₂O₃ tolerates a higher interface defect density than other passivation films with lower Q_f values. It will be shown that the post-deposition anneal increases the negative Q_f and lowers the interface defect density of the Si/SiO_x/Al₂O₃ system resulting in a significant improvement of the level of surface passivation obtained. The presence of an interfacial SiO_x film between c-Si and the Al₂O₃ appears to play a key role in both the origin of the negative Q_f and the interface defect density. As a negative Q_f in combination with a sufficiently low interface defect density are routinely reported for Al₂O₃ films deposited on c-Si, irrespective of the deposition technique, it is argued that the findings presented in this paper are not limited to Al₂O₃ films synthesized by (plasma-assisted) ALD.

The field-effect passivation of c-Si by Al₂O₃ is experimentally demonstrated in Fig. 1. A high quality 1.9 Ω cm *n*-type c-Si wafer with a thickness of 275 μm was passivated on both sides by a 26 nm thick Al₂O₃ film synthesized by plasma-assisted ALD.¹¹ The resulting effective lifetime of the passivated c-Si wafer exceeds 6 ms indicating that the c-Si surfaces are adequately passivated by Al₂O₃. Subsequently a positive charge density $Q_{surface}$ is applied at the Al₂O₃ surface in a corona charging experiment. In this case, the field-effect passivation is ruled by the sum of Q_f and $Q_{surface}$. From the figure it is clear that a positive $Q_{surface}$ up to 10^{13} cm^{-2} hardly affects the effective lifetime of the c-Si wafer. However, a positive $Q_{surface}$ in the range of $(1.2\text{-}1.4)\times10^{13} \text{ cm}^{-2}$ leads to a strong decrease in the effective lifetime. A minimum effective lifetime of $\sim100 \mu\text{s}$ is obtained for a positive $Q_{surface}$ of $1.3\times10^{13} \text{ cm}^{-2}$. At this stage the positive $Q_{surface}$ balances the negative Q_f in the Al₂O₃ film which nullifies the level of field-effect passivation. For a positive $Q_{surface}$ exceeding the amount of negative Q_f [$Q_{surface}$ in the range of $(1.3\text{-}2.0)\times10^{13} \text{ cm}^{-2}$] field-effect passivation is provided by the positive charge density at the c-Si surface. Summarizing, Fig. 1 clearly demonstrates the mechanism of field-effect passivation on c-Si and it reveals that the fixed negative charge density in this 26 nm thick Al₂O₃ film is $(1.3\pm0.1)\times10^{13} \text{ cm}^{-2}$.

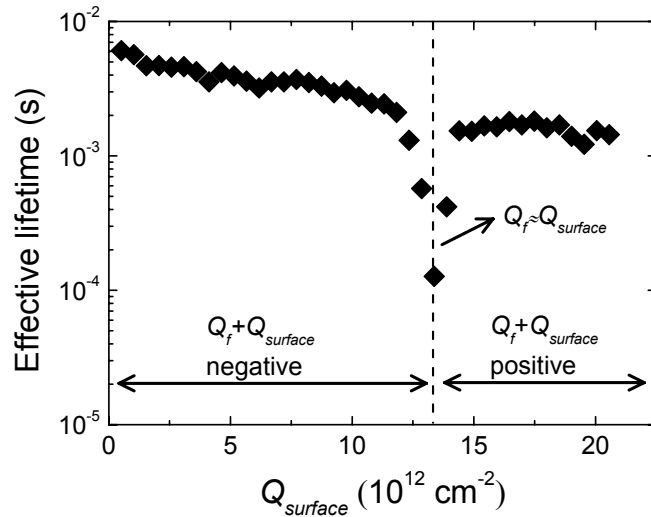


Figure 1: Effective lifetime of a $1.9 \Omega \text{ cm}$ n -type c-Si wafer passivated on both sides by a 26 nm thick Al_2O_3 film. The effective lifetime is presented as a function of the positive charge density Q_{surface} deposited at the Al_2O_3 on one side of the wafer in a corona charging experiment. Field-effect passivation is ruled by the sum of the negative fixed charge density Q_f in the Al_2O_3 film and the positive Q_{surface} . The effective lifetime was determined at an injection level of $10^{14}\text{-}10^{15} \text{ cm}^{-3}$.

Al_2O_3 has extensively been investigated for the application as gate and charge trapping dielectric on c-Si where also high negative Q_f have been reported. For gate dielectric applications in CMOS a low interface defect density and a low Q_f are essential,⁴ whereas a low interface defect density in combination with a high density of electronically active bulk defects is desired for charge trapping dielectrics such as applied in nonvolatile memory.^{12,13} Table I summarizes the bulk and interface electronic properties reported in the literature for Al_2O_3 films deposited on c-Si by various techniques. The sign of Q_f is always negative for the Al_2O_3 films after annealing, irrespective of the deposition technique.¹⁴ The magnitude of Q_f is typically in the range of $10^{12}\text{-}10^{13} \text{ cm}^{-2}$ for annealed Al_2O_3 films, in good agreement with our results in Fig. 1. From thickness dependent capacitance-voltage measurements it was deduced that the negative Q_f is independent of the Al_2O_3 thickness and is located at the interface with the substrate.¹⁵⁻¹⁷

It is interesting to note that negative fixed charges are detected in Al_2O_3 films deposited on H-terminated c-Si as well as Al_2O_3 films deposited on c-Si covered by a 1-100 nm thick SiO_2 film. Despite the fact that Al_2O_3 is thermodynamically stable on c-Si, Al_2O_3 deposition processes occur under non-equilibrium conditions and as a result

Table I: Bulk and interface electronic properties for Al₂O₃ films deposited on c-Si as reported in the literature. All films were deposited on H-terminated c-Si unless indicated otherwise. In all cases Q_f was extracted from the flat-band voltage shift determined from capacitance-voltage (C-V) measurements of MOS structures. The interface defect density was extracted from C-V and/or conductance measurements of MOS structures. Most samples were analyzed after a post-deposition anneal, however, some samples were also measured as-deposited (indicated with “a-d”).

Negative Q_f (10 ¹² cm ⁻²)	D_n at midgap (10 ¹¹ eV ⁻¹ cm ⁻²)	Deposition method	Deposition temperature (°C)	Post-deposition thermal treatment	Ref.
0.2-0.5	-	Pyrolysis of Al(C ₃ H ₈ O) ₃ on c-Si with 23-100 nm thermal SiO ₂	425	30 min FGA ^a at 425 °C	15
0.2-0.5	-	CVD from AlBr ₃ + NO on c-Si with 23-100 nm thermal SiO ₂	910	30 min FGA ^a at 425 °C	15
-0.5 (a-d) 3.2	15 (a-d) 0.8	Pyrolysis of Al(C ₃ H ₈ O) ₃ on c-Si with 1.5 nm native SiO ₂	360	15 min FGA ^a at 510 °C	¹⁸
10-11 (a-d)	-	Pyrolysis of AlCl ₃ in CO ₂ /H ₂ environment ^b	900	None	13
0.6 AD	~1	ALD from Al(CH ₃) ₃ +H ₂ O	450	None	¹⁹
~2	0.8	ALD from Al(CH ₃) ₃ and H ₂ O	350	Various at 585 °C and 800 °C	²⁰
-	0.3	Oxidation of evaporated Al	<400	800 °C in N ₂	²¹
7	1-3	ALD from AlCl ₃ and H ₂ O ^d	370	None	17
7 (a-d) 6-7	13 (a-d) 1	ALD from Al(CH ₃) ₃ and H ₂ O ^b	350	FGA ^a at 300-450 °C and anneal in N ₂ at 450 °C	²²
5-10 (a-d)	2-5 ^c (a-d)	Reactive target sputtering in Ar/O ₂	380	FGA ^a	²³
-	2-10 (a-d)	ALD from AlCl ₃ and H ₂ O	300-800	None	²⁴
-	20	ALD from Al(CH ₃) ₃ and H ₂ O	300	30 min FGA ^a at 400 °C	²⁵
13 ^c (a-d) 6 ^e	-	ALD from Al(CH ₃) ₃ and O ₃	400	None or 10 min at 800°C in N ₂	²⁶
3-9	-	Molecular beam epitaxy from Al and N ₂ O on c-Si with an interfacial layer formed from Al and chemical SiO ₂ . ^f	750	None or anneal at 600 °C in O ₂ , N ₂ , H ₂ or air	²⁷
3-8 (a-d)	-	ALD from Al(CH ₃) ₃ and H ₂ O on c-Si with 7 nm thermal SiO ₂	160-350	None	²⁸
Up to 10	-	ALD from Al(CH ₃) ₃ and H ₂ O ^b	<300	Yes, not specified	8
7	-	Remote plasma enhanced CVD from metal organic ^f and O ₂ on c-Si ^h	300	30 s anneal at 800°C and 30 min FGA ^a at 425 °C	16
0.2-2 (a-d) 5-8		ALD from Al(CH ₃) ₃ and O ₂ plasma	200	30 min anneal at 425 °C	²⁹

^aForming gas anneal, typically 5-10 % H₂ in N₂.

^bThe pre-treatment of the c-Si wafer was not specified.

^cThe Al₂O₃ films were grown under UV radiation.

^dThe defect density could be lowered by the addition of Zr or Si in the Al₂O₃ to values in the mid 10¹⁰ eV⁻¹ cm⁻² range.

^eThe Al₂O₃ film was covered with a HfO₂ film.

^fPoly-crystalline Al₂O₃ was grown in this study due to epitaxy process.

^g(CH₂)₃Al₂(C₄H₉O)₃

^hFilms were grown at H-terminated c-Si and c-Si with 1.0 nm or 1.6 nm thermal SiO₂ with no significant impact on the amount of fixed negative charge.

an interfacial SiO_x layer is commonly formed between the Al₂O₃ film and the c-Si substrate.³⁰⁻³³ This SiO_x layer can be formed during the Al₂O₃ deposition process but also during the post-deposition annealing treatment. The presence of an interfacial SiO_x is undesired for the application of Al₂O₃ as gate dielectric in CMOS devices as it lowers the effective dielectric constant of the layer stack. Nevertheless, only a very limited number of studies (e.g., in the work of Gusev *et al.*)³⁴ report the absence of an interfacial SiO_x

layer between the Al_2O_3 film and c-Si substrate.⁴ An interfacial SiO_x film was also detected by high resolution transmission electron microscopy (HR-TEM) in the Al_2O_3 films synthesized by plasma-assisted ALD, both in the as-deposited and annealed state, that demonstrated an excellent level of surface passivation on c-Si.⁹

The origin of the negative Q_f in Al_2O_3 deposited on c-Si has been attributed to intrinsic and extrinsic defects in Al_2O_3 . Matsunaga *et al.* have calculated the energetics of intrinsic vacancies and interstitials in Al_2O_3 from first-principles.³⁵ These calculations showed that each intrinsic point defect is most stable in their fully ionized form. Hence, Al vacancies and O interstitials exhibit a negative charge and Al interstitials and O vacancies exhibit a positive charge in good agreement with the ionic nature of the Al_2O_3 .³⁵ Extrinsic H has also been proposed as origin for the negative fixed charges in Al_2O_3 . Peacock *et al.* have calculated that interstitial H acts as a deep trap site for electrons in Al_2O_3 .³⁶ H is for example a common constituent in Al_2O_3 synthesized by ALD because H-containing precursors such as $\text{Al}(\text{CH}_3)_3$ and H_2O are used in the deposition process. Hence, Al vacancies, O interstitials, and interstitial H are proposed as the origin of the negative Q_f in Al_2O_3 . Based on the ionic nature of Al_2O_3 , Lucovsky postulated that Al_2O_3 consists of tetrahedrally coordinated Al in AlO_4^- units and octahedrally coordinated Al^{3+} in a ratio of 3:1 to assure charge neutrality.³⁷ Kimoto *et al.* have demonstrated that both tetrahedrally and octahedrally coordinated Al are present in Al_2O_3 grown by thermal ALD on H-terminated c-Si.³⁸ However, tetrahedrally coordinated Al was found to be dominant at the interface. This dominance was attributed to the fact that Si in the interfacial SiO_x film also has a tetrahedral coordination.³⁸ Consequently, the interfacial SiO_x film could fulfill an important role in the origin of the negative Q_f that is found in Al_2O_3 films grown on c-Si by inducing a high density of negatively charged Al vacancies close to the interface. This hypothesis is in good agreement with the location of the negative Q_f extracted from thickness dependent CV measurements by various authors.¹⁵⁻¹⁷

The polarity of Q_f plays an important role in the surface passivation of c-Si. The most commonly used dielectric passivation films on c-Si, i.e., thermal SiO_2 , a-SiC_x:H, and a-SiN_x:H contain a positive Q_f .³⁹⁻⁴¹ A positive Q_f has been shown to be detrimental for the passivation of highly B-doped surfaces such as in *p*-type emitters because the minority electrons are attracted to the c-Si surface and thereby enhance the recombination rate.¹⁰ Positive-charge dielectrics also demonstrate a strong injection level dependence for the surface passivation properties on lightly doped *p*-type c-Si.⁴¹⁻⁴³ The level of surface passivation decreases when going to lower excess carrier concentrations (i.e., injection levels) which is for example detrimental for the c-Si solar cell efficiency under low illumination conditions.³⁹ This injection level dependence is attributed to additional bulk recombination losses in the inversion layer close to the c-Si surface.⁴⁴ The inversion layer is created by the shielding of holes, which are the majority carriers in the *p*-type c-Si

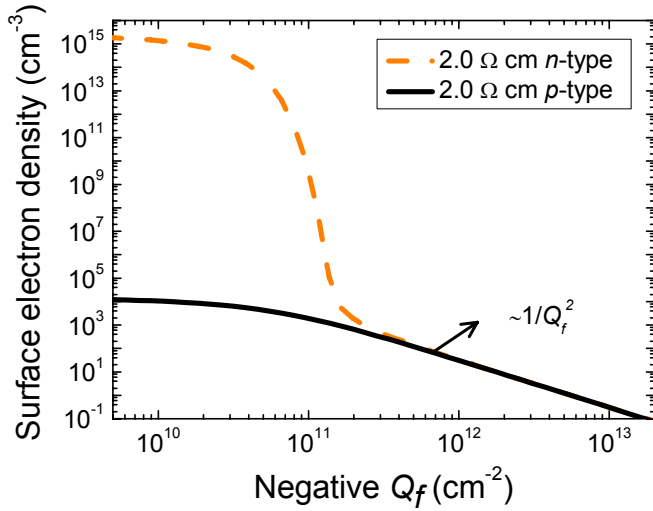


Figure 2: Simulated surface electron density for $2 \Omega \text{ cm}$ *p*- and *n*-type c-Si as a function of the density of the negative Q_f located at the c-Si surface. The electrons become the minority carriers at the surface of a $2 \Omega \text{ cm}$ *n*-type c-Si surface for a negative Q_f of $>1\times10^{11} \text{ cm}^{-2}$. The simulations were performed with the software package PC1D assuming no excess carrier generation by external illumination.⁴⁵

bulk, from the c-Si surface by the positive Q_f in the dielectric film. For the negative-charge dielectric Al_2O_3 it has, on the other hand, been demonstrated that the level of surface passivation is constant at low injection level for lightly doped *p*-type c-Si.⁹ Highly doped *p*-type c-Si surfaces are even more effectively passivated by Al_2O_3 compared to positive-charge dielectrics such as thermal SiO_2 and as-deposited a- $\text{SiN}_x:\text{H}$.¹⁰ On the contrary, when the negative-charge dielectric Al_2O_3 is used to passivate lightly doped *n*-type c-Si, the level of surface passivation decreases when going to lower injection level,⁹ whereas positive-charge dielectrics demonstrate a constant level of surface passivation in this case.^{42,43} Hence, a similar bulk recombination in the inversion layer could explain this injection level behavior of lightly doped *n*-type c-Si passivated by the negative-charge dielectric Al_2O_3 . Furthermore, the high positive Q_f in a- $\text{SiN}_x:\text{H}$ causes the so-called parasitic shunting effect when applied at the rear of *p*-type c-Si solar cells and thereby significantly decreases the short-circuit current of c-Si solar cells.⁴⁶ This effect is absent when the negative-charge dielectric Al_2O_3 is used at the rear of *p*-type c-Si solar cells which has resulted in solar cell efficiencies of 20.6 %.⁴⁷

It is evident that, besides the polarity of the fixed charge, also the amount of fixed charge is important for field-effect passivation. Figure 2 shows the surface electron density as a function of the negative Q_f located at the surface for $2.0 \Omega \text{ cm}$ *p*- and *n*-type c-Si. These simulations were performed in the software package PC1D that solves the

coupled electron and hole transport equations in semiconductors numerically.⁴⁵ Figure 2 clearly shows that a high density of negative Q_f results in a significant decrease in the electron density at the surface for both *p*- and *n*-type c-Si. For a negative $Q_f > 1 \times 10^{11} \text{ cm}^{-2}$ the electrons are the minority carriers at the surface of both *n*- and *p*-type c-Si. As already mentioned the surface recombination rate is proportional to the minority carrier concentration at the surface. For a negative Q_f in the range of $(3 \times 10^{11}-1 \times 10^{13}) \text{ cm}^{-2}$ the electron density is in fact approximately equal at the *n*- and *p*-type c-Si surface and scales with $1/Q_f^2$. Hence the field-effect passivation scales with Q_f^2 for a sufficiently high Q_f in the passivating film in agreement with results reported by Kuhlmann *et al.* for an inverted *p*-type c-Si surface.⁴⁸ It should be noted that this $1/Q_f^2$ scaling is also obtained under typical solar cell operation conditions.

The Q_f^2 dependence of the field-effect passivation allows us to compare the relative strength of field-effect passivation by Al_2O_3 and other charge containing dielectrics used for c-Si surface passivation. For thermal SiO_2 and a-SiC_x:H a relative low positive Q_f around 10^{11} cm^{-2} on *p*-type c-Si is commonly reported,^{39,41,44} whereas for a-SiN_x:H a positive Q_f in the range of 10^{12} cm^{-2} is typically found.⁴⁹ Consequently, the field-effect passivation provided by Al_2O_3 is up to four orders of magnitude stronger compared to thermal SiO_2 and a-SiC_x:H and up to two orders of magnitude stronger compared to a-SiN_x:H.

Besides field-effect passivation also chemical passivation reduces the recombination losses at c-Si surfaces. For example, the state-of-the-art surface passivation by thermal SiO_2 can mainly be attributed to chemical passivation due to its extremely low interface defect density. A strong field-effect passivation as in the case of Al_2O_3 , however, relaxes the requirements on the interface defect density. Using the Q_f^2 scaling of the field-effect passivation we can estimate the relative importance of the chemical passivation for Al_2O_3 compared to thermal SiO_2 for lightly doped c-Si. Assuming similar electron and hole capture cross sections for the dominant defects, the mid-gap defect density at the c-Si surface is allowed to be as high as $10^{13} \text{ eV}^{-1} \text{ cm}^{-2}$ to yield a similar level of surface passivation compared to thermal SiO_2 with a mid-gap interface defect density of $10^9 \text{ eV}^{-1} \text{ cm}^{-2}$.⁶ However from Fig. 1 it can be concluded that the Al_2O_3 film also provides a reasonable level of chemical passivation because the effective lifetime is still relative high at $\sim 100 \mu\text{s}$ when the negative Q_f in the Al_2O_3 film is balanced (for a poorly passivated surface the effective lifetime would only be $\sim 5 \mu\text{s}$). Hence, the interface defect density between the Al_2O_3 film and the c-Si substrate is expected to be reasonably low. As can be seen in Table I typically interface defect densities in the range of $10^{11} \text{ eV}^{-1} \text{ cm}^{-2}$ have been reported for annealed Al_2O_3 films on c-Si, which is up to two orders of magnitude higher compared to thermal SiO_2 . Similar to thermal SiO_2 the lowest interface defect density is obtained by post-deposition annealing treatments, either an anneal in a H_2 containing ambient in the $300-500^\circ\text{C}$ temperature range or a short high temperature anneal in N_2 below the crystallization temperature of

Al_2O_3 . The interface defect density of dielectrics on c-Si has, moreover, *empirically* been related to the average bonding concentration at the interface by Lucovsky *et al.*⁵⁰ Dielectrics with an average bonding concentration above 3 would exhibit a high interface defect density and vice versa. As the average bonding concentration of Al_2O_3 is 3.6 the interface defect density at the c-Si surface could be significantly lowered by the presence of a thin SiO_2 -like film between the c-Si and the Al_2O_3 film because SiO_2 has an average bonding density of 2.8.⁵⁰

The interface defect density is also of relevance due to the fact that interface defect states can trap charges and thereby could potentially cancel part of the field-effect passivation provided by the Q_f in the passivation film. The charging of interface defect states is clearly apparent in the surface passivating mechanism of a-Si:H on c-Si as demonstrated by Garin *et al.* and Obilet *et al.*^{51,52} Nevertheless, this effect becomes only of significance when the interface defect density is of the same order as Q_f . Hence, for Al_2O_3 on c-Si it is not expected that this effect is significant because the defect densities are typically at least one order of magnitude lower than the magnitude of the negative Q_f in the film (see Table I).

As mentioned, Al_2O_3 synthesized by plasma-assisted ALD provides no significant level of surface passivation on c-Si in the as-deposited state, whereas the level of surface passivation is excellent after a 30 min anneal at 425 °C in N_2 .^{9,10} This difference in surface passivation performance of the Al_2O_3 can for a large part be related to changes in the negative fixed charged density Q_f after anneal. In Fig. 3 the effective lifetime for c-Si wafers is shown for Al_2O_3 films with a thickness between 6 and 32 nm in the as deposited and annealed state. The films were deposited on both sides of 275 μm 1.9 $\Omega \text{ cm}$ *n*-type c-Si wafers by plasma-assisted ALD at a substrate temperature of 200 °C.²⁹ The Q_f in the Al_2O_3 films was determined by the contactless optical second-harmonic generation technique and the effective lifetime was determined by the contactless photoconductance technique.²⁹ The as-deposited Al_2O_3 films already contain a negative Q_f in the range of $(3\text{-}20)\times 10^{11} \text{ cm}^{-2}$ without demonstrating any level of surface passivation as indicated by the low effective lifetime in the range of 3–5 μs . After annealing the negative Q_f has increased for all films and is within the range of $(5\text{-}8)\times 10^{12} \text{ cm}^{-2}$. The effective lifetime also increases over more than two orders of magnitude and reaches a value of 1.2 ms for c-Si wafer passivated by the 32 nm thick Al_2O_3 film. Initial capacitance-voltage (CV) analysis also confirmed the increase in negative Q_f after the post-deposition anneal. It should also be noted that the negative Q_f in the as-deposited 32 nm Al_2O_3 film of $2\times 10^{12} \text{ cm}^{-2}$ is significantly higher compared to the negative Q_f of $\sim 3\times 10^{11} \text{ cm}^{-2}$ that is found in the as-deposited 6 and 11 nm thick Al_2O_3 films. This is most probably related to the significant longer deposition time of the 32 nm Al_2O_3 film which leads to an annealing effect during the deposition process itself. The difference in effective lifetime between the annealed 11 nm and 32 nm Al_2O_3 film scales with Q_f^2 and can consequently be

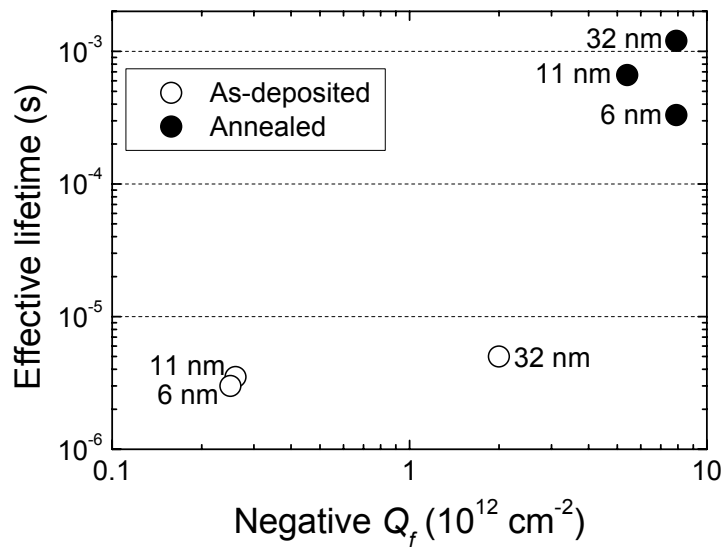


Figure 3: Measured effective lifetime at an injection level of $5 \times 10^{14} \text{ cm}^{-3}$ of a $275 \mu\text{m}$ $1.9 \Omega \text{ cm}$ n -type c-Si wafer passivated on both sides by a 6, 11 and 32 nm thick Al_2O_3 film plotted as a function of the measured negative Q_f in the Al_2O_3 film. Q_f and the effective lifetime were determined as-deposited and after a subsequent 30 min post-deposition anneal at 425°C in N_2 .

attributed to a difference in field-effect passivation. On the other hand, the relative low effective lifetime of the c-Si wafer passivated by the annealed 6 nm thick film indicates a lower chemical passivation and consequently a higher interface defect density compared to the annealed 11 and 32 nm thick Al_2O_3 films.

Using the Q_f^2 scaling of the field-effect passivation it can be argued that the increase in Q_f of the 32 nm Al_2O_3 film only results in an increase in the level of field-effect passivation by a factor 16 compared to the Al_2O_3 film in the as-deposited state. Consequently it can be concluded that the chemical passivation by the 32 nm thick Al_2O_3 film is also improved by the post-deposition anneal. The reduction of the interface defect density between the Al_2O_3 film and the c-Si substrate after the post-deposition annealing treatment was confirmed by capacitance-voltage (CV) measurements which showed a significant decrease in the parallel conductance after annealing.⁵³ It should be noted that a post-deposition anneal is routinely employed to improve the electrical quality of the interface between c-Si and dielectric films. This was also clearly demonstrated for the c-Si/ Al_2O_3 system in the studies of Hezel *et al.*¹⁸ and Jeon *et al.*²² In both studies the c-Si/ Al_2O_3 interface defect density was lowered over more than one order of magnitude

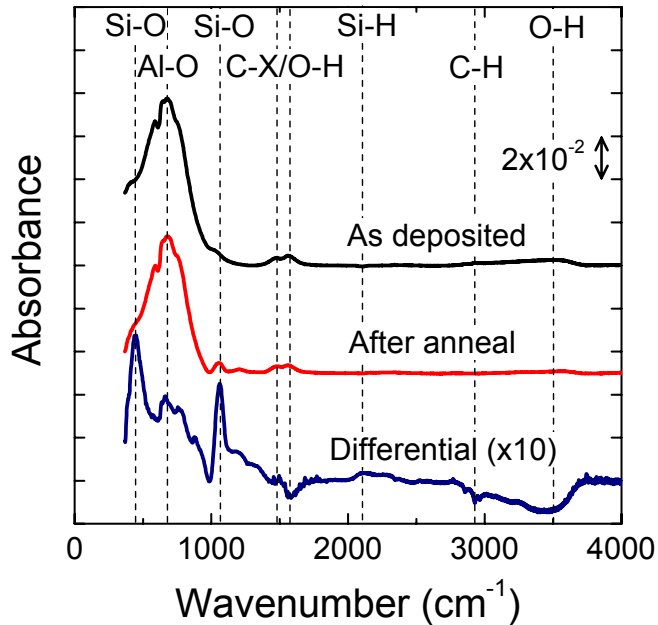


Figure 4: Infrared absorption spectra of a 30 nm thick Al_2O_3 film which was synthesized by plasma-assisted ALD on both sides of a high resistivity c-Si substrate. Data is presented in the as-deposited and annealed state. Absorption peaks related to $\text{Al}-\text{O}$, $\text{Si}-\text{O}$, $\text{C}-\text{H}_3$, $\text{O}-\text{H}$ and $\text{Si}-\text{H}$ bonds can clearly be distinguished in the spectra as indicated. For clarity also the differential absorption spectrum is shown that indicates the changes in the Al_2O_3 resulting from the post-deposition anneal.

(down to $\sim 1 \times 10^{11} \text{ eV}^{-1} \text{ cm}^{-2}$) by a post-deposition annealing step similar to the anneal applied to the Al_2O_3 films in Fig. 3.

Apart from changes in the bulk and interface electronic properties, also structural changes in the c-Si/ Al_2O_3 system are commonly reported after a post-deposition anneal.^{30,33} These structural changes are possibly related to the changes in the Al_2O_3 bulk and interface electronic properties. High resolution transmission electron microscopy revealed that the interfacial SiO_x thickness between Al_2O_3 and c-Si typically increased from 1.2 nm to 1.5 nm after the post-deposition anneal.⁹ The presence of $\text{Si}-\text{O}$ bonds is also confirmed by infrared absorbance spectra of as-deposited and annealed Al_2O_3 films as shown in Fig. 4. Particularly after the post-deposition anneal the $\text{Si}-\text{O}$ absorption peak in the infrared absorbance spectrum is very similar to the absorption peak observed for good quality thermal SiO_2 .⁵⁴ Chowdhurri *et al.* and Kuse *et al.* have also shown a strong increase in $\text{Si}-\text{O}$ related absorption by infrared spectroscopy and X-ray photoelectron spectroscopy (XPS) after annealing for Al_2O_3 films on c-Si as synthesized by ALD.^{30,33}

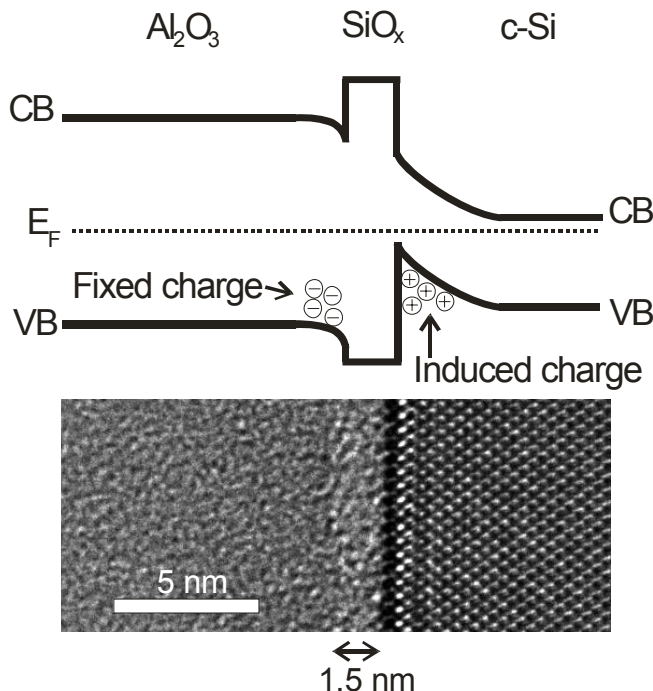


Figure 5: Schematic band diagram of the c-Si/SiO_x/Al₂O₃ system (VB: valence band energy, CB: conduction band energy, and E_F: Fermi energy). The high resolution transmission electron microscopy (TEM) image shows the c-Si/SiO_x/Al₂O₃ interface with the black line between the SiO_x and c-Si being a TEM artifact. A high negative Q_f is present in the Al₂O₃ film at the Al₂O₃/SiO_x interface effectively shields electrons from the c-Si surface. A relative good interface quality is assured by the presence of a thin interfacial SiO_x film between the c-Si substrate and the Al₂O₃ film.

As mentioned the interfacial SiO_x film could play an important role in the origin of the negative Q_f in the Al₂O₃ film and, hence, the changes in the Si-O related absorption could correlate with the change in the magnitude of the negative Q_f in the Al₂O₃ film. The infrared absorbance spectrum in Fig. 4 also confirms the presence of H in the form of O-H groups in the Al₂O₃ film. The O-H density decreases after the post-deposition anneal and this decrease coincides with the formation of both Al-O and Si-O bonds. The H atoms released during the anneal can possibly lead to passivation of Si dangling bond defects states at the interface as corroborated by an increase in Si-H related absorbance.

To summarize, it is demonstrated that the excellent surface passivation of c-Si by Al₂O₃ films synthesized by plasma-assisted ALD can mainly be attributed to a high negative charge density Q_f in the Al₂O₃ film. As schematically illustrated in Fig. 5 a high negative Q_f strongly reduces the electron concentration at the c-Si interface by means of electrostatic shielding. The negative charges are localized in the Al₂O₃ film close to the interface with the c-Si substrate that is separated from the Al₂O₃ through an interfacial SiO_x layer. The charges most likely originate from Al vacancies resulting from a

preferential tetrahedral coordination of Al in the region close to the interfacial SiO_x. The unique negative polarity of Q_f is especially beneficial for the passivation of *p*-type c-Si, including *p*-type emitters, as the bulk minority carriers are shielded from the c-Si surface. When the negative Q_f in the Al₂O₃ film is balanced by a positive $Q_{surface}$, still some level of chemical passivation is provided indicating that the interface defect density is also relatively low. The significant improvement in the level of c-Si surface passivation by Al₂O₃ after a post-deposition anneal can be related to changes in both surface passivating mechanisms, i.e., the negative Q_f significantly increases and the interface defect density decreases as indicated by the higher quality interfacial SiO_x. It has also been addressed that a high negative charge density Q_f tolerates a relatively high defect density at the c-Si interface while maintaining a good level of surface passivation. Because high negative Q_f values are routinely reported for Al₂O₃ films deposited on c-Si, irrespective of the deposition technique, it appears that the bulk and interface electrical quality required for excellent surface passivation of c-Si are not limited to Al₂O₃ films synthesized by ALD but are accessible for a broad range of deposition techniques.

ACKNOWLEDGEMENTS

The authors thank W. Keuning, J.L. van Hemmen, M.J.F. van de Sande, J.F.C. Jansen, and J.J.A. Zeebregts for their technical assistance and help during the experiments. Dr. I. Martin (Universitat Politecnica de Catalunya) and Dr. J. Schmidt (Institut für Solarenergieforschung Hameln/Emmerthal) are acknowledged for the fruitful discussions on the lifetime data. This work is supported by the Netherlands Technology Foundation STW. The work of B. Hoex is supported by OTB Solar.

REFERENCES:

- ¹ H. J. Queisser and E. E. Haller, *Science* **281** (5379), 945 (1998).
- ² M. Boroditsky, I. Gontijo, M. Jackson, R. Vrijen, E. Yablonovitch, T. Krauss, C. C. Cheng, A. Scherer, R. Bhat, and M. Krames, *J. Appl. Phys.* **87** (7), 3497 (2000).
- ³ M. J. Chen, Y. T. Shih, M. K. Wu, and F. Y. Tsai, *J. Appl. Phys.* **101** (3), 033130 (2007).
- ⁴ G. D. Wilk, R. M. Wallace, and J. M. Anthony, *J. Appl. Phys.* **89** (10), 5243 (2001).
- ⁵ A. G. Aberle, *Prog. Photovoltaics* **8** (5), 473 (2000).
- ⁶ H. Jin, K. J. Weber, N. C. Dang, and W. E. Jellett, *Appl. Phys. Lett.* **90** (26), 262109 (2007).
- ⁷ G. Lucovsky, *J. Vac. Sci. Technol. A* **19** (4), 1553 (2001).
- ⁸ G. Agostinelli, A. Delabie, P. Vitanov, Z. Alexieva, H. F. W. Dekkers, S. De Wolf, and G. Beaucarne, *Sol. Energ. Mat. Sol. Cells* **90** (18-19), 3438 (2006).
- ⁹ B. Hoex, S. B. S. Heil, E. Langereis, M. C. M. van de Sanden, and W. M. M. Kessels, *Appl. Phys. Lett.* **89** (4), 042112 (2006).
- ¹⁰ B. Hoex, J. Schmidt, R. Bock, P. P. Altermatt, M. C. M. van de Sanden, and W. M. M. Kessels, *Appl. Phys. Lett.* **91**, 112107 (2007).
- ¹¹ B. Hoex, J. Schmidt, P. Pohl, M. C. M. van de Sanden, and W. M. M. Kessels, Submitted for publication.
- ¹² M. Specht, H. Reisinger, F. Hofmann, T. Schulz, E. Landgraf, R. J. Luyken, W. Rosner, M. Grieb, and L. Risch, *Solid State Electron.* **49** (5), 716 (2005).
- ¹³ D. A. Mehta, S. R. Butler, and F. J. Feigl, *J. Appl. Phys.* **43** (11), 4631 (1972).
- ¹⁴ In the studies of Chin et al. (Ref 21) and Duenas et al. (Ref 24) also positive flatband voltage shifts were reported indicating a negative fixed charge density.
- ¹⁵ J. A. Aboaf, D. R. Kerr, and E. Bassous, *J. Electrochem. Soc.* **120** (8), 1103 (1973).
- ¹⁶ R. S. Johnson, G. Lucovsky, and I. Baumvol, *J. Vac. Sci. Technol. A* **19** (4), 1353 (2001).
- ¹⁷ S. Y. No, D. Eom, C. S. Hwang, and H. J. Kim, *J. Electrochem. Soc.* **153** (6), F87 (2006).
- ¹⁸ R. Hezel and K. Jaeger, *J. Electrochem. Soc.* **136** (2), 518 (1989).
- ¹⁹ G. S. Higashi and C. G. Fleming, *Appl. Phys. Lett.* **55** (19), 1963 (1989).
- ²⁰ D. G. Park, H. J. Cho, K. Y. Lim, C. Lim, I. S. Yeo, J. S. Roh, and J. W. Park, *J. Appl. Phys.* **89** (11), 6275 (2001).
- ²¹ A. Chin, Y.H. Wu, S.B. Chen, C.C. Liao, and W.J. Chen, Proc. of the VLSI Symp., Honolulu, 2000. p. 16

-
- ²² I. S. Jeon, J. Park, D. Eom, C. S. Hwang, H. J. Kim, C. J. Park, H. Y. Cho, J. H. Lee, N. I. Lee, and H. K. Kang, *Jpn. J. Appl. Phys.* **1** *42* (3), 1222 (2003).
- ²³ L. Manchanda, M. D. Morris, M. L. Green, R. B. van Dover, F. Klemens, T. W. Sorsch, P. J. Silverman, G. Wilk, B. Busch, and S. Aravamudhan, *Microelectron. Eng.* **59** (1-4), 351 (2001).
- ²⁴ S. Duenas, H. Castan, H. Garcia, A. de Castro, L. Bailon, K. Kukli, A. Aidla, J. Aarik, H. Mandar, T. Uustare, J. Lu, and A. Harsta, *J. Appl. Phys.* **99** (5), 054902 (2006).
- ²⁵ L. Truong, Y. G. Fedorenko, V. V. Afanasev, and A. Stesmans, *Microelectron. Reliab.* **45** (5-6), 823 (2005).
- ²⁶ M. Cho, H. B. Park, J. Park, S. W. Lee, C. S. Hwang, J. Jeong, H. S. Kang, and Y. W. Kim, *J. Electrochem. Soc.* **152** (5), F49 (2005).
- ²⁷ M. Shahjahan, T. Okada, K. Sawada, and M. Ishida, *Jpn. J. Appl. Phys.* **43** (8A), 5404 (2004).
- ²⁸ J. Buckley, B. De Salvo, D. Deleruyelle, M. Gely, G. Nicotra, S. Lombardo, J. F. Damlencourt, P. Hollinger, F. Martin, and S. Deleonibus, *Microelec. Engin.* **80**, 210 (2005).
- ²⁹ J. J. H. Gielis, B. Hoex, M. C. M. van de Sanden, and W. M. M. Kessels, to be published.
- ³⁰ A. R. Chowdhuri, C. G. Takoudis, R. F. Klie, and N. D. Browning, *Appl. Phys. Lett.* **80** (22), 4241 (2002).
- ³¹ S. C. Ha, E. Choi, S. H. Kim, and J. S. Roh, *Thin Solid Films* **476** (2), 252 (2005).
- ³² R. F. Klie, N. D. Browning, A. R. Chowdhuri, and C. G. Takoudis, *Appl. Phys. Lett.* **83** (6), 1187 (2003).
- ³³ R. Kuse, M. Kundu, T. Yasuda, N. Miyata, and A. Toriumi, *J. Appl. Phys.* **94** (10), 6411 (2003).
- ³⁴ E. P. Gusev, M. Copel, E. Cartier, I. J. R. Baumvol, C. Krug, and M. A. Gribelyuk, *Appl. Phys. Lett.* **76** (2), 176 (2000).
- ³⁵ K. Matsunaga, T. Tanaka, T. Yamamoto, and Y. Ikuhara, *Phys. Rev. B* **68** (8), 085110 (2003).
- ³⁶ P. W. Peacock and J. Robertson, *Appl. Phys. Lett.* **83** (10), 2025 (2003).
- ³⁷ G. Lucovsky, *J. Vac. Sci. Technol.* **19** (3), 456 (1981).
- ³⁸ K. Kimoto, Y. Matsui, T. Nabatame, T. Yasuda, T. Mizoguchi, I. Tanaka, and A. Toriumi, *Appl. Phys. Lett.* **83** (21), 4306 (2003).
- ³⁹ A. G. Aberle, S. Glunz, and W. Warta, *J. Appl. Phys.* **71** (9), 4422 (1992).
- ⁴⁰ R. Hezel and R. Schorner, *J. Appl. Phys.* **52** (4), 3076 (1981).
- ⁴¹ I. Martin, M. Vetter, M. Garin, A. Orpella, C. Voz, J. Puigdollers, and R. Alcubilla, *J. Appl. Phys.* **98** (11), 114912 (2005).
- ⁴² M. J. Kerr and A. Cuevas, *Semicond. Sci. Tech.* **17** (2), 166 (2002).
- ⁴³ M. J. Kerr and A. Cuevas, *Semicond. Sci. Tech.* **17** (1), 35 (2002).

- ⁴⁴ S. W. Glunz, D. Biro, S. Rein, and W. Warta, *J. Appl. Phys.* **86** (1), 683 (1999).
- ⁴⁵ P. A. Basore, *IEEE Trans. Electron. Dev.* **37** (2), 337 (1990).
- ⁴⁶ S. Dauwe, L. Mittelstadt, A. Metz, and R. Hezel, *Prog. Photovoltaics* **10** (4), 271 (2002).
- ⁴⁷ J. Schmidt, A. Merkle, R. Brendel, B. Hoex, M. C. M. van de Sanden, and W. M. M. Kessels, accepted for publication in *Progress in Photovoltaics* (2007).
- ⁴⁸ B. Kuhlmann, A. G. Aberle, and R. Hezel, *Proc. of the 13th European PVSEC*, Nice, France, 1995. p. 1209
- ⁴⁹ J. R. Elmiger, R. Schieck, and M. Kunst, *J. Vac. Sci. Technol. A* **15** (4), 2418 (1997).
- ⁵⁰ G. Lucovsky, Y. Wu, H. Niimi, V. Misra, and J. C. Phillips, *Appl. Phys. Lett.* **74** (14), 2005 (1999).
- ⁵¹ M. Garin, U. Rau, W. Brendle, I. Martin, and R. Alcubilla, *J. Appl. Phys.* **98** (9), 093711 (2005).
- ⁵² S. Olibet, E. Vallat-Sauvain, and C. Ballif, *Phys. Rev. B* **76** (3), 035326 (2007).
- ⁵³ E. H. Nicollian and A. Goetzberger, *Bell Syst. Tech. J.* **46** (6), 1055 (1967).
- ⁵⁴ C. T. Kirk, *Phys. Rev. B* **38** (2), 1255 (1988).

Chapter 8^{*}

Surface Passivation of High-Efficiency Solar Cells by Atomic-Layer-Deposited Al₂O₃

Atomic-layer-deposited aluminium oxide (Al₂O₃) is applied as rear-surface-passivating dielectric layer to PERC (Passivated Emitter and Rear Cell)-type crystalline silicon solar cells. The excellent passivation of low-resistivity *p*-type silicon by the negative-charge-dielectric Al₂O₃ is confirmed on the device level by an independently confirmed energy conversion efficiency of 20.6%. The best results are obtained for a stack consisting of a 30 nm Al₂O₃ film covered by a 200 nm plasma-enhanced-chemical-vapour-deposited silicon oxide (SiO_x) layer, resulting in a rear surface recombination velocity (SRV) of 70 cm/s. Comparable results are obtained for a 130 nm single-layer of Al₂O₃, resulting in a rear SRV of 90 cm/s.

^{*} J. Schmidt, A. Merkle, R. Brendel, B. Hoex, M.C.M. van de Sanden, W.M.M. Kessels, accepted for publication in Progress in Photovoltaics.

I. Introduction

The current trend in silicon-wafer-based photovoltaics towards thinner crystalline silicon (c-Si) wafers and higher efficiencies makes an effective reduction of surface recombination losses increasingly important. In high-efficiency laboratory silicon solar cells,¹⁻³ surface recombination is very effectively suppressed by means of silicon dioxide (SiO_2) grown in a high-temperature (≥ 900 °C) oxidation process. Very low surface recombination velocities (SRVs) are in particular realized at the lightly doped rear surface, where the combination of a thermally grown SiO_2 layer with an evaporated film of Al give – after an additional annealing treatment at $\sim 400^\circ\text{C}$ (the so-called ‘alneal’) – SRVs below 20 cm/s on un-metallized low-resistivity ($\sim 1 \Omega\text{cm}$) *p*-type c-Si wafers.⁴ In addition, the SiO_2/Al stack at the cell rear acts as an excellent reflector for near-bandgap photons, significantly improving the light trapping properties and hence the short-circuit current of the cell. One of the main reasons why high-temperature oxidation has not been implemented into the majority of industrial cell processes up to now is the high sensitivity of the silicon bulk lifetime to high-temperature processes. In particular in the case of multi-crystalline silicon wafers, thermal processes above 900°C typically lead to a significant degradation of the bulk lifetime.⁵ Hence, low-temperature surface passivation alternatives are required for future industrial high-efficiency silicon solar cells, which should have comparable properties as the alnealed SiO_2 . One intensively investigated alternative is silicon nitride (SiN_x), grown by plasma-enhanced chemical vapour deposition (PECVD) at $\sim 400^\circ\text{C}$, which has proven to give comparably low SRVs as alnealed SiO_2 on low-resistivity *p*-type c-Si.^{6,7} However, when applied to the rear of PERC (Passivated Emitter and Rear Cell)-type solar cells the short-circuit current density is strongly reduced compared to their SiO_2 -passivated counterparts.⁸ This effect has been attributed to the large density of fixed positive charges within the SiN_x layer, inducing an inversion layer in the crystalline silicon underneath the SiN_x . The coupling of this inversion layer to the base contact leads to a significant loss in the short-circuit current density. This detrimental effect is known as ‘parasitic shunting’.⁹ Another alternative low-temperature passivation scheme resulting in comparable SRVs as alnealed SiO_2 is intrinsic hydrogenated amorphous silicon (a-Si) deposited by PECVD in the temperature range between 200 and 250°C.¹⁰ Despite the fact that no parasitic shunting occurs in the case of an a-Si passivated cell rear, new problems arise from the high sensitivity of the a-Si passivation to thermal processes.

Recently, it was shown that thin films of aluminium oxide (Al_2O_3) grown by atomic layer deposition (ALD) provide an excellent level of surface passivation on *p*- and *n*-type silicon wafers, as determined from carrier lifetime measurements.^{11,12} Using low-temperature plasma-assisted ALD SRVs < 13 cm/s were demonstrated on low-resistivity

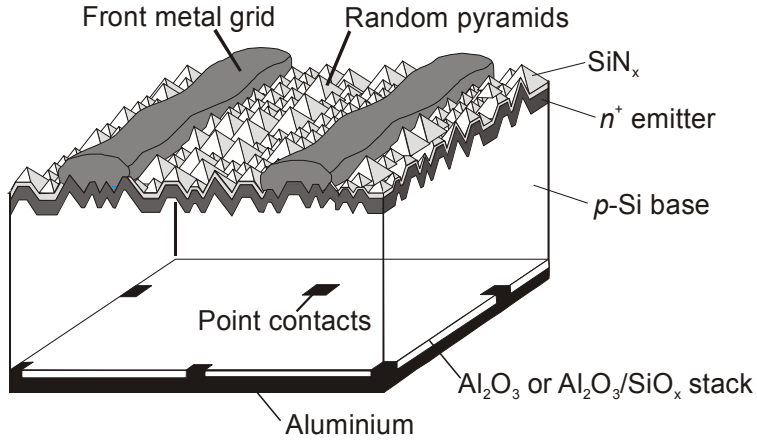


Figure 1: PERC-type solar cell structure used in this study to demonstrate the applicability of an Al_2O_3 rear surface passivation to high-efficiency solar cells.

p-type c-Si.¹² The fixed negative charge density within the Al_2O_3 layer induces an accumulation layer at the *p*-type c-Si surface that provides an effective field-effect passivation and the above-mentioned parasitic shunting effect at the solar cell rear is not expected. In combination with its very high transparency for near-bandgap photons, ALD-deposited Al_2O_3 should hence be an optimal choice for a dielectric layer at the c-Si solar cell rear. In this letter, we present first results of PERC-type solar cells with Al_2O_3 -passivated rear surface, demonstrating the large potential of atomic-layer-deposited Al_2O_3 films for future high-efficiency silicon solar cells.

II. Solar Cell Process

Figure 1 shows the PERC-type solar cell structure used in this study to demonstrate the applicability of Al_2O_3 rear surface passivation to high-efficiency silicon solar cells and Fig. 2 shows the corresponding process flow diagram. As starting material we use (100)-oriented boron-doped float-zone (FZ) c-Si wafers with a thickness of 310 μm and a resistivity of 0.5 Ωcm . After damage etching of $\sim 10 \mu\text{m}/\text{side}$ and wet chemical cleaning, a SiO_2 layer is grown on both wafer surfaces in a wet oxidation process at 1000°C. Subsequently, $2 \times 2 \text{ cm}^2$ diffusion windows are photolithographically opened on one wafer side and the silicon surface within the windows is textured with random pyramids in a KOH/isopropanol solution. A single-step phosphorus emitter is diffused from a POCl_3 source,¹³ resulting in an n^+ -emitter with a sheet resistance of 100 Ω/square , and the phosphorus glass is removed by a short HF dip. At this point of the process, the cell batch is split up into three batches, of which each one receives a different

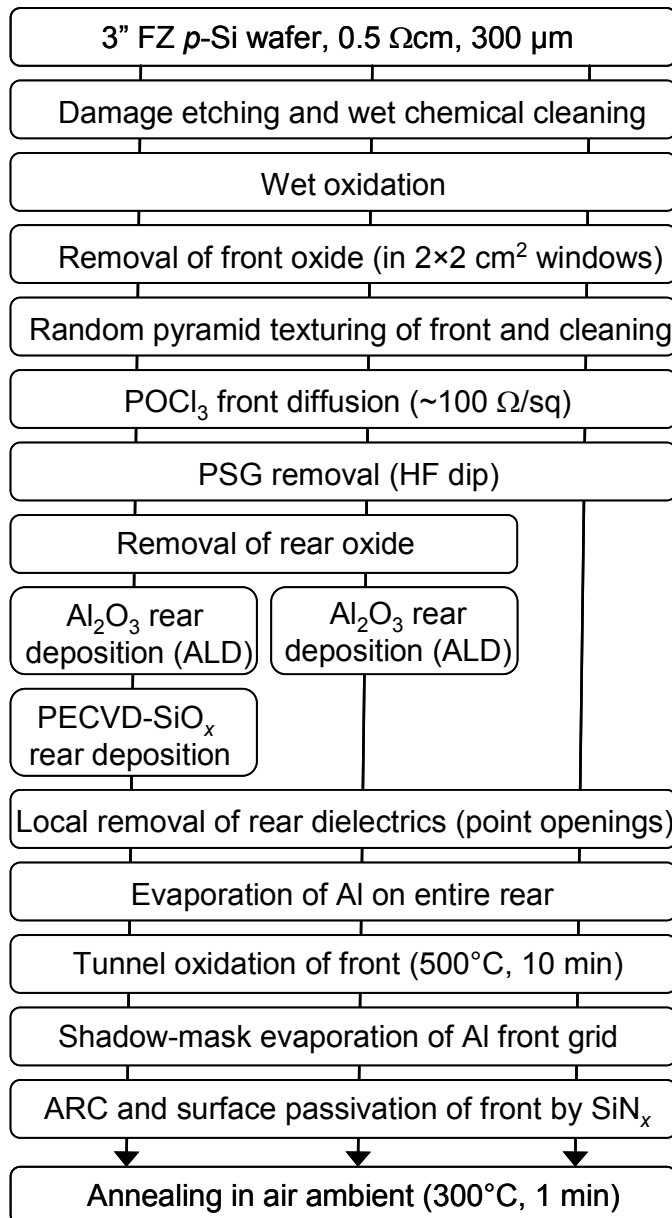


Figure 2: Process flow diagram for the PERC-type solar cells fabricated in this study.

rear surface passivation: (i) one batch of cells keeps the thermally grown SiO_2 , (ii) the second one is coated by a 130 nm Al_2O_3 film and (iii) the third batch is passivated by a stack consisting of a 30 nm Al_2O_3 layer and a 200 nm thick PECVD- SiO_x layer deposited in a Plasmalab 80+ parallel-plate reactor (Oxford Instruments) at 425°C. The Al_2O_3 films are deposited by plasma-assisted ALD in a commercial ALD reactor (FlexAL™, Oxford Instruments) at a deposition temperature of 200 °C.¹⁴ The plasma-assisted ALD Al_2O_3

process is split up into two self-limiting reactions consisting of a tri-methyl-aluminium [$\text{Al}(\text{CH}_3)_3$] exposure and an O_2 plasma. The subsequent annealing step as applied in the study of Hoex *et al.*¹² is omitted in this case as adequate post-deposition annealing steps are already present in the process flow shown in Fig. 2. The SiO_x layer is deposited in a continuous PECVD process using silane (SiH_4) and nitrous oxide (N_2O) as process gases. The remaining process steps are identical for all three cell batches. Using photolithography point contact openings are etched into the dielectric layers at the rear. A photolithography mask resulting in a point contact pitch of 2 mm and a metallization fraction of 4% is used. 20 μm of aluminium is evaporated on the entire cell rear using electron-beam evaporation. A tunnel oxidation of the n^+ -emitter is performed at 500°C for 10 min, resulting in an ~1.5 nm thick oxide layer.¹⁵ The 20 μm thick Al front metal grid is then evaporated through a shadow mask onto the tunnel oxide. Finally, a surface-passivating SiN_x antireflection coating is deposited onto the front of the PERC solar cell by remote-PECVD at 300°C.⁶ Before characterization all solar cells receive an additional 1-min 300°C anneal in air, which slightly improves the fill factor and the open-circuit voltage. The aperture area of all solar cells fabricated in this study is 4 cm^2 and the entire front metallization, including the busbar, is within the active cell area.

III. Solar Cell Results

Table I summarizes the one-sun parameters of the processed PERC-type solar cells featuring different rear surface passivation schemes, as measured under standard testing conditions (25°C, 100 mW/cm², AM 1.5 G). The results marked with an asterisk were independently confirmed at Fraunhofer ISE CalLab. The best reference solar cell with annealed SiO_2 rear surface passivation is characterized by an efficiency of $\eta = 20.5\%$, an open-circuit voltage of $V_{\text{oc}} = 656 \text{ mV}$ and a short-circuit current density of $J_{\text{sc}} = 38.9 \text{ mA/cm}^2$. The analysis of the internal quantum efficiency (IQE) shows that the V_{oc} is limited by the front emitter. The average values of all 4 cells with SiO_2 rear passivation show only a very small scatter, demonstrating the high reproducibility of the process. The average parameters of the cells with Al_2O_3 , $\text{Al}_2\text{O}_3/\text{SiO}_x$ and SiO_2 rear passivation agree within the scatter ranges. In particular it is noticeable that the J_{sc} of the cells with Al_2O_3 and $\text{Al}_2\text{O}_3/\text{SiO}_x$ rear surface passivation is not reduced compared to the SiO_2 -passivated cells. In the case of high-positive-charge dielectrics, such as SiN_x with fixed positive charge densities $>10^{12} \text{ cm}^{-2}$, it was reported that J_{sc} is reduced by 1-2 mA/cm² compared to the thermal SiO_2 reference, due to the above-described parasitic shunting effect.^{8,9} This effect is not expected in the case of Al_2O_3 as it is a negative-charge-dielectric inducing an accumulation layer instead of an inversion layer in the *p*-type c-Si underneath the rear surface. Al_2O_3 films are generally characterized by a high

Table I: One-sun parameters measured under standard testing conditions of 290 μm thick PERC-type silicon solar cells with three different rear surface passivations: (i) thermal SiO_2 (220 nm), (ii) ALD- Al_2O_3 (130 nm) and (iii) ALD- Al_2O_3 (30 nm)/PECVD- SiO_x (200 nm). All cells were fabricated on 0.5- Ωcm FZ p -Si wafers. The aperture cell area is 4 cm^2 . Average values and standard deviations for all cells processed in the batch are also provided.

Rear side	Cell ID	V_{oc} [mV]	J_{sc} [mA/cm 2]	FF [%]	η [%]
Thermal SiO_2 (220 nm)	7_1	656	38.9	80.3	20.5
	Average of 4	655 \pm 1	38.4 \pm 0.5	80.3 \pm 1.3	20.2 \pm 0.3
ALD- Al_2O_3 (130 nm)	3_3	655	38.7	78.9	20.0*
	Average of 4	656 \pm 2	38.6 \pm 0.1	79.4 \pm 1.4	20.0 \pm 0.4
ALD- Al_2O_3 (30 nm)/ PECVD- SiO_x (200 nm)	2_4	660	39.0	80.1	20.6*
	Average of 8	657 \pm 2	38.6 \pm 0.3	80.4 \pm 1.1	20.4 \pm 0.4

*Calibrated measurement at Fraunhofer ISE CalLab.

fixed negative charge density up to -10^{13} cm $^{-2}$.^{12,16} The cell results summarized in Table 1 confirm the expected non-existence of the parasitic shunting for Al_2O_3 -passivated as well as for $\text{Al}_2\text{O}_3/\text{SiO}_x$ -passivated rear surfaces. The best cell of the entire batch is obtained for the $\text{Al}_2\text{O}_3/\text{SiO}_x$ -passivated cell, resulting in an independently confirmed efficiency of $\eta = 20.6\%$, a V_{oc} of 660 mV and a J_{sc} of 39.0 mA/cm 2 .

It is not possible to quantify the exact rear surface passivation quality from comparison of the cell parameters given in Table I, as these solar cells are largely limited by recombination losses in the front emitter. Hence, we analyze the IQE in the wavelength range 800-1200 nm to determine the rear SRVs of the different rear surface passivation schemes. The symbols in Fig. 3 show the IQE as a function of wavelength λ of three representative PERC cells with the different rear passivation schemes, measured at a fixed bias light intensity of 0.3 suns. The solid lines in Fig. 3 show the fits to the measured data. To model the $IQE(\lambda)$ dependence we use the software LASSIE,^{17,18} which combines the extended IQE evaluation by Basore¹⁹ with the improved optical model developed by Brendel.²⁰ The bulk lifetime is assumed to be limited by Auger recombination, resulting in a bulk diffusion length of $L_b = 1500 \mu\text{m}$ for the 0.5 Ωcm p -type silicon material used in this work.²¹ As we assume the intrinsic upper limit for the bulk lifetime, the SRVs determined from the IQE analysis are upper limits as well. Table II summarizes the rear SRVs S_r and the internal rear reflectances R_r extracted from the IQE analysis. All three rear structures are equally effective reflectors for near-

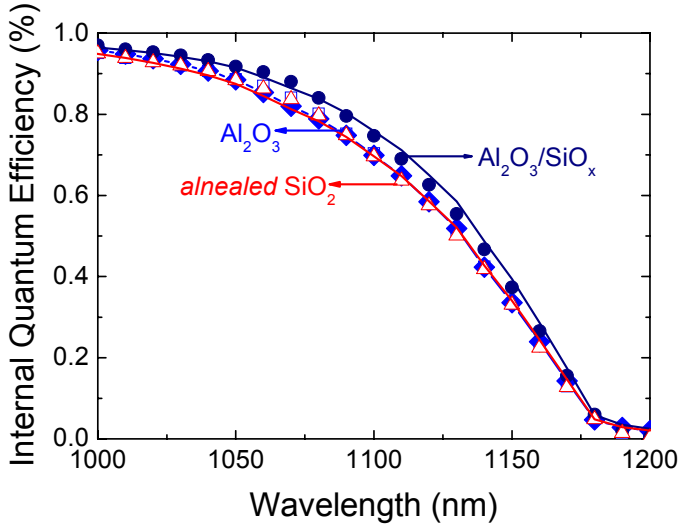


Figure 3: Measured internal quantum efficiency IQE as a function of wavelength λ (symbols) for solar cells with three different rear surface passivations: (i) thermal SiO_2 (220 nm), (ii) ALD- Al_2O_3 (130 nm) and (iii) ALD- Al_2O_3 (30 nm)/PECVD- SiO_x (200 nm). The lines show the fitted $IQE(\lambda)$ curves. All measurements were taken with a white bias light intensity of ~ 0.3 suns.

bandgap photons ($R_r = 91\%$). The rear SRV of the reference cell with annealed SiO_2 amounts to $S_r = (90 \pm 20) \text{ cm/s}$. The extracted S_r for the cell with single-layer Al_2O_3 rear passivation is the same as for the SiO_2 -passivated reference cell, showing that ALD-deposited Al_2O_3 performs as good as aluminium-annealed high-temperature-grown SiO_2 . A further reduction in the S_r is obtained for the $\text{Al}_2\text{O}_3/\text{SiO}_x$ stack, resulting in a S_r of only $(70 \pm 20) \text{ cm/s}$, which we attribute to the hydrogenation of interface states at the $\text{Al}_2\text{O}_3/\text{Si}$ interface during deposition of the hydrogen-rich SiO_x layer.

The effective SRV of a point-contacted rear is given by Fischer's equation:¹⁷

$$S_r = \frac{D_n}{W} \left[\frac{p}{2W\sqrt{\pi f}} \arctan \left(\frac{2W}{p} \sqrt{\frac{\pi}{f}} \right) - \exp \left(-\frac{W}{p} \right) + \frac{D_n}{fWS_{\text{met}}} \right]^{-1} + \frac{S_{\text{pass}}}{1-f}, \quad (1)$$

where D_n is the electron diffusion coefficient, W the wafer thickness, p the contact pitch, f the metallization fraction and S_{met} and S_{pass} are the SRVs on the metallized and on the passivated areas of the rear. Equation (1) holds for arbitrary values of S_{met} as long as low-injection conditions prevail. It has been verified experimentally on lifetime test structures²² as well as on solar cells.²³ According to Eqn. (1) the minimum SRV $S_{r,\min}$ for a point-contact rear with perfect passivation in the non-metallized area (i.e., $S_{\text{pass}} = 0$) is

Table II: Effective rear surface recombination velocity S_r and internal rear reflectance R_r extracted from the IQE measurements shown in Fig. 3.

Rear side	Rear surface recombination velocity S_r [cm/s]	Internal rear reflectance R_r [%]
Thermal SiO_2 (220 nm)	90 ± 20	91 ± 1
Al_2O_3 (130 nm)	90 ± 20	90 ± 1
Al_2O_3 (30 nm)/ SiO_x (200 nm)	70 ± 20	91 ± 1

given by the first summand on the right-hand side of Eqn. (1). For our cell structure we determine $S_{r,\min} = 73$ cm/s ($D_n = 23$ cm²/s, $W = 290$ μm , $p = 2000$ μm , $f = 4\%$, $S_{\text{met}} \geq 10^5$ cm/s), clearly demonstrating that in the case of the $\text{Al}_2\text{O}_3/\text{SiO}_x$ stack, recombination in the passivated area of the cell rear can be completely neglected. Note that, although a slightly better passivation is obtained in the case of the $\text{Al}_2\text{O}_3/\text{SiO}_x$ stacks, the rear SRV of the single-layer Al_2O_3 -passivated cells is also for the most part determined by recombination at the metal contacts. The IQE results clearly prove that atomic-layer-deposited Al_2O_3 is a very effective new dielectric passivation layer for high-efficiency silicon solar cells.

IV. Conclusions

We have demonstrated that Al_2O_3 films deposited by plasma-assisted ALD are suitable for the surface passivation of point-contacted rear surfaces of high-efficiency solar cells. Independently confirmed efficiencies above 20% have been obtained for PERC-type solar cells with the point-contacted rear passivated by a 130 nm Al_2O_3 layer as well with a double layer consisting of a 30 nm Al_2O_3 film and a 200 nm PECVD- SiO_x layer. Internal quantum efficiency measurements have revealed that the effective surface recombination velocities of the single-layer Al_2O_3 -passivated cells are comparable and that of the $\text{Al}_2\text{O}_3/\text{SiO}_x$ -passivated cells are even below that measured on reference cells passivated by an annealed thermal SiO_2 . The measured effective rear surface recombination velocities of all cells were shown to be clearly dominated by recombination at the metal point contacts.

In addition to the excellent surface passivation provided by Al_2O_3 films deposited by plasma-assisted ALD, the deposition process itself is also beneficial from an application point of view. In contrast to the conventionally applied PECVD, ALD consists of two self-limiting half-reactions, which implies several advantages: (i) ALD

gives highly conformal coatings, which allows to deposit and passivate e.g. deep trenches or even pores in silicon, (ii) pin-hole and particle free deposition is achieved, (iii) as ALD is a self-limiting process uniform films can be deposited over large areas with mono-layer growth control, and (iv) very low impurity concentrations of deposited films and hence very high film quality is achieved. The main disadvantage of ALD for photovoltaic applications is its relatively low deposition rate. However, as shown in this study, this disadvantage can be overcome by depositing ultrathin (2-30 nm) ALD-Al₂O₃ films and capping them with a thicker film of e.g. PECVD-SiO_x. Apart of the advantageous optical properties of these stacks, we have demonstrated that the passivation quality of such ALD-Al₂O₃/PECVD-SiO_x stacks can even be superior to that of single layers of Al₂O₃, which we attribute to the hydrogenation of interface states at the Al₂O₃/Si interface during deposition of the hydrogen-rich SiO_x layer. The same beneficial effect is expected from other hydrogen-rich PECVD-deposited films, such as SiN_x or SiC_x. Combination of ALD and PECVD might hence be a key technology for future industrial high-efficiency solar cells.

ACKNOWLEDGMENTS

The authors thank all members of the photovoltaic groups at ISFH for their contributions to this work and W. Keuning (Eindhoven University of Technology) for carrying out the Al₂O₃ depositions. We gratefully acknowledge the financial support provided by the German State of Lower Saxony and the Netherlands Technology Foundation STW.

REFERENCES:

- ¹ A. G. Aberle, W. Warta, J. Knobloch, and B. Voss, Proc. of the 21st IEEE PVSEC, Orlando, (IEEE, Piscataway, NJ, 1990), p. 233.
- ² M. A. Green, A. W. Blakers, J. H. Zhao, A. M. Milne, A. H. Wang, and X. M. Dai, IEEE Trans. Electronic Devices **37**, 331 (1990).
- ³ J. Zhao, A. H. Wang, and M. A. Green, Sol. Energy Mat. Sol. Cells **66**, 27 (2001).
- ⁴ M. J. Kerr and A. Cuevas, Semicond. Sci. Tech. **17**, 35 (2002).
- ⁵ M.J. Stocks and A. Cuevas, Proc. of the 14th EU-PVSEC, Barcelona, (H.S. Stephens & Assoc., Bedford (UK), 1997), p. 770.
- ⁶ T. Lauinger, J. Schmidt, A. G. Aberle, and R. Hezel, Appl. Phys. Lett. **68**, 1232 (1996).
- ⁷ J. Schmidt, J.D. Moschner, J. Henze, S. Dauwe, and R. Hezel, Proc. of the 19th EU-PVSEC, Paris, (WIP Renewable Energies, Munich, 2004), p. 391.
- ⁸ S. Dauwe, L. Mittelstädt, A. Metz, J. Schmidt, and R. Hezel, Proc. of the 3rd World Conference PVSEC, Osaka, (Arisumi Printing Inc., Japan, 2003), p. 1395.
- ⁹ S. Dauwe, L. Mittelstadt, A. Metz, and R. Hezel, Prog. Photovoltaics **10**, 271 (2002).
- ¹⁰ S. Dauwe, J. Schmidt, and R. Hezel, Proc. of the 29th IEEE Photovoltaic Specialist Conference, New Orleans, (IEEE, Piscataway, NJ, 2002), p. 1246.
- ¹¹ G. Agostinelli, A. Delabie, P. Vitanov, Z. Alexieva, H. F. W. Dekkers, S. De Wolf, and G. Beaucarne, Sol. Energy Mat. Solar Cells **90**, 3438 (2006).
- ¹² B. Hoex, S. B. S. Heil, E. Langereis, M. C. M. van de Sanden, and W. M. M. Kessels, Appl. Phys. Lett. **89**, 042112 (2006).
- ¹³ A. Hubner, C. Hampe, and A. G. Aberle, Sol. Energy Mat. Sol. Cells **46**, 67 (1997).
- ¹⁴ J.L. van Hemmen, S. B. S. Heil, J. Klootwijk, F. Roozeboom, C.J. Hodson, M. C. M. van de Sanden, and W. M. M. Kessels, J. Electrochem. Soc. **154**, G165 (2007).
- ¹⁵ R. Hezel and A. Metz, Proc. of the 16th EU-PVSEC, Glasgow, Uk, (James & James, London, 2000), p. 2000.
- ¹⁶ R. Hezel and K. Jaeger, J. Electrochem. Soc. **136**, 518 (1989).
- ¹⁷ www.fischer-pv.de
- ¹⁸ B. Fischer, Ph.D. Thesis, University of Konstanz, 2003.
- ¹⁹ P. A. Basore, Proc. of the 23rd IEEE PVSEC, Louisville, (IEEE, Piscataway, NJ, 1993), p. 147.
- ²⁰ R. Brendel and R. Plieninger, Proc. of the 9th International PVSEC, Miyazaki, Japan, (Techical Digest, 1996), p. 521.
- ²¹ P. P. Altermatt, J. Schmidt, G. Heiser, and A. G. Aberle, J. Appl. Phys. **82**, 4938 (1997).

-
- ²² H. Plagwitz, M. Schaper, and J. Schmidt, Proc. of the 31st IEEE PVSEC, Lake Buena Vista, FL, (IEEE, Piscataway, NJ, 2005), p. 999.
- ²³ D. Kray and S. Glunz, Progr. Photovoltaics **14**, 195 (2006).

Summary

Functional Thin Films for High-Efficiency Solar Cells

Photovoltaics (PV) is widely recognized as one of the main future sources of renewable energy. Currently, the PV industry is a “booming” business with an annual growth of 30-40 %. This growth is driven by subsidy programs with a strong incentive to decrease the costs per kWh. In the field of crystalline silicon (c-Si) PV there is consequently a continuous drive to reduce the c-Si wafer thickness and to increase the solar cell energy conversion efficiency. A reduction of the solar cell thickness will significantly increase the surface-to-volume ratio and as a result recombination losses at the c-Si surface will become the most dominant loss mechanism in c-Si solar cells. Simultaneously the amount of usable light reaching the rear surface of the c-Si solar cells will increase due to the low light absorption related to the indirect nature of the c-Si bandgap.

The work described in this Ph.D. dissertation has focused on dielectric and semiconductor thin films that can improve the optical and electrical quality of c-Si solar cells. Such functional thin films with a thickness < 100 nm can effectively reduce the undesired recombination losses of photo-generated charge carriers at the c-Si surface. This strong reduction in recombination losses can be attributed to the fact that these thin films strongly reduce the amount of recombination active defect centers and/or electrostatically shield charge carriers by an internal electric field at the c-Si surface. Additionally, the dielectric contrast between c-Si and these thin films can effectively be employed for (anti)-reflection coating purposes at the front and the rear side of solar cells.

Silicon nitride (a-SiN_x:H) deposited from plasmas with NH₃-SiH₄ reactant mixtures was the first thin film material that was investigated in this Ph.D. research. From carrier-lifetime measurements it was demonstrated that a-SiN_x:H films deposited at ultra-high rates (> 5 nm/s) by the expanding thermal plasma (ETP) technique could significantly reduce recombination losses at the c-Si surface. Moreover these a-SiN_x:H films served as an excellent antireflection coating and improved the bulk electronic properties of c-Si by bulk passivation. From compositional and optical analysis, using techniques such as spectroscopic ellipsometry, Rutherford backscattering, and Fourier transform infrared spectroscopy, it was shown that a-SiN_x:H with a high mass density is of vital importance for the surface and bulk passivation performance. This fundamental insight allowed the optimization of a-SiN_x:H without actual fabrication of c-Si solar cells. In collaboration with the company OTB Solar these results have lead to an industrial high-rate deposition process of a-SiN_x:H which is currently adopted in industry by several leading solar cell manufacturers.

$\text{a-SiN}_x\text{:H}$ does, however, not exhibit the ideal properties for the passivation of p -type c-Si. At the rear side of a p -type c-Si solar cell the solar cell efficiency is reduced by the so-called parasitic shunting effect. Moreover, $\text{a-SiN}_x\text{:H}$ even increases electronic losses at highly p -doped c-Si surfaces. For this reason plasma-deposited silicon dioxide (a-SiO_2) and amorphous silicon (a-Si:H) were also investigated. It was demonstrated that both a-SiO_2 and a-Si:H grown by the ETP technique can improve the electrical quality of the c-Si surface. In addition SiO_2 films also have the ideal optical properties to serve as reflection coating at the back of c-Si solar cells. Both the SiO_2 and a-Si:H films were deposited at significantly higher rates (up to 10 nm/s) than typically reported for conventional techniques, which is beneficial from an application point of view. A joint patent application describing the SiO_2 process developed was filed with OTB Solar.

A relative new material that was investigated for c-Si surface passivation was aluminum oxide (Al_2O_3) synthesized by the plasma-assisted atomic layer deposition (ALD) technique. From carrier-lifetime measurements it was demonstrated that thin Al_2O_3 films (7-30 nm) can provide a state-of-the-art level of surface passivation on low resistivity p -type and n -type c-Si. The underlying physical mechanism was studied in detail revealing the important role of a high negative fixed charge density in the Al_2O_3 thin film. These fixed negative charges can most likely be attributed to the presence of Al vacancies in the Al_2O_3 film close to the interface with the interfacial SiO_x film that is formed between the Al_2O_3 and the c-Si substrate. Both the magnitude and polarity of the fixed charge density make Al_2O_3 a very interesting material for c-Si surface passivation. The passivation induced by the fixed charge density in Al_2O_3 is up to four orders of magnitude stronger than for other charge-containing films used for surface passivation. Moreover, the unique polarity of the fixed charge in Al_2O_3 results in an excellent passivation of p -type c-Si (including highly doped p -type emitter surfaces) as the minority electrons are effectively shielded from the c-Si surface. In collaboration with the solar cell institute ISFH in Germany the performance of Al_2O_3 on p -type emitters and at the rear side of p -type c-Si solar cells was tested. These experiments demonstrated that Al_2O_3 provides a significant better device performance compared to the current state-of-the-art thermally grown SiO_2 in good correspondence with the theoretical understanding of the c-Si surface passivation mechanism.

Publications related to this research

Journal publications:

B. Hoex, A.J.M. van Erven, R.C.M. Bosch, W.T.M. Stals, M.D. Bijker, P.J. van den Oever, and W.M.M. Kessels, M.C.M. van de Sanden, *Industrial high-rate ($\sim 5 \text{ nm/s}$) deposited silicon nitride yielding high-quality bulk and surface passivation under optimum antireflection coating conditions*, Progress in Photovoltaics: Research and Application **13**, p. 705 (2005).

B. Hoex, S.B.S. Heil, E. Langereis, M.C.M. van de Sanden, and W.M.M. Kessels, *Ultralow surface recombination of c-Si substrates passivated by plasma-assisted atomic layer deposited Al_2O_3* , Applied Physics Letters **89**, 042112 (2006).

B. Hoex, F.J.J. Peeters, M. Creatore, M.A. Blauw, W.M.M. Kessels, and M.C.M. van de Sanden, *High-rate plasma deposited SiO_2 films for surface passivation of crystalline silicon*, Journal of Vacuum and Science and Technology A **24(5)**, 1823 (2006).

B. Hoex, J. Schmidt, R. Bock, P.P. Altermatt, M.C.M. van de Sanden, and W.M.M. Kessels, *Excellent passivation of highly doped p-type Si surfaces by the negative-charge-dielectric Al_2O_3* , Applied Physics Letters **91**, 1120107 (2007).

J. Schmidt, A. Merkle, R. Brendel, B. Hoex, M.C.M. van de Sanden, and W.M.M. Kessels, *Surface Passivation of High-Efficiency Silicon Solar Cells by Atomic-Layer-Deposited Al_2O_3* , accepted for publication in Progress in Photovoltaics.

S. He, B. Hoex, D. Inns, I.C. Brazil, P.I. Windenborg, and A.G. Aberle, *Crystal Quality Improvement of Solid Phase Crystallized Evaporated Silicon Films by in situ Densification Anneal*, submitted for publication.

B. Hoex, J. Schmidt, P. Pohl, M.C.M. van de Sanden, and W.M.M. Kessels, *Silicon Surface Passivation by Atomic Layer Deposited Al_2O_3* , submitted for publication.

J.J.H. Gielis, P.J. van den Oever, B. Hoex, M.C.M. van de Sanden, and W.M.M. Kessels, *A Real Time Study of a-Si / c-Si Heterointerface Formation and Epitaxial Growth by Spectroscopic Ellipsometry, Infrared spectroscopy and Second-Harmonic-Generation*, submitted for publication.

B. Hoex, J.J.H. Gielis, M.C.M. van de Sanden, and W.M.M. Kessels, *On the c-Si Surface Passivation Mechanism by the Negative Charge Dielectric Al₂O₃*, in preparation for publication.

J.J.H. Gielis, B. Hoex, M.C.M. van de Sanden, and W.M.M. Kessels, *Negative Charge and Charging Dynamics in Al₂O₃ films on Si Characterized by Second-Harmonic Generation*, in preparation for publication.

Conference proceedings:

P. J. van den Oever, W.M.M. Kessels, B. Hoex, R.C.M. Bosch, A.J.M. van Erven, R.L.J.R. Pennings, W.T.M. Stals, M.D. Bijker, and M.C.M. van de Sanden, *Plasma properties of a novel commercial plasma source for high-throughput processing of c-Si solar cells*, Proceedings of the 31th IEEE PVSEC, Lake Buana Vista, p. 1320 (2005).

W.M.M. Kessels, P.J. van den Oever, B. Hoex, R.C.M. Bosch, A.J.M. van Erven, M.D. Bijker, and M.C.M. van de Sanden, *Controlling the silicon nitride film density for ultrahigh-rate deposition of top quality antireflection coatings*, of the 31th IEEE PVSEC, Lake Buana Vista, p. 1253 (2005).

B. Hoex, A.J.M. van Erven, M.D. Bijker, P.J. van den Oever, W.M.M. Kessels, and M.C.M. van de Sanden, *Industrial High-Rate (≥ 4 nm/s) Deposited Silicon Nitride with Low Surface Recombination Velocities under Optimum Antireflection Coating Conditions*, Proceedings of the 20th EU-PVSEC Barcelona, p. 1387 (2005).

P.J. van den Oever, W.M.M. Kessels, B. Hoex, R.C.M. Bosch, A.J.M. Van Erven, M.D. Bijker, and M.C.M. van de Sanden, *A Novel Commercial Plasma Source for Ultra High-Rate Deposition of Silicon Nitride for c-Si Solar Cells*, Proceedings of the 20th EU-PVSEC Barcelona, p. 1395 (2005).

A.J.M. van Erven, R.C.M. Bosch, B. Hoex, M Bennett, B. Kumar, S. Narayanan, T. Koval, and M.D. Bijker, *Application of Ultra High-Rate ETP Deposited Silicon Nitride for Screen Printed Crystalline Silicon Solar Cells*, Proceedings of the 20th EU-PVSEC Barcelona, p. 1450 (2005).

B. Hoex, F.J.J. Peeters, A.J.M. van Erven, M.D. Bijker, W.M.M. Kessels, and M.C.M. van de Sanden, *High-rate deposition of silicon nitride and silicon oxide films for surface passivation and (anti)reflection coating applications*, Proceedings of the 15th International Photovoltaic Science and Engineering Conference, Shanghai, p. 1106 (2005).

P.J. van den Oever, J.J.H. Gielis, B. Hoex, M.C.M. van de Sanden, and W.M.M. Kessels, *A real-time study of the a-Si/c-Si interface formation using ellipsometry, infrared spectroscopy, and second-harmonic generation*, Proceedings of the WCPEC-4, Hawaii, p. 1610 (2005).

B. Hoex, F.J.J. Peeters, M. Creatore, M.D. Bijker, W.M.M. Kessels, and M.C.M. van de Sanden, *Good surface passivation for high rate plasma deposited silicon oxide*, Proceedings of the WCPEC-4, Hawaii, p. 1134 (2005).

B. Hoex, F.J.J. Peeters, A.J.M van Erven, M.D. Bijker, W.M.M. Kessels, and M.C.M. van de Sanden, *High-quality surface passivation obtained by high-rate deposited silicon nitride, silicon oxide, and amorphous silicon using the versatile expanding thermal plasma technique*, Proceedings of the WCPEC-4, Hawaii, p. 1036 (2005).

B. Hoex, W.M.M. Kessels, M.D. Bijker and M.C.M. van de Sanden, *Excellent Surface Passivation by Hydrogenated Amorphous Silicon Deposited at Rates > 1 nm/s by the Expanding Thermal Plasma Technique*, Proceedings of the 21th EU-PVSEC, Dresden, p. 435 (2006).

A. Aberle, P. Widenborg, P. Campbell, A. Sproul, M. Griffin, J. Weber, D. Inns, M. Terry, T. Walsh, O. Kunz, S. He, B. Hoex, L. Shi, T. Sakano, R.F. Bamberg, S.V. Chan, D. Di, Y. Zhou, F. Fecker, and S. Pohlner, *Poly-Si on glass thin-film PV research at UNSW*, Proceedings of the 22nd EU-PVSEC, Milan, p. 1884 (2007).

S. He, B. Hoex, I.C. Brazil, P. Winderborg, and A.G. Aberle, *Crystal Quality Improvement of Solid Phase Crystallized Evaporated Silicon Film by in-situ densification anneal*, Proceedings of the 17th International-PVSEC, Fukuoka, p. 563 (2007).

Patent publications:

Method for passivating a substrate surface

M.D. Bijker, B. Hoex, W.M.M. Kessels, and M.C.M. van de Sanden
WO 2007/013806 A1, 1 February 2007

Werkwijze voor het passiveren van ten minste een deel van een substraatoppervlak

M.D. Bijker, B. Hoex, W.M.M. Kessels, en M.C.M. van de Sanden
Dutch patent 1029647, 2 April 2007

Acknowledgments

Een proefschrift in de Technische Natuurkunde is bijna nooit de vrucht van een enkele persoon maar veelal het resultaat van een vruchtbare samenwerking met een grote groep mensen. Ik wil daarom iedereen die een bijdrage aan mijn promotie werk heeft geleverd hartelijk bedanken.

Allereerst wil ik mijn copromotor Erwin bedanken. Jouw ongekend enthousiasme en (bijna onmenselijke) werklust werken erg aanstekelijk. Ik kon bijna altijd bij je binnenlopen om onmiddellijk te discussiëren over de laatste ontwikkelingen waardoor ik weer met volle kracht vooruit kon. Jouw uitmuntende schrijfstijl en oog voor detail hebben mij enorm vooruit geholpen in de afgelopen vier jaar en dit zal mij de rest van mijn carrière nog goed van pas komen.

Ook mijn promotor Richard ben ik veel dank verschuldigd. Jij gaf mij de mogelijkheid om een promotie “à la carte” te doen waarin ik zeer veel vrijheid kreeg om nieuwe projecten te ontplooien. Ondanks dat de meeste projecten vanzelfsprekend mislukte (zo is het leven nu eenmaal), hebben we uiteindelijk toch supermooi werk neergezet en tellen we nu echt mee in het veld van c-Si zonnecellen. Ook de vele discussies over de meer economische aspecten van ons onderzoek heb ik enorm gewaardeerd.

De rest van de PMP-groep heeft natuurlijk ook een belangrijke rol vervuld in de totstandkoming van dit proefschrift. De technische ondersteuning van Ries, Jo, Janneke, Herman en Bertus was essentieel voor het goed geolied verlopen van de experimenten. Ook is het harde werk van het ALD-team (met name Erik, Hans, Stephan en Wytze) enorm belangrijk geweest voor de snelle resultaten die we op het gebied van Al₂O₃ hebben bereikt. Ook de SHG-experimenten tezamen met Joost zijn enorm belangrijk geweest en hebben super mooie resultaten opgeleverd. Ook ben ik erg veel dank verschuldigd aan mijn interne stagiaires Floran en Luc die enorme bergen mooi werk hebben verzet. Mijn afstudeerde Paul ben ik zeer dankbaar voor de buitengewoon prettige professionele en sociale interactie die we gedurende anderhalf jaar gehad hebben. Jouw afstudeerwerk werk werd zelfs door het oliebedrijf Shell op de juiste waarde geschat!

De samenwerking met OTB is ook een belangrijke bijdrage geweest voor dit proefschrift en voor mijn eigen ontwikkeling. Die ene dag per week bij OTB gaf mij een goede voelspriet voor de praktijk en maakte mij duidelijk dat het commercialiseren van innovatieve technologie geen sinecure is. Ik wil met name Martin, Rob en Roel bedanken voor de samenwerking op het experimentele vlak. Het was ook zeer leerzaam om met eigen ogen te zien hoe OTB Solar zich onder leiding van Chris en Martin zich van een projectgeoriënteerd naar een productgeoriënteerd bedrijf ontwikkelde.

I also want to acknowledge the people at the University of New South Wales for the pleasant time I had during my time there. It was an honor to work in the group of

Prof. Armin Aberle, and I want to thank him for having me in his group which allowed me to learn a lot about challenges in developing a novel solar cell design. I also enjoyed the experimental work I did with Song, Daniel and Oliver on the (occasionally operational) e-beam evaporator. I will also cherish the famous beer on steps (BOS) meetings with especially Ian, Stephan, and Florian, which routinely ended in the Coogee Bay Hotel after midnight.

With respect to the ALD Al_2O_3 project I would like to acknowledge a whole range of people. First of all I want to acknowledge Dr. Jan Schmidt of the solar cell institute ISFH in Germany. The experiments and discussions during my two visits to ISFH in 2006 have been essential for the outcome of the Al_2O_3 project. Especially the nice corona charging experiment which I conducted together with Dr. Peter Pohl has been invaluable in our work. Moreover, the collaboration with ISFH has proved the device performance of Al_2O_3 on *p*-type emitters and on solar cells which turned out to be even better than we could have imagined. In this respect I also want to thank Dr. Pietro Altermatt for the device simulations on the *p*-type emitters and Agnes Merkle for the (bulk) of the solar cell processing. Furthermore I want to acknowledge Dr. Thorsten Trupke (UNSW) and Dr. Keith McIntosh (ANU) for the help in solving the “weird” lifetime measurements which we obtained on lightly doped c-Si wafer passivated by Al_2O_3 . Finally I want to thank Dr. Isidro Martin for the insightful discussions we had about the modeling of the lifetime measurements.

Gelukkig is er ook nog een leven naast het werk. Binnen het kader van PMP ben ik met veel plezier bijna zes jaar actief (speler en coach) geweest in het PEST zaalvoetbal team. Ook heb ik met heel veel plezier “stoeptegels getild” met mijn fitness maatje Göksel die mij nog steeds naar zwaardere gewichten dwingt te gaan. Ook de vele gezellige avonden met “De Gekste” clubje (Alex, Bas, Björn, Floris, Giel, Jeroen, Kuno, Martin, Nick, Nieke, Marjolein, Yvonne, Renée, Sylvie en Wout) en met “het bioscoopclubje” (Bart, Marlie, Miranda en Wouter) waren essentieel voor de broodnodige afleiding. Mijn huisgenoot Floris wil ik bedanken voor de gezelligheid en vele discussies over van alles en nog wat en voor het proeflezen van hoofdstuk één van mijn proefschrift. Als laatste wil ik mijn ouders, mijn zus Astrid en Robert bedanken voor hun onvoorwaardelijke steun en liefde.

Curriculum Vitae

7 May 1979

Born in Horst, The Netherlands

June 1997

Diploma VWO

Blariacum College, Venlo-Blerick, The Netherlands

June 2003

Master of Science degree in Applied Physics

Eindhoven University of Technology, Eindhoven, The Netherlands

Three-month traineeship (2001-2002) in Prof. E.S. Aydil group, Faculty of Chemical
Engineering

University of California, Santa Barbara, United States

Master thesis project in the group of Equilibrium and Transport in Plasmas, Department
of Applied Physics

Eindhoven University of Technology, Eindhoven, The Netherlands

Including:

Two-month working visit (summer 2002) in Prof. E.S. Aydil group, Faculty of Chemical
Engineering

University of California, Santa Barbara, United States

November 2003 to May 2008

Ph.D. research in the group Plasma & Materials Processing, Department of Applied
Physics

Eindhoven University of Technology, Eindhoven, The Netherlands

In collaboration with:

OTB Solar B.V.

Eindhoven, The Netherlands

Three-month (fall 2006) working visit in Prof. A.G. Aberle group, School of
Photovoltaic and Renewable Energy Engineering
University of New South Wales, Sydney, Australia

